

NNLO QCD subtraction for top-antitop production in the $q\bar{q}$ channel

Gabriel Abelof,^a Aude Gehrmann-De Ridder,^{b,c} Philipp Maierhöfer^c and Stefano Pozzorini^c

^a*Department of Physics & Astronomy, Northwestern University, Evanston, IL 60208, U.S.A.*

^b*Institute for Theoretical Physics, ETH, CH-8093 Zürich, Switzerland*

^c*Physics Institute, University of Zürich, Winterthurerstrasse 190, CH-8057, Zürich*

E-mail: gabriel.abelof@northwestern.edu, gehra@itp.phys.ethz.ch, philipp@physik.uzh.ch, pozzorin@physik.uzh.ch

ABSTRACT: We present the computation of the double real and real-virtual contributions to top-antitop pair production in the quark-antiquark channel at leading colour. The $q\bar{q} \rightarrow t\bar{t}g$ amplitudes contributing to the real-virtual part are computed with OPENLOOPS, and their numerical stability in the soft and collinear regions is found to be sufficiently high to perform a realistic NNLO calculation in double precision. The subtraction terms required at real-real and real-virtual levels are constructed within the antenna subtraction formalism extended to deal with the presence of coloured massive final state particles. We show that those subtraction terms approximate the real-real and real-virtual matrix elements in all their singular limits.

KEYWORDS: QCD Phenomenology, Hadronic Colliders

ARXIV EPRINT: [1404.6493](https://arxiv.org/abs/1404.6493)

Contents

1	Introduction	1
2	Top-antitop production in the $q\bar{q}$ channel at NLO	6
2.1	Notation and conventions	6
2.2	$t\bar{t}$ production at LO	6
2.3	$t\bar{t}$ production at NLO	7
2.3.1	Real radiation contributions	8
2.3.2	Virtual contributions	11
2.3.3	The mass factorisation counter term at NLO	12
3	The massive initial-final antenna $A_4^0(1_Q, 3_g, 4_g, \hat{2}_q)$	13
3.1	Universal double unresolved factors	14
3.1.1	Double soft factor of two colour-connected gluons	14
3.1.2	Soft-collinear factor in the colour-connected configuration	15
3.1.3	Triple collinear factor	15
3.2	Infrared limits of $A_4^0(1_Q, 3_g, 4_g, \hat{2}_q)$	16
4	The massive initial-final antenna $A_3^1(1_Q, 3_g, \hat{2}_q)$	17
4.1	One-loop antenna functions	17
4.2	Single unresolved factors at one-loop	18
4.2.1	Collinear splitting functions	19
4.2.2	Massive soft factors	19
4.3	Infrared properties of $A_3^{1,lc}(1_Q, 3_g, \hat{2}_q)$	20
5	Double real contributions to $q\bar{q} \rightarrow t\bar{t}$ at leading colour	21
5.1	The double real contribution $d\hat{\sigma}_{q\bar{q},\text{NNLO},N_c^2}^{\text{RR}}$	21
5.2	The double real subtraction term $d\hat{\sigma}_{q\bar{q},\text{NNLO},N_c^2}^{\text{S}}$	22
6	General structure of the real-virtual contributions to $q\bar{q} \rightarrow t\bar{t}$ at leading-colour	24
7	Real-virtual contributions to top-antitop production in the quark-antiquark channel with OPENLOOPS	26
8	Real-virtual subtraction terms	28
8.1	The mass factorisation counter term $d\hat{\sigma}_{\text{NNLO}}^{\text{MF},1}$	28
8.2	Cancellation of explicit infrared poles in $d\hat{\sigma}_{\text{NNLO},q\bar{q},N_c^2}^{\text{RV}}$	30
8.3	Construction of $d\hat{\sigma}_{q\bar{q},\text{NNLO},N_c^2}^{\text{VS}}$	31
8.3.1	Construction of $d\hat{\sigma}_{q\bar{q},\text{NNLO},N_c^2}^{\text{VS},a}$	31
8.3.2	Construction of $d\hat{\sigma}_{q\bar{q},\text{NNLO},N_c^2}^{\text{VS},b}$	31
8.3.3	Construction of $d\hat{\sigma}_{q\bar{q},\text{NNLO},N_c^2}^{\text{VS},d}$	33
8.3.4	The complete real-virtual subtraction term $d\hat{\sigma}_{q\bar{q},\text{NNLO},N_c^2}^{\text{T}}$	33

9	Numerical tests of soft and collinear cancellations	35
9.1	Tests of the double real contributions	35
9.1.1	Double soft limits	36
9.1.2	Triple collinear limits	36
9.1.3	Soft-collinear limits	36
9.1.4	Double collinear limits	38
9.1.5	Single soft limits	38
9.1.6	Final-final single collinear limit	38
9.1.7	Initial-final single collinear limits	40
9.2	Tests of the real-virtual contributions	40
10	Stability of the integration over the three-particle phase space	42
11	Summary and outlook	43
A	Single unresolved tree-level universal factors	45
A.1	The collinear splitting functions	45
A.2	The massive soft eikonal factor	46
B	Colour-ordered infrared singularity operators	47
C	The complete expression of $A_4^0(1_Q, 3_g, 4_g, \hat{2}_q)$	48

1 Introduction

Top quark physics has become precision physics at the LHC. Some observables, like the total cross section for $t\bar{t}$ production, are expected to be measured with accuracies at the percent level. In addition, the ATLAS and CMS collaborations at CERN have reported first measurements of differential observables in top-quark pair production, such as the transverse momentum and rapidity of the $t\bar{t}$ system [1], its invariant mass [2], and the top quark transverse momentum [3]. Those measurements will allow for a much more detailed probe of the top quark production mechanism than what can be obtained from the total cross section. To reliably interpret these data, these precise measurements have to be matched onto equally accurate theoretical predictions. Those can be obtained by computing these hadron collider observables at the next-to-next-to leading order (NNLO) in perturbative QCD. At present, a fully differential NNLO calculation of the cross section for top pair production including all partonic channels is still missing. Intermediate results have recently become available in [4–15].

Most notably, the inclusive total hadronic $t\bar{t}$ production cross section has been presented in [16].

At NNLO, perturbative calculations of collider observables, like jet or heavy quark cross sections and associated kinematical distributions, are typically carried out using parton-level event generators. These programs generate events for all parton-level subprocesses

relevant to a given final state configuration up to NNLO accuracy and provide full kinematical information on an event-by-event basis. Towards this ultimate goal for top-pair production observables, in this paper we consider the quark-antiquark initiated channel at leading colour and compute two essential contributions to the NNLO top pair production cross section, namely the double real and real-virtual parts.

An NNLO event generator for observables with n final-state particles or jets involves three main building blocks: the two-loop corrections to the n -parton production process, denoted as double-virtual contributions $d\sigma^{VV}$, the one-loop corrections to the $(n+1)$ -parton production process, called real-virtual contribution $d\sigma^{RV}$, and the tree-level $(n+2)$ -parton double real contribution, $d\sigma^{RR}$. These three building blocks involve infrared divergences that arise from the exchange or emission of soft and collinear partons and cancel only in their sum. In addition, the real-virtual and virtual-virtual contributions to hadron collider observables involve initial-state collinear singularities that must be absorbed into mass factorisation counter terms. Those are labelled as $d\sigma^{MF,1}$ and $d\sigma^{MF,2}$, respectively.

The combination of subprocesses of different particle multiplicity and the consistent cancellation of the respective infrared singularities is one of the major challenges in the construction of NNLO parton-level event generators. In each subprocess, infrared singularities assume a different form: in the virtual corrections they are explicit, while in the real contributions they are implicit and become explicit only after phase space integration. To compute an observable beyond leading order, a regularization procedure is therefore required to extract and cancel the infrared singularities among different partonic channels before those can be implemented in the parton-level event generator. This goal is typically achieved by means of subtraction methods, where all relevant singularities of the matrix elements are subtracted by means of universal auxiliary terms, which are sufficiently simple to be added back after analytic integration over the unresolved phase space. In the past, this approach was successfully applied to various NNLO calculations using sector decomposition [17–20], q_T -subtraction [21], antenna subtraction [22] and most recently with an approach based on sector-improved residue subtraction [12, 23].

Two of these methods have been extended to treat massive final state fermions and applied to top pair hadro-production. In [16] the total cross section for inclusive $t\bar{t}$ production was obtained with the STRIPPER method [23, 24], which combines the FKS subtraction method [25] and sector decomposition [18, 19]. Moreover, the antenna subtraction formalism with massive fermions has been applied to the evaluation of the double real contributions to $t\bar{t}$ production for the pure fermionic processes [4] and for the gluon initiated process $gg \rightarrow t\bar{t}q\bar{q}$ [26]. In this paper, we shall employ the massive extension of antenna subtraction to extract the infrared behaviour of double real and real-virtual NNLO contributions to the $q\bar{q} \rightarrow t\bar{t}$ channel at leading colour.

While the computation of NNLO corrections to observables involving massive particles require the same kind of ingredients as for massless observables, namely real-real, real-virtual and virtual-virtual contributions, the presence of massive fermions in the final state introduces a few simplifications as well as new complications. First, due to the presence of massive final states, the ultraviolet renormalisation procedure of one and two loop amplitudes is more involved than for their massless counterparts. Not only couplings

but also mass and wave function ultraviolet renormalisations are required. For all loop amplitudes encountered in this paper, we shall use the ultraviolet regularisation procedure described in [8, 10]. Concerning infrared singularities, massive quarks do not give rise to final-state collinear singularities, and the quasi-collinear effects described in [27, 28] can be safely ignored for $t\bar{t}$ production at the LHC. Thus only divergencies associated with soft radiation and with collinear emissions off massless partons require explicit subtraction terms. On the other hand, the non-vanishing parton masses introduce a new scale, which represents a considerable source of complexity both for the final-state kinematics and for the integration of the subtraction terms.

Employing a subtraction method, the NNLO partonic cross section for top-pair production in a given partonic channel (and proportional to a specific colour factor) has the general structure [22]

$$\begin{aligned}
 d\hat{\sigma}_{\text{NNLO}} = & \int_{\Phi_4} (d\hat{\sigma}_{\text{NNLO}}^{\text{RR}} - d\hat{\sigma}_{\text{NNLO}}^{\text{S}}) + \int_{\Phi_4} d\hat{\sigma}_{\text{NNLO}}^{\text{S}} \\
 & + \int_{\Phi_3} (d\hat{\sigma}_{\text{NNLO}}^{\text{RV}} - d\hat{\sigma}_{\text{NNLO}}^{\text{VS}}) + \int_{\Phi_3} d\hat{\sigma}_{\text{NNLO}}^{\text{VS}} + \int_{\Phi_3} d\hat{\sigma}_{\text{NNLO}}^{\text{MF},1} \\
 & + \int_{\Phi_2} d\hat{\sigma}_{\text{NNLO}}^{\text{VV}} + \int_{\Phi_2} d\hat{\sigma}_{\text{NNLO}}^{\text{MF},2}.
 \end{aligned} \tag{1.1}$$

Two types of subtraction terms are introduced: $d\hat{\sigma}_{\text{NNLO}}^{\text{S}}$ for the 4-parton final state, and $d\hat{\sigma}_{\text{NNLO}}^{\text{VS}}$ for the 3-parton final state. The former approximates the behaviour of the double real contributions $d\hat{\sigma}_{\text{NNLO}}^{\text{RR}}$ in their single and double unresolved limits, whereas the latter reproduces the single unresolved behaviour of the mixed real-virtual contributions $d\hat{\sigma}_{\text{NNLO}}^{\text{RV}}$.

In the context of the antenna subtraction framework employed in this paper, we decompose further the double real subtraction term $d\hat{\sigma}_{\text{NNLO}}^{\text{S}}$. This term contains distinct pieces corresponding to different limits and different colour-ordered configurations. Some of these pieces ought to be integrated analytically over the unresolved phase space of one particle and combined with the 3-parton final state, while the remaining terms are to be integrated over the unresolved phase space of two particles and combined with the 2-parton contributions. This separation amounts to splitting the integrated form of $d\hat{\sigma}_{\text{NNLO}}^{\text{S}}$ as [29–32]

$$\int_{\Phi_4} d\hat{\sigma}_{\text{NNLO}}^{\text{S}} = \int_{\Phi_3} \int_1 d\hat{\sigma}_{\text{NNLO}}^{\text{S},1} + \int_{\Phi_3} \int_2 d\hat{\sigma}_{\text{NNLO}}^{\text{S},2}, \tag{1.2}$$

which allows us to rearrange the different terms in eq. (1.1) into the more convenient form

$$\begin{aligned}
 d\hat{\sigma}_{\text{NNLO}} = & \int_{\Phi_4} [d\hat{\sigma}_{\text{NNLO}}^{\text{RR}} - d\hat{\sigma}_{\text{NNLO}}^{\text{S}}] \\
 & + \int_{\Phi_3} [d\hat{\sigma}_{\text{NNLO}}^{\text{RV}} - d\hat{\sigma}_{\text{NNLO}}^{\text{T}}] \\
 & + \int_{\Phi_2} [d\hat{\sigma}_{\text{NNLO}}^{\text{VV}} - d\hat{\sigma}_{\text{NNLO}}^{\text{U}}],
 \end{aligned} \tag{1.3}$$

with

$$d\hat{\sigma}_{\text{NNLO}}^{\text{T}} = d\hat{\sigma}_{\text{NNLO}}^{\text{VS}} - \int_1 d\hat{\sigma}_{\text{NNLO}}^{\text{S},1} - d\hat{\sigma}_{\text{NNLO}}^{\text{MF},1}, \quad (1.4)$$

$$d\hat{\sigma}_{\text{NNLO}}^{\text{U}} = - \int_1 d\hat{\sigma}_{\text{NNLO}}^{\text{VS}} - \int_2 d\hat{\sigma}_{\text{NNLO}}^{\text{S},2} - d\hat{\sigma}_{\text{NNLO}}^{\text{MF},2}. \quad (1.5)$$

In this paper, we shall explicitly construct the antenna subtraction terms $d\hat{\sigma}_{\text{NNLO}}^{\text{S}}$ and $d\hat{\sigma}_{\text{NNLO}}^{\text{T}}$ entering at the four- and three-parton contributions to the NNLO top pair production cross section (1.3) for the quark-antiquark channel at leading colour. The virtual-virtual subtraction term, $d\hat{\sigma}_{\text{NNLO}}^{\text{U}}$, will be derived elsewhere.

Based on the universal factorisation properties of QCD colour-ordered amplitudes, the antenna formalism [4, 22, 26, 27, 31, 33–42] provides a general framework for the construction of subtraction terms that reproduce the singular behaviour of the double real and mixed real-virtual NNLO corrections. Subtraction terms are constructed as products of antenna functions and reduced matrix elements squared with remapped momenta, and the subtraction procedure is based on the colour ordering representation.

The antenna functions capture all the unresolved radiation emitted between a pair of hard partons, referred to as hard radiators. In hadronic collisions, the hard radiators can be initial or final state partons, and therefore three types of antennae must be distinguished: final-final (f-f), initial-final (i-f) and initial-initial (i-i). While NLO subtraction terms only involve three-parton tree-level antennae, at NNLO four-parton tree-level antennae and three-parton antennae are also needed in the double real and real-virtual contributions, respectively. In addition, $3 \rightarrow 2$ and $4 \rightarrow 2$ phase space mappings are required for the reduced matrix elements multiplying the antenna functions in the subtraction terms. Moreover, the analytic integration of the subtraction terms over the appropriate unresolved patch of the phase space requires an exact and Lorentz invariant factorisation of the phase space. Both the mappings and the factorisations are different in f-f, i-f, and i-i configurations. They can all be found for the massive case in [4, 27].

The framework outlined above for the construction of NNLO antenna subtraction terms was set up in [31, 32, 42] in the context of a proof-of-principle implementation of the purely gluonic leading-colour NNLO contributions to di-jet production at hadron colliders. In [31, 32], the correctness of the method was checked by showing a complete cancellation of all explicit and implicit infrared divergences that arise in the intermediate steps of the calculation. These results were numerically implemented in the NNLOJET parton-level event generator [43], producing the first NNLO results for hadronic di-jet production. A considerable reduction of the theoretical scale uncertainty was observed, and for the first time double differential distributions in p_T and η for inclusive-jet and di-jet NNLO cross sections were presented. Recently, these results have been upgraded to include the full colour dependence in [29].

As outlined above, the goal of this paper is to employ the antenna subtraction method in its extension to the massive case to compute the double real and real-virtual corrections to $t\bar{t}$ hadro-production in the $q\bar{q}$ channel. In particular we shall focus on the leading-colour pieces of processes $q\bar{q} \rightarrow t\bar{t}gg$ at tree-level and $q\bar{q} \rightarrow t\bar{t}g$ at one-loop and their corresponding antenna subtraction terms denoted as $d\hat{\sigma}_{\text{NNLO}}^{\text{S}}$ and $d\hat{\sigma}_{\text{NNLO}}^{\text{T}}$ in eq. (1.3).

This will require the use of known phase space factorisations and mappings [4, 27, 44] and several massive antennae. From those, the three-parton massive antennae are known. New tree-level four-parton and three-parton antennae will be derived here for the first time. The general structure of the subtraction terms remains unchanged with respect to the massless case [22, 31, 32, 42] though, and we shall not repeat it here. We shall instead restrict our presentation to the new elements that are relevant for the present calculation and are related to the presence of massive final states.

Besides antenna subtraction, also the calculation of the $2 \rightarrow 3$ one-loop amplitudes represent a nontrivial ingredient of the $2 \rightarrow 2$ NNLO calculation at hand. Thanks to the recent advent of fully automated NLO tools, such contributions can be in principle computed on a routinely basis. However, the application of NLO tools in the framework of NNLO calculations poses new and still poorly explored challenges. First of all, depending on the employed tool, the numerical character of the new one-loop algorithms might imply a serious CPU speed penalty as compared to analytic approaches. Moreover, the integration of the (subtracted) one-loop contributions over the soft and collinear regions of phase space can lead to serious numerical instabilities. In particular, the well known spurious singularities related to small Gram determinants are inevitably enhanced in the infrared phase space regions, and the resulting loss of numerical accuracy can be strongly enhanced by the large cancellations between matrix elements and subtraction terms. It is thus a priori not clear if automated one-loop generators can guarantee an adequate level of numerical stability and speed for NNLO applications. In this paper we address these issues using the OPENLOOPS [45] one-loop generator in combination with the CUTTOOLS [46] reduction library, which allows us to study the behaviour of one-loop matrix elements in the deep infrared regime using quadruple precision. As we will show, in spite of the presence of severe instabilities associated with very soft gluon emissions, in the antenna subtraction framework the employed tools turn out to be sufficiently stable to perform a realistic NNLO calculation in double precision. Given the high speed of OPENLOOPS and the fact that quadruple precision can be avoided almost completely, this guarantees a highly efficient integration of the real-virtual NNLO contributions.

The paper is organised as follows: in section 2, we shall present the cross section for the top-antitop production up to the NLO level. This will enable us to set up the normalisation and present the NLO ingredients required for the computation of the top-pair production cross section at NNLO. The new tree-level four-parton antenna and the three-parton antenna functions required at the double real and real-virtual level of this computation will be presented in sections 3 and 4, respectively. The double real contributions and their subtraction terms are derived in section 5. Sections 6 and 7 contain the real-virtual contributions. Their general structure is presented in section 6 while their computation with OPENLOOPS is described in section 7. In section 8, we explicitly construct the real-virtual subtraction terms which cancel the explicit infrared poles of the real-virtual contributions and approximate these contributions in all their single unresolved limits. Sections 9 and 10 present various detailed checks on the consistency and numerical stability of the double real and real-virtual subtractions. Finally, section 11 contains our conclusions. In appendix A, the universal single unresolved soft and collinear factors are presented, in appendix B the

colour-ordered infrared singularity operators are included, while in appendix C the full expression of the antenna presented in section 3 is given.

2 Top-antitop production in the $q\bar{q}$ channel at NLO

In this section we shall present the main ingredients that are required in the computation of the NLO cross section for $t\bar{t}$ hadronic production in the $q\bar{q}$ channel. Besides setting up the notation and the general framework that we will follow throughout the present paper, those NLO contributions will be an essential input for the NNLO mass factorisation counter term $d\hat{\sigma}_{q\bar{q},\text{NNLO}}^{\text{MF},1}$ which shall be derived explicitly in section 8.

2.1 Notation and conventions

To facilitate the reading of our expressions, we shall closely follow the notation in [4, 27] for the matrix elements and subtractions terms. In order to identify the colour-ordered sub-amplitudes with the colour factors that multiply them in the colour decomposition of the full amplitude, we use the following conventions: different colour strings are separated with double semicolons. A colour string $(T^{a_1} \dots T^{a_n})_{ij}$ corresponds to $\dots;;i, a_1, \dots, a_n, j;;\dots$ in the argument of the corresponding sub-amplitude. Adjacent partons within one colour string are colour-connected. An antiquark (or an initial state quark) at the end of a colour chain and a like-flavour quark (or initial state antiquark) at the beginning of a different colour chain are also colour-connected, since the two chains merge in the collinear limit where the $q\bar{q}$ pair clusters into a gluon. When decoupling identities are used, we denote the gluons which are photon-like and only couple to quark lines with the index γ instead of g . In sub-amplitudes where all gluons are photon-like no semicolons are used, since the concept of colour connection is not meaningful. Finally, a hat over the label of a certain parton indicates that it is an initial state particle (for example, $\hat{1}_q$ is an initial state quark with momentum p_1).

Concerning the kinematics, we will use the following definition of invariants:

$$s_{ij} = 2p_i \cdot p_j, \quad s_{ijk} = 2p_i \cdot p_j + 2p_i \cdot p_k + 2p_j \cdot p_k, \quad (2.1)$$

both for massless and massive momenta to make the mass-dependent terms explicitly proportional to m_Q . The momenta $p_{i,j,k}$ in eq. (2.1) have to be understood as physical incoming or outgoing momenta with $p_{i,j,k}^0 > 0$. The above invariants are thus always positive, and crossing transformations have to be accompanied by sign-flips $s_{ij} \rightarrow -s_{ij}$, $s_{ijk} \rightarrow -s_{ijk}$ whenever appropriate.

2.2 $t\bar{t}$ production at LO

The hadronic cross section for $t\bar{t}$ production at leading order involves two partonic channels, with either a $q\bar{q}$ pair or a pair of gluons in the initial state. It is given by

$$d\sigma_{\text{LO}}(H_1, H_2) = \int \frac{d\xi_1}{\xi_1} \frac{d\xi_2}{\xi_2} \left(f_g(\xi_1, \mu) f_g(\xi_2, \mu) d\hat{\sigma}_{gg,\text{LO}}(p_1, p_2) + \sum_q f_q(\xi_1, \mu) f_{\bar{q}}(\xi_2, \mu) d\hat{\sigma}_{q\bar{q},\text{LO}}(p_1, p_2) \right), \quad (2.2)$$

where H_1 and H_2 are the momenta of the incoming hadrons, $p_i = \xi_i H_i$, and the sum runs over all quark flavours. Restricting ourselves to the $q\bar{q}$ initiated process, the leading order partonic cross section takes the form:

$$d\hat{\sigma}_{q\bar{q},\text{LO}} = \mathcal{N}_{\text{LO}}^{q\bar{q}} \int d\Phi_2(p_3, p_4; p_1, p_2) |\mathcal{M}_4^0(3_Q, 4_{\bar{Q}}, \hat{2}_{\bar{q}}, \hat{1}_q)|^2 J_2^{(2)}(p_3, p_4), \quad (2.3)$$

where, $d\Phi_2(p_3, p_4; p_1, p_2)$ is the $2 \rightarrow 2$ partonic phase space, $J_2^{(2)}(p_3, p_4)$ is a so-called measurement function, which ensures that a pair of final state massive quarks of momenta p_3 and p_4 are observed. $\mathcal{M}_4^0(\dots)$ is the colour-ordered and coupling-stripped tree-level amplitude. It is related to the full amplitude through the (trivial) colour decomposition

$$M_4^0(q_1\bar{q}_2 \rightarrow Q_3\bar{Q}_4) = g_s^2 \left(\delta_{i_3 i_1} \delta_{i_2 i_4} - \frac{1}{N_c} \delta_{i_3 i_4} \delta_{i_2 i_1} \right) \mathcal{M}_4^0(3_Q, 4_{\bar{Q}}, \hat{2}_{\bar{q}}, \hat{1}_q). \quad (2.4)$$

The normalisation factor is

$$\mathcal{N}_{\text{LO}}^{q\bar{q}} = \frac{1}{2s} \left(\frac{\alpha_s(\mu)}{2\pi} \right)^2 \frac{\bar{C}(\epsilon)^2}{C(\epsilon)^2} \frac{(N_c^2 - 1)}{4N_c^2}, \quad (2.5)$$

where s is the energy squared in the hadronic center-of-mass frame. Included in this normalisation factor are the flux factor, as well as the sum and average over colour and spin.

The constants $C(\epsilon)$ and $\bar{C}(\epsilon)$ are defined as:

$$C(\epsilon) = \frac{(4\pi)^\epsilon}{8\pi^2} e^{-\epsilon\gamma_E} \quad \bar{C}(\epsilon) = (4\pi)^\epsilon e^{-\epsilon\gamma_E}, \quad (2.6)$$

providing the useful relation

$$g_s^2 = 4\pi\alpha_s = \left(\frac{\alpha_s}{2\pi} \right) \frac{\bar{C}(\epsilon)}{C(\epsilon)}. \quad (2.7)$$

2.3 $t\bar{t}$ production at NLO

At the next-to-leading order, three different partonic channels enter: the $q\bar{q}$, the gg and the qg channels. The hadronic cross section for $t\bar{t}$ production at this order is therefore given by

$$\begin{aligned} d\sigma_{\text{NLO}}(P_1, P_2) = & \int \frac{d\xi_1}{\xi_1} \frac{d\xi_2}{\xi_2} \left[f_g(\xi_1, \mu) f_g(\xi_2, \mu) d\hat{\sigma}_{gg,\text{NLO}}(p_1, p_2) \right. \\ & + \sum_q \left(f_q(\xi_1, \mu) f_{\bar{q}}(\xi_2, \mu) d\hat{\sigma}_{q\bar{q},\text{NLO}}(p_1, p_2) \right. \\ & + \left(f_q(\xi_1, \mu) + f_{\bar{q}}(\xi_1, \mu) \right) f_g(\xi_2, \mu) d\hat{\sigma}_{qg,\text{NLO}}(p_1, p_2) \\ & \left. \left. + f_g(\xi_1, \mu) \left(f_q(\xi_2, \mu) + f_{\bar{q}}(\xi_2, \mu) \right) d\hat{\sigma}_{gq,\text{NLO}}(p_1, p_2) \right) \right], \quad (2.8) \end{aligned}$$

where we have used the fact that the partonic cross sections for the qg and the $\bar{q}g$ are identical due to their invariance under charge conjugation.

Restricting ourselves to the $q\bar{q}$ channel and employing a subtraction method at NLO, the partonic cross section takes the form,

$$d\hat{\sigma}_{q\bar{q},\text{NLO}} = \int_{d\Phi_3} (d\hat{\sigma}_{q\bar{q},\text{NLO}}^{\text{R}} - ds_{q\bar{q},\text{NLO}}^{\text{S}}) + \int_{d\Phi_2} \left(d\hat{\sigma}_{q\bar{q},\text{NLO}}^{\text{V}} + \int_1 d\hat{\sigma}_{q\bar{q},\text{NLO}}^{\text{S}} + d\hat{\sigma}_{q\bar{q},\text{NLO}}^{\text{MF}} \right). \quad (2.9)$$

The three-parton final state contains the real radiation contributions $d\hat{\sigma}_{q\bar{q},\text{NLO}}^{\text{R}}$ and their corresponding subtraction term $d\hat{\sigma}_{q\bar{q},\text{NLO}}^{\text{S}}$, whereas the two-parton final state includes the virtual contributions $d\hat{\sigma}_{q\bar{q},\text{NLO}}^{\text{V}}$, the integrated subtraction term $\int_1 d\hat{\sigma}_{q\bar{q},\text{NLO}}^{\text{S}}$ and the NLO mass factorisation counter term $d\hat{\sigma}_{q\bar{q},\text{NLO}}^{\text{MF}}$. The latter is related to the leading order partonic cross section and will be given below.

By grouping the different contributions to the NLO partonic cross section as in eq. (2.9), the difference $(d\hat{\sigma}_{q\bar{q},\text{NLO}}^{\text{R}} - d\hat{\sigma}_{q\bar{q},\text{NLO}}^{\text{S}})$ is numerically well behaved in all regions of the $2 \rightarrow 3$ phase space. It can be integrated numerically in four dimensions. Furthermore, the two-parton contributions $(d\hat{\sigma}_{q\bar{q},\text{NLO}}^{\text{V}} + \int_1 d\hat{\sigma}_{q\bar{q},\text{NLO}}^{\text{S}} + d\hat{\sigma}_{q\bar{q},\text{NLO}}^{\text{MF}})$ are free of poles in the dimensional regulator ϵ as we shall demonstrate below.

2.3.1 Real radiation contributions

The real radiation corrections to the $q\bar{q}$ channel for $t\bar{t}$ hadronic production are due to the process $q\bar{q} \rightarrow t\bar{t}g$. The colour decomposition of the corresponding tree-level amplitude is

$$M_5^0(q_1\bar{q}_2 \rightarrow Q_3\bar{Q}_4g_5) = \quad (2.10)$$

$$g_s^3\sqrt{2} \left\{ \left[(T^{a_5})_{i_3i_1} \delta_{i_2i_4} \mathcal{M}_5^0(3_Q, 5_g, \hat{1}_q; ; \hat{2}_{\bar{q}}, 4_{\bar{Q}}) + (T^{a_5})_{i_2i_4} \delta_{i_3i_1} \mathcal{M}_5^0(3_Q, \hat{1}_q; ; \hat{2}_{\bar{q}}, 5_g, 4_{\bar{Q}}) \right] \right.$$

$$\left. - \frac{1}{N_c} \left[(T^{a_5})_{i_3i_4} \delta_{i_2i_1} \mathcal{M}_5^0(3_Q, 5_g, 4_{\bar{Q}}; ; \hat{2}_{\bar{q}}, \hat{1}_q) + (T^{a_5})_{i_2i_1} \delta_{i_3i_4} \mathcal{M}_5^0(3_Q, 4_{\bar{Q}}; ; \hat{2}_{\bar{q}}, 5_g, \hat{1}_q) \right] \right\}.$$

Squaring this expression and combining it with the $2 \rightarrow 3$ phase space, the appropriate over-all factors and the measurement function, we can write the real radiation contributions as

$$d\hat{\sigma}_{q\bar{q},\text{NLO}}^{\text{R}} = \mathcal{N}_{\text{NLO}}^{\text{R},q\bar{q}} d\Phi_3(p_3, p_4, p_5; p_1, p_2)$$

$$\times \left\{ N_c \left[|\mathcal{M}_5^0(3_Q, 5_g, \hat{1}_q; ; \hat{2}_{\bar{q}}, 4_{\bar{Q}})|^2 + |\mathcal{M}_5^0(3_Q, \hat{1}_q; ; \hat{2}_{\bar{q}}, 5_g, 4_{\bar{Q}})|^2 \right] \right.$$

$$+ \frac{1}{N_c} \left[|\mathcal{M}_5^0(3_Q, 5_g, 4_{\bar{Q}}; ; \hat{2}_{\bar{q}}, \hat{1}_q)|^2 + |\mathcal{M}_5^0(3_Q, 4_{\bar{Q}}; ; \hat{2}_{\bar{q}}, 5_g, \hat{1}_q)|^2 \right.$$

$$\left. \left. - 2|\mathcal{M}_5^0(3_Q, 4_{\bar{Q}}, \hat{2}_{\bar{q}}, \hat{1}_q, 5_g)|^2 \right] \right\} J_3^{(2)}(p_3, p_4, p_5) \quad (2.11)$$

where we have defined

$$\mathcal{M}_5^0(3_Q, 4_{\bar{Q}}, \hat{2}_{\bar{q}}, \hat{1}_q, 5_g) = \mathcal{M}_5^0(3_Q, 5_g, \hat{1}_q; ; \hat{2}_{\bar{q}}, 4_{\bar{Q}}) + \mathcal{M}_5^0(3_Q, \hat{1}_q; ; \hat{2}_{\bar{q}}, 5_g, 4_{\bar{Q}})$$

$$= \mathcal{M}_5^0(3_Q, 5_g, 4_{\bar{Q}}; ; \hat{2}_{\bar{q}}, \hat{1}_q) + \mathcal{M}_5^0(3_Q, 4_{\bar{Q}}; ; \hat{2}_{\bar{q}}, 5_g, \hat{1}_q) \quad (2.12)$$

in which the gluon is U(1)-like. The normalisation factor $\mathcal{N}_{\text{NLO}}^{\text{R},q\bar{q}}$ is given by

$$\mathcal{N}_{\text{NLO}}^{\text{R},q\bar{q}} = \mathcal{N}_{\text{LO}}^{q\bar{q}} \frac{\alpha_s(\mu)}{2\pi} \frac{\bar{C}(\epsilon)}{C(\epsilon)}, \quad (2.13)$$

and the measurement or jet function denoted by $J_3^{(2)}(p_3, p_4, p_5)$ guarantees that out of three-parton with momenta p_3, p_4 and p_5 a final state with a massive heavy quark pair is formed.

The matrix elements squared in eq. (2.11) can become singular when the gluon, whose momentum is denoted by p_5 in the above equation, is either soft or collinear to either of the incoming partons. The antenna subtraction term that reproduces the behaviour of $d\hat{\sigma}_{q\bar{q},\text{NLO}}^{\text{R}}$ in those limits is known [27]. It is constructed entirely with products of A-type antennae and reduced matrix elements in final-final, initial-final and initial-initial kinematical configurations

$$\begin{aligned}
 d\hat{\sigma}_{q\bar{q},\text{NLO}}^{\text{S}} &= \mathcal{N}_{\text{NLO}}^{\text{R},q\bar{q}} d\Phi_3(p_3, p_4, p_5; p_1, p_2) \\
 &\times \left\{ N_c \left[A_3^0(3_Q, 5_g, \hat{1}_q) |\mathcal{M}_4^0((\tilde{35})_Q, 4_{\bar{Q}}, \hat{2}_{\bar{q}}, \hat{1}_q)|^2 J_2^{(2)}(\tilde{p}_{35}, p_4) \right. \right. \\
 &\quad \left. \left. + A_3^0(4_{\bar{Q}}, 5_g, \hat{2}_{\bar{q}}) |\mathcal{M}_4^0(3_Q, (\tilde{45})_{\bar{Q}}, \hat{2}_{\bar{q}}, \hat{1}_q)|^2 J_2^{(2)}(p_3, \tilde{p}_{45}) \right] \right. \\
 &\quad + \frac{1}{N_c} \left[2A_3^0(3_Q, 5_g, \hat{2}_{\bar{q}}) |\mathcal{M}_4^0((\tilde{35})_Q, 4_{\bar{Q}}, \hat{2}_{\bar{q}}, \hat{1}_q)|^2 J_2^{(2)}(\tilde{p}_{35}, p_4) \right. \\
 &\quad \left. + 2A_3^0(4_{\bar{Q}}, 5_g, \hat{1}_q) |\mathcal{M}_4^0(3_Q, (\tilde{45})_{\bar{Q}}, \hat{2}_{\bar{q}}, \hat{1}_q)|^2 J_2^{(2)}(p_3, \tilde{p}_{45}) \right. \\
 &\quad - 2A_3^0(3_Q, 5_g, \hat{1}_q) |\mathcal{M}_4^0((\tilde{35})_Q, 4_{\bar{Q}}, \hat{2}_{\bar{q}}, \hat{1}_q)|^2 J_2^{(2)}(\tilde{p}_{35}, p_4) \\
 &\quad - 2A_3^0(4_{\bar{Q}}, 5_g, \hat{2}_{\bar{q}}) |\mathcal{M}_4^0(3_Q, (\tilde{45})_{\bar{Q}}, \hat{2}_{\bar{q}}, \hat{1}_q)|^2 J_2^{(2)}(p_3, \tilde{p}_{45}) \\
 &\quad - A_3^0(3_Q, 5_g, 4_{\bar{Q}}) |\mathcal{M}_4^0((\tilde{35})_Q, (\tilde{45})_{\bar{Q}}, \hat{2}_{\bar{q}}, \hat{1}_q)|^2 J_2^{(2)}(\tilde{p}_{35}, \tilde{p}_{45}) \\
 &\quad \left. \left. - A_3^0(\hat{1}_q, 5_g, \hat{2}_{\bar{q}}) |\mathcal{M}_4^0(\tilde{3}_Q, \tilde{4}_{\bar{Q}}, \hat{2}_{\bar{q}}, \hat{1}_q)|^2 J_2^{(2)}(\tilde{p}_3, \tilde{p}_4) \right] \right\}. \quad (2.14)
 \end{aligned}$$

The reduced matrix elements and measurement functions in the equation above contain redefined momenta that are obtained from the original ones through Lorentz invariant on-shell mappings, whose form is different in subtraction terms involving final-final, initial-final and initial-initial antennae. Final state and initial state remapped momenta are denoted with tildes (e.g. \tilde{p}_{35}) and bars (e.g. \bar{p}_1), respectively. In final-final subtraction terms the mappings employed are of the form $\{p_i, p_j, p_k\} \rightarrow \{\tilde{p}_{ij}, \tilde{p}_{jk}\}$ and both redefined momenta are obtained from all three original momenta in the antenna system. Initial-final mappings are of the form $\{p_i, p_j, p_k\} \rightarrow \{\bar{p}_i, \tilde{p}_{jk}\}$, where p_i is an initial state momentum which the mapping rescales, and \tilde{p}_{jk} is obtained from all three momenta in the antenna system. For subtraction terms in initial-initial configurations, the mapping rescales both initial state momenta and performs a Lorentz boost on all remaining final state particles in order to preserve momentum conservation in the reduced matrix elements. The precise definitions of all these mappings can be found, for example, in [27].

The construction of the subleading colour pieces ($1/N_c$) of eq. (2.14) requires a special procedure, which was explained in [4, 27].

The integrated form of the NLO subtraction term $d\hat{\sigma}_{q\bar{q},\text{NLO}}^{\text{S}}$ is obtained by factorising the $2 \rightarrow 3$ phase space into an antenna phase space and a reduced $2 \rightarrow 2$ phase space, and integrating the antenna functions A_3^0 in eq. (2.14) inclusively over the antenna phase space. This factorisation, as well as the specific form of the antenna phase space is different for final-final (f-f), initial-final (i-f) and initial-initial (i-i) configurations. It has been derived in the massless case in [22, 36] and in the massive case in [27, 40]. The integrated forms of the A-type antennae in eq. (2.14) are denoted as \mathcal{A} . We shall only make explicit use of their pole parts, which can be entirely written in terms of universal splitting kernels and infrared singularity operators as

$$\begin{aligned}
 \text{Poles}(\mathcal{A}_{QgQ}^0(\epsilon, s_{ij}, x_1, x_2)) &= -2\mathbf{I}_{QQ}^{(1)}(\epsilon, s_{ij})\delta(1-x_1)\delta(1-x_2) \\
 \text{Poles}(\mathcal{A}_{q,Qg}^0(\epsilon, s_{ij}, x_1, x_2)) &= -2\mathbf{I}_{Qq}^{(1)}(\epsilon, s_{ij})\delta(1-x_1)\delta(1-x_2) + \frac{1}{2}\Gamma_{qq}^{(1)}(x_1)\delta(1-x_2) \\
 \text{Poles}(\mathcal{A}_{q\bar{q},Q}^0(\epsilon, s_{ij}, x_1, x_2)) &= -2\mathbf{I}_{q\bar{q}}^{(1)}(\epsilon, s_{ij})\delta(1-x_1)\delta(1-x_2) \\
 &\quad + \frac{1}{2}\Gamma_{qq}^{(1)}(x_1)\delta(1-x_2) + \frac{1}{2}\Gamma_{q\bar{q}}^{(1)}(x_2)\delta(1-x_1). \tag{2.15}
 \end{aligned}$$

The colour-ordered infrared singularity operators of the form $\mathbf{I}_{ij}^{(1)}$ appearing in the above equation are given in appendix B. The splitting kernel $\Gamma_{qq}^{(1)}(x)$ in $D = 4 - 2\epsilon$ dimensions is given by

$$\Gamma_{qq}^{(1)}(x) = -\frac{1}{\epsilon} \left(\frac{3}{2}\delta(1-x) + 2\mathcal{D}_0(x) - 1 - x \right), \tag{2.16}$$

with

$$\mathcal{D}_0(x) = \left(\frac{1}{1-x} \right)_+. \tag{2.17}$$

From these equations, we can express the pole part of the integrated form of eq. (2.14) compactly as

$$\begin{aligned}
 \text{Poles} \left(\int_1 d\hat{\sigma}_{q\bar{q},\text{NLO}}^{\text{S}} \right) &= \mathcal{N}_{\text{NLO}}^{\text{V},q\bar{q}} \int \frac{dx_1}{x_1} \frac{dx_2}{x_2} d\Phi_2(p_3, p_4; x_1 p_1, x_2 p_2) |\mathcal{M}_4^0(3_Q, 4_{\bar{Q}}, \hat{2}_{\bar{q}}, \hat{1}_q)|^2 \\
 &\times \left\{ \delta(1-x_1)\delta(1-x_2) \left[N_c \left(-2\mathbf{I}_{Q\bar{q}}^{(1)}(\epsilon, s_{13}) - 2\mathbf{I}_{Q\bar{q}}^{(1)}(\epsilon, s_{24}) \right) - \frac{1}{N_c} \left(4\mathbf{I}_{Q\bar{q}}^{(1)}(\epsilon, s_{14}) \right. \right. \right. \\
 &\quad \left. \left. \left. + 4\mathbf{I}_{Q\bar{q}}^{(1)}(\epsilon, s_{23}) - 4\mathbf{I}_{Q\bar{q}}^{(1)}(\epsilon, s_{13}) - 4\mathbf{I}_{Q\bar{q}}^{(1)}(\epsilon, s_{24}) - 2\mathbf{I}_{Q\bar{Q}}^{(1)}(\epsilon, s_{34}) - 2\mathbf{I}_{q\bar{q}}^{(1)}(\epsilon, s_{12}) \right) \right] \right. \\
 &\quad \left. + \left(\frac{N_c^2 - 1}{2N_c} \right) \left[\Gamma_{qq}^{(1)}(x_1)\delta(1-x_2) + \Gamma_{q\bar{q}}^{(1)}(x_2)\delta(1-x_1) \right] \right\} J_2^{(2)}(p_3, p_4), \tag{2.18}
 \end{aligned}$$

with the normalisation factor $\mathcal{N}_{\text{NLO}}^{\text{V},q\bar{q}}$ given by

$$\mathcal{N}_{\text{NLO}}^{\text{V},q\bar{q}} = \mathcal{N}_{\text{LO}}^{q\bar{q}} \frac{\alpha_s(\mu)}{2\pi} \bar{C}(\epsilon) = \mathcal{N}_{\text{NLO}}^{\text{R},q\bar{q}} C(\epsilon). \tag{2.19}$$

2.3.2 Virtual contributions

The virtual contributions denoted by $d\hat{\sigma}_{q\bar{q},\text{NLO}}^{\text{V}}$ in eq. (2.9) are due to the process $q\bar{q} \rightarrow t\bar{t}$ at. The colour decomposition of the relevant one loop amplitude is

$$M_4^1(q_1\bar{q}_2 \rightarrow Q_3\bar{Q}_4) = g_s^4 C(\epsilon) \left[\delta_{i_3 i_1} \delta_{i_2 i_4} \mathcal{M}_{4,1}^1(3_Q, 4_{\bar{Q}}, \hat{2}_{\bar{q}}, \hat{1}_q) + \delta_{i_3 i_4} \delta_{i_2 i_1} \mathcal{M}_{4,2}^1(3_Q, 4_{\bar{Q}}, \hat{2}_{\bar{q}}, \hat{1}_q) \right]. \quad (2.20)$$

Each of the partial amplitudes can be still decomposed into primitives as

$$\begin{aligned} \mathcal{M}_{4,i}^1(3_Q, 4_{\bar{Q}}, \hat{2}_{\bar{q}}, \hat{1}_q) &= N_c \mathcal{M}_{4,i}^{[lc]}(3_Q, 4_{\bar{Q}}, \hat{2}_{\bar{q}}, \hat{1}_q) + N_l \mathcal{M}_{4,i}^{[l]}(3_Q, 4_{\bar{Q}}, \hat{2}_{\bar{q}}, \hat{1}_q) \\ &\quad + N_h \mathcal{M}_{4,i}^{[h]}(3_Q, 4_{\bar{Q}}, \hat{2}_{\bar{q}}, \hat{1}_q) - \frac{1}{N_c} \mathcal{M}_{4,i}^{[slc]}(3_Q, 4_{\bar{Q}}, \hat{2}_{\bar{q}}, \hat{1}_q), \end{aligned} \quad (2.21)$$

where N_l and N_h are respectively the number of light and heavy flavours. Using eqs. (2.20) and (2.21) together with the colour decomposition given in eq. (2.4) for the corresponding tree-level amplitude, we can write the virtual contributions to the $t\bar{t}$ production cross section in the $q\bar{q}$ channel as

$$\begin{aligned} d\hat{\sigma}_{q\bar{q},\text{NLO}}^{\text{V}} &= \mathcal{N}_{\text{NLO}}^{\text{V},q\bar{q}} d\Phi_2(p_3, p_4; p_1, p_2) \\ &\quad \times \left\{ N_c |\mathcal{M}_{4,1}^{[lc]}(3_Q, 4_{\bar{Q}}, \hat{2}_{\bar{q}}, \hat{1}_q)|_{\text{NLO}}^2 + N_l |\mathcal{M}_{4,1}^{[l]}(3_Q, 4_{\bar{Q}}, \hat{2}_{\bar{q}}, \hat{1}_q)|_{\text{NLO}}^2 \right. \\ &\quad \left. + N_h |\mathcal{M}_{4,1}^{[h]}(3_Q, 4_{\bar{Q}}, \hat{2}_{\bar{q}}, \hat{1}_q)|_{\text{NLO}}^2 - \frac{1}{N_c} |\mathcal{M}_{4,1}^{[slc]}(3_Q, 4_{\bar{Q}}, \hat{2}_{\bar{q}}, \hat{1}_q)|_{\text{NLO}}^2 \right\} J_2^{(2)}(p_3, p_4), \end{aligned} \quad (2.22)$$

where we have introduced the following compact notation

$$|\mathcal{M}_{4,1}^X(3_Q, 4_{\bar{Q}}, \hat{2}_{\bar{q}}, \hat{1}_q)|_{\text{NLO}}^2 = 2\text{Re} \left(\mathcal{M}_{4,1}^X(3_Q, 4_{\bar{Q}}, \hat{2}_{\bar{q}}, \hat{1}_q) \mathcal{M}_4^0(3_Q, 4_{\bar{Q}}, \hat{2}_{\bar{q}}, \hat{1}_q)^\dagger \right). \quad (2.23)$$

Interestingly, the partial amplitude $\mathcal{M}_{4,2}^1(3_Q, \hat{1}_g, \hat{2}_g, 4_{\bar{Q}})$ present in eq. (2.20) vanishes when interfered with the tree-level amplitude of eq. (2.4) and it drops out of $d\hat{\sigma}_{q\bar{q},\text{NLO}}^{\text{V}}$. These virtual contributions have been computed in [47–49]. Our expressions are in full agreement with those known results.

The matrix elements in eq. (2.22) contain ultraviolet as well as infrared divergences. While the infrared divergences cancel when added to the integrated subtraction terms and mass factorisation terms, the UV poles are removed by renormalisation. For all loop amplitudes throughout this paper we shall follow the renormalisation scheme described in [8, 9], in which the heavy quark mass and wave function are renormalised on shell, while the strong coupling constant is renormalised in the $\overline{\text{MS}}$ scheme. In the particular case of the amplitude for the process $q\bar{q} \rightarrow Q\bar{Q}$ no mass renormalisation is needed since the corresponding tree-level process does not contain any internal massive propagators. With this simplification, the amplitude is renormalised as

$$M_{\text{ren}}^{(1)} = M_{\text{bare}}^{(1)} + \left(\delta Z_{WF,Q}^{(1)} + 2\delta Z_{\alpha_s}^{(1)} \right) M_{\text{bare}}^{(0)}, \quad (2.24)$$

where the subscripts (bare) and (ren) stand for bare and renormalised respectively, and the renormalisation constants are given by

$$\delta Z_{\alpha_s}^{(1)} = \bar{C}(\epsilon) \left(-\frac{\beta_0}{\epsilon} \right) \tag{2.25}$$

$$\delta Z_{WF,Q}^{(1)} = \delta Z_{m_Q}^{(1)} = (4\pi)^\epsilon \Gamma(1 + \epsilon) \left(\frac{\mu^2}{m_Q^2} \right)^\epsilon C_F \left(-\frac{3}{2\epsilon} - \frac{2}{1 - 2\epsilon} \right) \tag{2.26}$$

with

$$\beta_0 = \frac{11}{6} C_A - \frac{1}{3} (N_h + N_l). \tag{2.27}$$

C_A and C_F are the $SU(N_c)$ Casimir operators, given by $C_A = N_c$, and $C_F = (N_c^2 - 1) / 2N_c$.

The explicit infrared pole structure of the UV-renormalised virtual contributions $d\hat{\sigma}_{q\bar{q},\text{NLO}}^V$ can be casted in terms of massless and massive colour-ordered infrared singularity operators $\mathbf{I}_{ij}^{(1)}$ as,

$$\begin{aligned} \text{Poles} (d\hat{\sigma}_{q\bar{q},\text{NLO}}^V) &= \mathcal{N}_{\text{NLO}}^{V,q\bar{q}} d\Phi_2(p_3, p_4; p_1, p_2) |\mathcal{M}_4^0(3_Q, 4_{\bar{Q}}, \hat{2}_{\bar{q}}, \hat{1}_q)|^2 \\ &\times \left[N_c \left(2\mathbf{I}_{Q\bar{q}}^{(1)}(\epsilon, s_{13}) + 2\mathbf{I}_{Q\bar{q}}^{(1)}(\epsilon, s_{24}) \right) + \frac{1}{N_c} \left(4\mathbf{I}_{Q\bar{q}}^{(1)}(\epsilon, s_{23}) + 4\mathbf{I}_{Q\bar{q}}^{(1)}(\epsilon, s_{14}) \right) \right. \\ &\left. - 4\mathbf{I}_{Q\bar{q}}^{(1)}(\epsilon, s_{13}) - 4\mathbf{I}_{Q\bar{q}}^{(1)}(\epsilon, s_{24}) - 2\mathbf{I}_{Q\bar{Q}}^{(1)}(\epsilon, s_{34}) - 2\mathbf{I}_{q\bar{q}}^{(1)}(\epsilon, s_{12}, 0) \right] J_2^{(2)}(p_3, p_4). \end{aligned} \tag{2.28}$$

As can be seen in the equation above, after UV renormalisation, the remaining infrared poles of the virtual contributions are proportional to the colour factors N_c and $1/N_c$. The absence of infrared poles in the closed-fermion-loop contributions, that is, the contributions proportional to N_l and N_h , is expected, since the real radiation contributions in eq. (2.11) have no terms proportional to N_l or N_h .

We have cross checked eq. (2.28) against the known universal pole structure of QCD amplitudes with massive fermions [50], and found complete agreement.

2.3.3 The mass factorisation counter term at NLO

The general form of the NLO mass factorisation counter term is related to the leading order cross section through

$$d\hat{\sigma}_{ij,\text{NLO}}^{\text{MF}}(p_1, p_2) = - \int \frac{dx_1}{x_1} \frac{dx_2}{x_2} \mathbf{\Gamma}_{ij;kl}^{(1)}(x_1, x_2) d\hat{\sigma}_{kl,\text{LO}}(x_1 p_1, x_2 p_2), \tag{2.29}$$

with the kernel $\mathbf{\Gamma}_{ij;kl}^{(1)}$ defined as

$$\mathbf{\Gamma}_{ij;kl}^{(1)}(x_1, x_2) = \delta(1 - x_2) \delta_{lj} \mathbf{\Gamma}_{ki}^{(1)}(x_1) + \delta(1 - x_1) \delta_{ki} \mathbf{\Gamma}_{lj}^{(1)}(x_2), \tag{2.30}$$

and $\mathbf{\Gamma}_{ab}^{(1)}(z)$ are Altarelli-Parisi kernels [51].

Applying this expression to the $q\bar{q}$ initiated channel we find

$$\begin{aligned} d\hat{\sigma}_{q\bar{q},\text{NLO}}^{\text{MF}}(p_1, p_2) &= -\mathcal{N}_{\text{NLO}}^{V,q\bar{q}} \left(\frac{N_c^2 - 1}{2N_c} \right) \int \frac{dx_1}{x_1} \frac{dx_2}{x_2} d\Phi_2(p_3, p_4; x_1 p_1, x_2 p_2) \\ &\times \left(\mathbf{\Gamma}_{qq}^{(1)}(x_1) \delta(1 - x_2) + \mathbf{\Gamma}_{qq}^{(1)}(x_2) \delta(1 - x_1) \right) |\mathcal{M}_4^0(3_Q, 4_{\bar{Q}}, \hat{2}_{\bar{q}}, \hat{1}_q)|^2 J_2^{(2)}(p_3, p_4), \end{aligned} \tag{2.31}$$

where $\hat{1}_q$ and $\hat{2}_{\bar{q}}$ have momenta $x_1 p_1$ and $x_2 p_2$ respectively and $\Gamma_{q\bar{q}}^{(1)}(x)$ was given in eq. (2.16).

Combining eqs. (2.18), (2.28) and (2.31), it is straightforward to see that

$$Poles \left(d\hat{\sigma}_{q\bar{q},\text{NLO}}^V + \int_1 d\hat{\sigma}_{q\bar{q},\text{NLO}}^S + d\hat{\sigma}_{q\bar{q},\text{NLO}}^{\text{MF}} \right) = 0. \tag{2.32}$$

3 The massive initial-final antenna $A_4^0(1_Q, 3_g, 4_g, \hat{2}_q)$

Within the antenna formalism [22], the singular limits of the double real contributions that occur when a pair of colour-connected partons become simultaneously unresolved are captured by tree-level four-parton antenna functions. In general, these four-parton antenna functions are denoted as $X_4^0(i, j, k, l)$, and depend on the parton momenta p_i, p_j, p_k, p_l and the masses of the hard radiators m_i and m_l in the massive case. They are obtained from ratios of colour-ordered matrix elements squared as

$$X_4^0(i, j, k, l) = S_{ijkl,IL} \frac{|\mathcal{M}_4^0(i, j, k, l)|^2}{|\mathcal{M}_2^0(I, L)|^2}, \tag{3.1}$$

where $S_{ijkl,IL}$ denotes a symmetry factor associated with the antenna which accounts both for potential identical particle symmetries and for the presence of more than one antenna in the basic two-parton process. This factor is fixed by demanding that the antennae collapse exactly into the unresolved factors appropriate to each unresolved limit. The flavours of the partons I and L in the two-parton matrix element are determined by the flavour of the two particles that the matrix elements $\mathcal{M}_4^0(i, j, k, l)$ collapses onto when j and k become unresolved. According to the species of partons I and L , antennae can be classified as quark-antiquark, quark-gluon, and gluon-gluon antennae, and depending on whether the hard radiators i and l are in the initial or in the final state, we distinguish between final-final (f-f), initial-final (i-f) and initial-initial (i-i) antennae.

In the context of this paper, one new massive tree-level four-parton antenna is needed to capture the double unresolved behaviour of the real matrix elements squared associated to the partonic channel $q\bar{q} \rightarrow t\bar{t}g$ in the leading colour component. It is an A-type initial-final flavour-violating antenna which is denoted as $A_4^0(1_Q, 3_g, 4_g, \hat{2}_q)$. It is evaluated from the flavour violating tree-level process $\gamma^* q \rightarrow Qgg$ through the ratio

$$\frac{|\mathcal{M}_4^0(1_Q, 3_g, 4_g, \hat{2}_q)|^2}{|\mathcal{M}_2^0(\widetilde{(134)}_Q, \hat{2}_q)|^2}. \tag{3.2}$$

The full expression of this antenna is rather lengthy and it will be left for appendix C. In the remaining part of this section, we shall present the single and double unresolved limits of this antenna $A_4^0(1_Q, 3_g, 4_g, \hat{2}_q)$. We will start by presenting the double unresolved factors related to its double unresolved limits. The single unresolved factors are well known and are collected in appendix A for completeness. The integrated form of $A_4^0(1_Q, 3_g, 4_g, \hat{2}_q)$ is presently unknown, it will be obtained by integrating the antenna over the appropriate initial-final antenna phase space, using the techniques developed in [44]. This integrated form will be part of $d\hat{\sigma}_{\text{NNLO}}^U$ given in eq. (1.5) which will be derived elsewhere.

3.1 Universal double unresolved factors

When a pair of massless particles becomes simultaneously unresolved, colour-ordered amplitudes squared factorise into a product of a double unresolved factor and a reduced matrix element with two particles less. The form of the double unresolved factor depends crucially on the colour-connection of the unresolved particles: when these are colour-connected a genuine double unresolved factor is obtained, whereas when they are colour-unconnected a product of two single unresolved factors is obtained. In the following we shall present the genuine colour-connected double unresolved factors that we encounter in the unresolved limits of the double real matrix elements squared associated with the partonic process $q\bar{q} \rightarrow t\bar{t}gg$. These are a massless triple collinear factor corresponding to the triple collinear limit of both final state gluons and one of the initial state fermions, a massive double soft factor, and a massive soft-collinear factor.

3.1.1 Double soft factor of two colour-connected gluons

When two colour-connected gluons j and k become soft between their neighbours i and l an m -particle colour-ordered matrix element factorises as

$$\mathcal{M}_m^0(\dots, i, j, k, l, \dots) \xrightarrow{p_j, p_k \rightarrow 0} \epsilon^{\mu_1}(p_j, \lambda_1) \epsilon^{\mu_2}(p_k, \lambda_2) J_{\mu_1 \mu_2}(p_i, p_j, p_k, p_l) \mathcal{M}_{m-2}^0(\dots, i, l, \dots), \quad (3.3)$$

with the double soft current given by [52]

$$\begin{aligned} J^{\mu_1 \mu_2}(p_i, p_j, p_k, p_l) = & \frac{1}{2} \left[\frac{g^{\mu_1 \mu_2}}{p_j \cdot p_k} \left(1 - \frac{p_i \cdot p_j}{p_i \cdot (p_j + p_k)} - \frac{p_k \cdot p_l}{p_l \cdot (p_j + p_k)} \right) - \frac{p_i^{\mu_1} p_l^{\mu_2}}{(p_i \cdot p_j)(p_k \cdot p_l)} \right. \\ & + \frac{p_i^{\mu_1} p_i^{\mu_2}}{(p_i \cdot p_j)(p_i \cdot (p_j + p_k))} + \frac{p_l^{\mu_1} p_l^{\mu_2}}{(p_k \cdot p_l)(p_l \cdot (p_j + p_k))} + \frac{p_i^{\mu_1} p_j^{\mu_2}}{(p_j \cdot p_k)(p_i \cdot (p_j + p_k))} \\ & \left. + \frac{p_k^{\mu_1} p_l^{\mu_2}}{(p_j \cdot p_k)(p_l \cdot (p_j + p_k))} - \frac{p_i^{\mu_2} p_k^{\mu_1}}{(p_j \cdot p_k)(p_i \cdot (p_j + p_k))} - \frac{p_j^{\mu_2} p_k^{\mu_1}}{(p_j \cdot p_l)(p_l \cdot (p_j + p_k))} \right]. \end{aligned} \quad (3.4)$$

Squaring eq. (3.3) and summing over the polarisations of the soft gluons we find

$$|\mathcal{M}_m^0(\dots, i, j, k, l, \dots)|^2 \xrightarrow{p_j, p_k \rightarrow 0} \mathcal{S}_{ijkl}(m_i, m_l) |\mathcal{M}_{m-2}^0(\dots, i, l, \dots)|^2, \quad (3.5)$$

with the massive double soft eikonal factor

$$\begin{aligned} \mathcal{S}_{ijkl}(m_i, m_l) = & \frac{2s_{il}^2}{s_{ij}s_{kl}(s_{ij} + s_{ik})(s_{jl} + s_{kl})} + \frac{2s_{il}}{s_{jk}} \left[\frac{1}{s_{ij}s_{kl}} + \frac{1}{s_{ij}(s_{jl} + s_{kl})} \right. \\ & \left. + \frac{1}{s_{kl}(s_{ij} + s_{ik})} - \frac{4}{(s_{ij} + s_{ik})(s_{jl} + s_{kl})} \right] + \frac{2(1 - \epsilon)}{s_{jk}^2} \left(1 - \frac{s_{ij}}{s_{ij} + s_{ik}} - \frac{s_{kl}}{s_{jl} + s_{kl}} \right)^2 \\ & - \frac{4m_i^2}{s_{ij}s_{jk}(s_{ij} + s_{ik})} \left(\frac{s_{ik}}{s_{ij} + s_{ik}} + \frac{s_{il}s_{jk}}{s_{ij}s_{kl}} + \frac{s_{jl}}{s_{kl}} - \frac{s_{jl}}{s_{jl} + s_{kl}} \right) + \frac{4m_i^4}{s_{ij}^2(s_{ij} + s_{ik})^2} \\ & - \frac{4m_l^2}{s_{jk}s_{kl}(s_{jl} + s_{kl})} \left(\frac{s_{jl}}{s_{jl} + s_{kl}} + \frac{s_{il}s_{jk}}{s_{ij}s_{kl}} + \frac{s_{ik}}{s_{ij}} - \frac{s_{ik}}{s_{ij} + s_{ik}} \right) + \frac{4m_l^4}{s_{kl}^2(s_{jl} + s_{kl})^2} \\ & + \frac{4m_i^2 m_l^2}{s_{ij}^2 s_{kl}^2}. \end{aligned} \quad (3.6)$$

This result converges to the massless colour-ordered double soft factor of [53] in the limit where $m_i, m_l \rightarrow 0$.

3.1.2 Soft-collinear factor in the colour-connected configuration

Soft-collinear singularities occur in those regions of phase space in which a gluon becomes soft and two other massless partons become simultaneously collinear. The factorisation of colour-ordered matrix elements in these limits is different depending on the colour connection of the unresolved particles. When the soft gluon j is colour connected to the collinear particles k and l , the soft-collinear factorisation is given by

$$|\mathcal{M}_m^0(\dots, i, j, k, l, \dots)|^2 \xrightarrow{p_k \parallel p_l, p_j \rightarrow 0} \frac{1}{s_{kl}} P_{kl \rightarrow m}(z) S_{c_{i,jkl}}(m_i) |\mathcal{M}_{m-2}^0(\dots, i, m, \dots)|^2, \quad (3.7)$$

where $P_{kl \rightarrow m}(z)$ is one of the single collinear splitting functions in eqs. (A.2)–(A.4). If either parton k or l are in the initial state, $P_{kl \rightarrow m}(z)$ will be an initial-final Altarelli-Parisi splitting function.

In the final-final case, the soft-collinear factor $S_{c_{i,jkl}}(m_i)$ reads

$$S_{c_{i,jkl}}(m_i) = \frac{2(s_{ik} + s_{il})}{s_{ij}(s_{jk} + s_{jl})} - \frac{2m_i^2}{s_{ij}^2}, \quad (3.8)$$

whereas in initial-final configurations they are

$$S_{c_{i,jkl}}(m_i) = \mathcal{S}_{ijl}(m_i, 0) \quad S_{c_{i,jkl}}(m_i) = \mathcal{S}_{ijk}(m_i, 0), \quad (3.9)$$

with $\mathcal{S}_{ijk}(m_i, 0)$ being the single massive soft factor given in eq. (A.10).

3.1.3 Triple collinear factor

In those regions of phase space where three colour-connected massless partons (i, j, l) become collinear, a generic colour-ordered amplitude squared denoted by $|\mathcal{M}_n^0(\dots, i, j, k, \dots)|^2$ factorises as

$$|\mathcal{M}_m^0(\dots, i, j, k, \dots)|^2 \xrightarrow{p_i \parallel p_j \parallel p_k \rightarrow 0} P_{ijk \rightarrow l} |\mathcal{M}_{m-2}^0(\dots, l, \dots)|^2, \quad (3.10)$$

where the three colour-connected final state particles (i, j, k) cluster to form a single parent particle l . The limit is approached in phase space when

$$p_i \rightarrow z_1 p_l \quad p_j \rightarrow z_2 p_l \quad p_k \rightarrow z_3 p_l \quad (3.11)$$

with

$$z_1 + z_2 + z_3 = 1 \quad \text{and} \quad p_l^2 \rightarrow 0. \quad (3.12)$$

The triple collinear splitting functions generally depend on the momentum fractions z_1, z_2 and z_3 , as well as on the invariants s_{ij}, s_{jk}, s_{ik} . The explicit functional form of $P_{ijk \rightarrow l}$ varies according to the flavours of the three collinear particles as well as on their colour connection. There are two triple collinear splitting functions involving a fermion and two gluons, each of which applies to different colour orderings. In this paper we will need the

one corresponding to a colour-ordering of the form $\dots;;i_q, j_g, k_g, \dots$, in which case the splitting function is

$$\begin{aligned}
 P_{q_i g_j g_k \rightarrow q_l}(z_1, z_2, z_3, s_{ij}, s_{ik}, s_{jk}) = & \\
 & \frac{1}{s_{ij}s_{jk}} \left[(1-\epsilon) \left(\frac{1+z_1^2}{z_3} + \frac{1+(1-z_3)^2}{(1-z_1)} \right) + 2\epsilon \left(\frac{z_1}{z_3} + \frac{1-z_3}{1-z_1} \right) \right] \\
 & + \frac{1}{s_{ij}s_{ijk}} \left[(1-\epsilon) \left(\frac{(1-z_3)^3 + z_1(1-z_2) - 2z_3}{z_3(1-z_1)} \right) - \epsilon \left(\frac{2(1-z_3)(z_3-z_1) - z_2}{z_3(1-z_1)} - \epsilon^2 z_2 \right) \right] \\
 & + \frac{1}{s_{jk}s_{ijk}} \left[(1-\epsilon) \left(\frac{(1-z_3)^2(2-z_3) + z_2^3 + 2z_2 z_1 - 2 - z_3}{z_3(1-z_1)} \right) + 2\epsilon \frac{(z_2 z_1 - z_3 - 2z_3 z_1)}{z_3(1-z_1)} \right] \\
 & + (1-\epsilon) \left[\frac{2(z_2 s_{ijk} - (1-z_1)s_{ij})^2}{s_{jk}^2 s_{ijk}^2 (1-z_1)^2} + \frac{1}{s_{ijk}^2} \left(4 \frac{s_{ij}}{s_{jk}} + (1-\epsilon) \frac{s_{jk}}{s_{ij}} + (3-\epsilon) \right) \right]. \quad (3.13)
 \end{aligned}$$

This triple collinear splitting function corresponds to a configuration in which the three collinear particles are in the final state. However, in the double real corrections for top pair production, only collinear limits of an initial state parton and two final state particles are relevant, given the fact that the tree-level matrix elements contain only two massless final state particles. The initial-final triple collinear splitting functions can always be obtained from their final-final counterparts. For example, the splitting function for the clustering $(\hat{i}, j, k) \rightarrow \hat{l}$ can be related to the final-final case $(i, j, k) \rightarrow l$ as [54]

$$\begin{aligned}
 P_{\hat{i}jk \rightarrow \hat{l}}(z_1, z_2, z_3, s_{ij}, s_{ik}, s_{jk}) = & \\
 & (-1)^\Delta P_{ijk \rightarrow l} \left(\frac{1}{1-z_2-z_3}, -\frac{z_2}{1-z_2-z_3}, -\frac{z_3}{1-z_2-z_3}, -s_{ij}, -s_{ik}, s_{jk} \right), \quad (3.14)
 \end{aligned}$$

where $\Delta = 0$ if the number of incoming fermions is the same before and after the crossing, and $\Delta = 1$ otherwise.

3.2 Infrared limits of $A_4^0(1_Q, 3_g, 4_g, \hat{2}_q)$

The four-parton tree-level initial-final massive flavour-violating A-type antenna function denoted by $A_4^0(1_Q, 3_g, 4_g, \hat{2}_q)$ has the following single and double unresolved limits

$$A_4^0(1_Q, 3_g, 4_g, \hat{2}_q) \xrightarrow{3_g, 4_g \rightarrow 0} \mathcal{S}_{1342}(m_Q, 0) \quad (3.15)$$

$$A_4^0(1_Q, 3_g, 4_g, \hat{2}_q) \xrightarrow{\hat{2}_q \parallel 4_g, 3_g \rightarrow 0} \frac{1}{s_{24}} P_{\hat{q}g \rightarrow \hat{q}}(z) \mathcal{S}_{c_{1;342}}(m_Q) \quad (3.16)$$

$$A_4^0(1_Q, 3_g, 4_g, \hat{2}_q) \xrightarrow{\hat{2}_q \parallel 3_g \parallel 4_g} P_{\hat{q}gg \rightarrow \hat{q}}(z_1, z_2, z_3, s_{23}, s_{24}, s_{34}) \quad (3.17)$$

$$A_4^0(1_Q, 3_g, 4_g, \hat{2}_q) \xrightarrow{3_g \rightarrow 0} \mathcal{S}_{134}(m_Q, 0) A_3^0(1_Q, 4_g, \hat{2}_q) \quad (3.18)$$

$$A_4^0(1_Q, 3_g, 4_g, \hat{2}_q) \xrightarrow{4_g \rightarrow 0} \mathcal{S}_{342}(0, 0) A_3^0(1_Q, 3_g, \hat{2}_q) \quad (3.19)$$

$$A_4^0(1_Q, 3_g, 4_g, \hat{2}_q) \xrightarrow{\hat{2}_q \parallel 4_g} \frac{1}{s_{24}} P_{\hat{q}g \rightarrow \hat{q}}(z) A_3^0(1_Q, 3_g, (\hat{2}\hat{4})_q) \quad (3.20)$$

$$A_4^0(1_Q, 3_g, 4_g, \hat{2}_q) \xrightarrow{3_g \parallel 4_g} \frac{1}{s_{34}} P_{gg \rightarrow g}(z) A_3^0(1_Q, (\tilde{3}\hat{4})_g, \hat{2}_q) + (\text{ang.}). \quad (3.21)$$

In this last equation (ang.), stands for angular dependent terms. Those terms arise when a gluon splitting is involved in a collinear limit. In this case, the unresolved single collinear factor is not a spin-averaged Altarelli-Parisi splitting function as given in appendix A but it also involves spin-dependent terms [4].

4 The massive initial-final antenna $A_3^1(1_Q, 3_g, \hat{2}_q)$

The construction of a subtraction term for the real-virtual corrections to $t\bar{t}$ production in the $q\bar{q}$ channel in the leading-colour approximation requires a new initial-final massive one-loop antenna function which we will present in this section.

4.1 One-loop antenna functions

Within the antenna formalism, the infrared limits of the real-virtual contributions are captured by three-parton one-loop antennae [22, 31]. These are generally denoted as $X_3^1(i, j, k)$ and they depend on the antenna momenta p_i, p_j, p_k as well as on the masses of the hard radiators in the massive case. In general, these one-loop antenna functions are constructed out of colour-ordered three-parton and two-parton matrix elements as

$$X_3^1(i, j, k) = S_{ijk, IK} \frac{|\mathcal{M}_3^1(i, j, k)|_{\text{NLO}}^2}{|\mathcal{M}_2^0(I, K)|^2} - X_3^0(i, j, k) \frac{|\mathcal{M}_2^1(I, K)|^2}{|\mathcal{M}_2^0(IK)|^2}, \quad (4.1)$$

where the tree-level antenna function, denoted by $X_3^0(i, j, k)$, is given by

$$X_3^0(i, j, k) = S_{ijk, IK} \frac{|\mathcal{M}_{ijk}^0|^2}{|\mathcal{M}_{IK}^0|^2}. \quad (4.2)$$

$S_{ijk, IK}$ denotes the symmetry factor associated with the antenna, which accounts both for potential identical particle symmetries and for the presence of more than one antenna in the basic two-parton process. Initial-final and initial-initial antennae can be obtained from their final-final counterparts by the appropriate crossing of partons to the initial-state. This procedure is straightforward at tree-level but requires some care in the one-loop case, since antennae contain polylogarithms or hypergeometric functions that must be analytically continued to the appropriate kinematical region [37, 38].

In any of the three kinematical configurations, the antenna functions can be conveniently decomposed according to their colour factors as follows:¹

$$X_3^1(i, j, k) = N_c X_3^{1,lc}(i, j, k) + N_l X_3^{1,l}(i, j, k) + N_h X_3^{1,h}(i, j, k) - \frac{1}{N_c} X_3^{1,slc}(i, j, k). \quad (4.3)$$

In general the sub-antennae have ultraviolet and infrared divergences of explicit and implicit nature. In order to remove the ultraviolet poles, we renormalise the amplitudes in eq. (4.1)

¹In [22], the leading colour contribution was denoted by $X_3^1(i, j, k)$, the subleading colour part by $\tilde{X}_3^1(i, j, k)$, and the N_F part was denoted by $\hat{X}_3^1(i, j, k)$. We shall not use this notation here but instead follow that of eq. (4.3), which we find more transparent.

following the scheme of [8, 9], with the renormalisation constants given in eq. (2.25). We find that the renormalisation prescription of the different sub-antennae is

$$X_3^{1,lc}(i, j, k) = X_{3,b}^{1,lc}(i, j, k) - \mu^{-2\epsilon} \bar{C}(\epsilon) \frac{b_0}{\epsilon} X_3^0(i, j, k) - m_Q^{-2\epsilon} (4\pi)^\epsilon \Gamma(1 + \epsilon) \left(\frac{3}{2\epsilon} + \frac{2}{1 - 2\epsilon} \right) X_{3,1M}^0(i, j, k) \quad (4.4)$$

$$X_3^{1,N_l}(i, j, k) = X_{3,b}^{1,N_l}(i, j, k) - \mu^{-2\epsilon} \bar{C}(\epsilon) \frac{b_{0,F}}{\epsilon} X_3^0(i, j, k) \quad (4.5)$$

$$X_3^{1,N_h}(i, j, k) = X_{3,b}^{1,N_h}(i, j, k) - \mu^{-2\epsilon} \bar{C}(\epsilon) \frac{b_{0,F}}{\epsilon} X_3^0(i, j, k) \quad (4.6)$$

$$X_3^{1,slc}(i, j, k) = X_{3,b}^{1,slc}(i, j, k) + m_Q^{-2\epsilon} (4\pi)^\epsilon \Gamma(1 + \epsilon) \left(\frac{3}{2\epsilon} + \frac{2}{1 - 2\epsilon} \right) X_{3,1M}^0(i, j, k), \quad (4.7)$$

where $b_0 = 11/6$ and $b_{0,F} = -1/3$ are the colour-ordered components of the QCD beta function. We have also defined

$$X_{3,1M}^0(i, j, k) = S_{ijk,IK} \frac{\text{Re} \left(\mathcal{M}_{3,1M}^0(i, j, k) (\mathcal{M}_3^0(i, j, k))^\dagger \right)}{|\mathcal{M}_2^0(I, K)|^2}, \quad (4.8)$$

where $\mathcal{M}_{3,1M}^0(i, j, k)$ is the tree-level amplitude with a mass insertion in the massive propagators. Interestingly, the wave function renormalisation counter terms coming from $\mathcal{M}_3^1(i, j, k)$ cancel against those coming from $\mathcal{M}_2^1(I, K)$, in such a way that the antenna function itself does not require wave function renormalisation.

The antennae that we employ in the real-virtual subtraction terms are renormalised at $\mu^2 = |s_{ijk}|$. To ensure that the matrix elements in the real-virtual contributions and the antennae are renormalised at the same scale, we must substitute

$$X_{ijk}^{1,lc} \rightarrow X_{ijk}^{1,lc} + \frac{b_0}{\epsilon} X_{ijk}^0 \left((|s_{ijk}|)^{-\epsilon} - (\mu^2)^{-\epsilon} \right) \quad (4.9)$$

$$X_{ijk}^{1,N_l} \rightarrow X_{ijk}^{1,N_l} + \frac{b_{0,F}}{\epsilon} X_{ijk}^0 \left((|s_{ijk}|)^{-\epsilon} - (\mu^2)^{-\epsilon} \right) \quad (4.10)$$

$$X_{ijk}^{1,N_h} \rightarrow X_{ijk}^{1,N_h} + \frac{b_{0,F}}{\epsilon} X_{ijk}^0 \left((|s_{ijk}|)^{-\epsilon} - (\mu^2)^{-\epsilon} \right) \quad (4.11)$$

$$X_{ijk}^{1,slc} \rightarrow X_{ijk}^{1,slc}. \quad (4.12)$$

After UV renormalisation, one-loop antennae still have explicit and implicit infrared divergences. The structure of the former can be entirely captured by colour-ordered infrared singularity operators; the latter occur when massless partons in the antenna become soft or collinear.

4.2 Single unresolved factors at one-loop

The factorisation properties of colour-ordered amplitudes in their soft and collinear limits has been extensively studied in [7, 55–66]. Like at tree-level, the interference of a one-loop amplitude with its tree-level counterpart yields soft eikonal factors and collinear splitting functions in its soft and collinear limits respectively. Those singular factors are also found in the unresolved limits of antennae.

In general, when a gluon becomes soft or a pair of massless partons become collinear, the interference of a one-loop and a tree-level colour-ordered amplitude factorises as

$$|\mathcal{M}_m^1|_{\text{NLO}}^2 \rightarrow \text{Sing}_1^{(0)} |\mathcal{M}_{m-1}^1|_{\text{NLO}}^2 + \text{Sing}_1^{(1)} |\mathcal{M}_{m-1}^0|^2, \quad (4.13)$$

where $\text{Sing}_1^{(1)}$ is a single unresolved factor and $|\mathcal{M}_{m-1}^1|_{\text{NLO}}^2$ is the interference of a reduced one-loop sub-amplitude and its tree-level counterpart. Following the decomposition of the colour-ordered amplitudes into primitives, the unresolved factors can be decomposed as

$$\text{Sing}_1^{(1)} = N_c \text{Sing}_1^{(1),[lc]} + N_l \text{Sing}_1^{(1),[l]} + N_h \text{Sing}_1^{(1),[h]} - \frac{1}{N_c} \text{Sing}_1^{(1),[slc]}. \quad (4.14)$$

In the following we shall present the explicit form of the singular factors that must be considered in the construction of subtraction terms for the leading-colour real-virtual corrections to top pair production in the $q\bar{q}$ channel.

4.2.1 Collinear splitting functions

For the partonic process that we are presently considering, i.e. $q\bar{q} \rightarrow t\bar{t}g$, the splitting function that occurs when the final-state gluon becomes collinear to either of the incoming fermions is $P_{qg \leftarrow Q}^1(z)$. In the leading-colour approximation, only the N_c part of this splitting function is needed, and it is given by

$$P_{\hat{q}g \rightarrow \hat{q}}^{(1),[lc]}(z) = \left[-\frac{b_0}{\epsilon} - \frac{c_\Gamma}{\bar{C}(\epsilon)} \left(\frac{s_{qg}}{\mu^2} \right)^{-\epsilon} \left(\frac{\Gamma(1-\epsilon)}{\epsilon^2} \left(\frac{z}{(1+\epsilon)\Gamma(-\epsilon)} {}_2F_1(1, 1+\epsilon, 2+\epsilon; z) \right. \right. \right. \\ \left. \left. \left. + (-z)^{-\epsilon} \Gamma(1+\epsilon) \right) - \frac{\epsilon}{2} \right] P_{\hat{q}g \rightarrow \hat{q}}(z) - \frac{c_\Gamma}{\bar{C}(\epsilon)} \left(\frac{s_{qg}}{\mu^2} \right)^{-\epsilon} \left(\frac{2\epsilon + z - z^2(1-\epsilon^2)}{z(1-z)} \right). \quad (4.15)$$

In this equation, z is the momentum fraction carried by the gluon and $P_{\hat{q}g \rightarrow \hat{q}}(z)$ is the tree-level splitting function whose expression is

$$P_{\hat{q}g \rightarrow \hat{q}}(z) = \frac{1 + (1-z)^2 - \epsilon z^2}{z(1-z)}. \quad (4.16)$$

4.2.2 Massive soft factors

As it occurs at tree-level, when a soft gluon is emitted between massive fermions in the colour chain, the soft factor contains mass dependent terms. While at tree-level the massless soft factor can be obtained from the massive one by setting the masses of the hard radiators to zero, this is no longer the case at the one-loop level: masses are present in the arguments of logarithms that diverge in the massless limit. We must therefore consider separately the soft factors with: (a) two massless hard radiators, (b) one massless and one massive hard radiator, (c) two massive hard radiators. When treating the real-virtual corrections to top pair hadro-production within the leading-colour approximation, only case (b) must be considered. Furthermore, only the N_c part of the soft currents and eikonal factors are needed.

When a gluon j becomes soft in a primitive amplitude where it is colour-connected to the hard particles i and k , the amplitude factorises as

$$\mathcal{M}_m^{1,[X]}(\dots, i, j, k, \dots) \xrightarrow{p_j \rightarrow 0} \epsilon^\mu(p_j, \lambda) J_\mu(p_i, p_j, p_k) \mathcal{M}_{m-1}^{1,[X]}(\dots, i, k, \dots) + \epsilon^\mu(p_j, \lambda) J_\mu^{(1),[X]}(p_i, p_j, p_k; m_i, m_k) \mathcal{M}_{m-1}^0(\dots, i, k, \dots), \quad (4.17)$$

where $X = lc, l, h, slc$, and the tree-level current $J_\mu(p_i, p_j, p_k)$ is given by

$$J_\mu(p_i, p_j, p_k) = \frac{p_i^\mu}{\sqrt{2} p_i \cdot p_j} - \frac{p_k^\mu}{\sqrt{2} p_j \cdot p_k}. \quad (4.18)$$

The primitive currents $J_\mu^{(1),[X]}(p_i, p_j, p_k; m_i, m_k)$ take a different form depending on whether m_i and/or m_k vanish. These massive soft currents were derived in [7] as tensors in colour space that describe the soft factorisation of full amplitudes rather than of colour-ordered sub-amplitudes. The renormalised colour-ordered currents can be obtained from their results. In the case of one vanishing mass, the leading-colour current that we are presently interested in, reads

$$J_\mu^{(1),[lc]}(p_i, p_j, p_k; m_i, 0) = -\frac{1}{2} \left\{ \frac{b_0}{\epsilon} + \left(\frac{\mu^2 s_{ik}}{s_{ij} s_{jk}} \right)^{-\epsilon} \left[\frac{1}{2\epsilon^2} + \frac{i\pi}{2\epsilon} - \frac{5\pi^2}{12} + \frac{m_i^2 s_{jk}}{2(s_{ij} s_{ik} - m_i^2 s_{jk})} \left(2i\pi \ln \left(\frac{m_i^2 s_{jk}}{s_{ij} s_{ik}} \right) + \ln^2 \left(\frac{m_i^2 s_{jk}}{s_{ij} s_{ik}} \right) \right) + \mathcal{O}(\epsilon) \right] \right\} J_\mu(p_i, p_j, p_k). \quad (4.19)$$

From the one-loop and tree-level soft currents, massive soft eikonal factors are obtained as

$$S_{ijk}^{(1),[X]}(m_i, m_k) = -2 g^{\mu\nu} \text{Re} \left(J_\mu^{(1),[X]}(p_i, p_j, p_k; m_i, m_k) J_\nu(p_i, p_j, p_k) \right). \quad (4.20)$$

We find

$$S_{ijk}^{(1),[lc]}(m_i, 0) = - \left\{ \frac{b_0}{\epsilon} + \left(\frac{\mu^2 s_{ik}}{s_{ij} s_{jk}} \right)^{-\epsilon} \left[\frac{1}{2\epsilon^2} - \frac{5\pi^2}{12} + \frac{m_i^2 s_{jk}}{2(s_{ij} s_{ik} - m_i^2 s_{jk})} \ln^2 \left(\frac{m_i^2 s_{jk}}{s_{ij} s_{ik}} \right) + \mathcal{O}(\epsilon) \right] \right\} \mathcal{S}_{ijk}(m_i, 0) \quad (4.21)$$

with the massive tree-level eikonal factor $\mathcal{S}_{ijk}(m_i, 0)$ given in appendix A.2.

4.3 Infrared properties of $A_3^{1,lc}(1_Q, 3_g, \hat{2}_q)$

As mentioned above, in the context of this paper, a new massive antenna is needed to subtract the unresolved infrared limits of the real-virtual contributions related to the partonic process $q\bar{q} \rightarrow t\bar{t}g$. It is a flavour-violating quark-antiquark antenna denoted by $A_3^1(1_Q, 3_g, \hat{2}_q)$, which we compute directly in the initial-final kinematics following the definition of eq. (4.1). Working in the leading-colour approximation, only the leading-colour part of the antenna $A_3^{1,lc}(1_Q, 3_g, \hat{2}_q)$ needs to be considered. The full expression of this sub-antenna is too lengthy to be presented in this paper, but its pole part can be compactly written in terms of colour-ordered $\mathbf{I}_{ij}^{(1)}$ operators. This pole part will be explicitly needed in section 8 and is given by

$$\text{Poles} \left(A_3^{1,lc}(1_Q, 3_g, \hat{2}_q) \right) = 2 \left(\mathbf{I}_{Qg}^{(1)}(\epsilon, s_{13}) + \mathbf{I}_{qg}^{(1)}(\epsilon, s_{23}) - \mathbf{I}_{Q\bar{q}}^{(1)}(\epsilon, s_{123}) \right) A_3^0(1_Q, 3_g, \hat{2}_q). \quad (4.22)$$

Also the unresolved limits of $A_3^{1,lc}(1_Q, 3_g, \hat{2}_q)$ will be required in section 8 in the context of the construction of our real-virtual subtraction terms. They read

$$A_3^{1,lc}(1_Q, 3_g, \hat{2}_q) \xrightarrow{p_3 \rightarrow 0} S_{132}^{(1),[lc]}(m_Q^2, 0) \quad (4.23)$$

$$A_3^{1,lc}(1_Q, 3_g, \hat{2}_q) \xrightarrow{p_2 \parallel p_3} \frac{1}{s_{23}} P_{\hat{q}g \rightarrow \hat{q}}^{1,[lc]}(z), \quad (4.24)$$

with the soft and collinear factors defined in eqs. (4.21) and (4.15) respectively. The integrated form of $A_3^{1,lc}(1_Q, 3_g, \hat{2}_q)$ is not known at present. It will be part of $d\hat{\sigma}_{\text{NNLO}}^{\text{U}}$ given in eq. (1.5) which will be derived elsewhere.

5 Double real contributions to $q\bar{q} \rightarrow t\bar{t}$ at leading colour

It is the purpose of this section to present the structure of the double real contributions associated to the tree-level process $q\bar{q} \rightarrow t\bar{t}gg$ at leading colour, and to construct the corresponding subtraction terms.

5.1 The double real contribution $d\hat{\sigma}_{q\bar{q},\text{NNLO},N_c^2}^{\text{RR}}$

The colour-decomposition of the tree-level amplitude for the partonic process $q\bar{q} \rightarrow t\bar{t}gg$ reads

$$\begin{aligned} M_6^0(q_1\bar{q}_2 \rightarrow Q_3\bar{Q}_4g_5g_6) = 2g_s^4 \sum_{(i,j) \in P(5,6)} \left[(T^{a_i}T^{a_j})_{i_3i_1} \delta_{i_2i_4} \mathcal{M}_6^0(3_Q, i_g, j_g, \hat{1}_q; ; \hat{2}_{\bar{q}}, 4_{\bar{Q}}) \quad (5.1) \right. \\ + (T^{a_i})_{i_3i_1} (T^{a_j})_{i_2i_4} \mathcal{M}_6^0(3_Q, i_g, \hat{1}_q; ; \hat{2}_{\bar{q}}, j_g, 4_{\bar{Q}}) \\ + \delta_{i_3i_1} (T^{a_i}T^{a_j})_{i_2i_4} \mathcal{M}_6^0(3_Q, \hat{1}_q; ; \hat{2}_{\bar{q}}, i_g, j_g, 4_{\bar{Q}}) \\ - \frac{1}{N_c} (T^{a_i}T^{a_j})_{i_3i_4} \delta_{i_2i_1} \mathcal{M}_6^0(3_Q, i_g, j_g, 4_Q; ; \hat{2}_{\bar{q}}, \hat{1}_q) \\ - \frac{1}{N_c} (T^{a_i})_{i_3i_4} (T^{a_j})_{i_2i_1} \mathcal{M}_6^0(3_Q, i_g, 4_Q; ; \hat{2}_{\bar{q}}, j_g, \hat{1}_q) \\ \left. - \frac{1}{N_c} \delta_{i_3i_4} (T^{a_i}T^{a_j})_{i_2i_1} \mathcal{M}_6^0(3_Q, 4_Q; ; \hat{2}_{\bar{q}}, i_g, j_g, \hat{1}_q) \right]. \end{aligned}$$

Squaring this expression, combining it with all appropriate prefactors, phase space and measurement function, and retaining only the terms multiplied by N_c^2 , we have

$$\begin{aligned} d\hat{\sigma}_{q\bar{q},\text{NNLO},N_c^2}^{\text{RR}} = \frac{1}{2} \mathcal{N}_{\text{NNLO}}^{q\bar{q},\text{RR}} N_c^2 \sum_{(i,j) \in P(5,6)} d\Phi_4(p_3, p_4, p_5, p_6; p_1, p_2) \left[|\mathcal{M}_6^0(3_Q, i_g, j_g, \hat{1}_q; ; \hat{2}_{\bar{q}}, 4_{\bar{Q}})|^2 \right. \\ \left. + |\mathcal{M}_6^0(3_Q, i_g, \hat{1}_q; ; \hat{2}_{\bar{q}}, j_g, 4_{\bar{Q}})|^2 + |\mathcal{M}_6^0(3_Q, \hat{1}_q; ; \hat{2}_{\bar{q}}, i_g, j_g, 4_{\bar{Q}})|^2 \right] J_2^{(4)}(p_3, p_4, p_5, p_6), \quad (5.2) \end{aligned}$$

where the overall factor 1/2 accounts for the identical gluons in the final state. The normalisation factor is

$$\mathcal{N}_{\text{NNLO}}^{q\bar{q},\text{RR}} = \mathcal{N}_{\text{LO}}^{q\bar{q}} \left(\frac{\alpha_s(\mu)}{2\pi} \right)^2 \frac{\bar{C}(\epsilon)}{C(\epsilon)}, \quad (5.3)$$

and $\mathcal{N}_{\text{LO}}^{q\bar{q}}$ has been given in eq. (2.5).

This contribution is singular in several single and double unresolved limits namely

- single soft limits: $p_i \rightarrow 0$ with $i = 5, 6$
- single collinear limits: $p_5 || p_6$, and $p_i || p_j$ with $i = 5, 6, j = 1, 2$
- double soft limit: $p_5, p_6 \rightarrow 0$
- triple collinear limits: $p_i || p_5 || p_6$ with $i = 1, 2$
- soft-collinear limits: $p_5 \rightarrow 0, p_i || p_6$ and $p_6 \rightarrow 0, p_i || p_6$ with $i = 1, 2$
- double collinear limits: $p_i || p_5, p_j || p_6$ with $i, j = 1, 2, i \neq j$.

5.2 The double real subtraction term $d\hat{\sigma}_{q\bar{q},\text{NNLO},N_c^2}^S$

The general structure of the double real subtraction terms obtained within the framework of the antenna formalism has been presented in [22, 42] in the massless case and extended to the massive case in [4, 26]. Without entering into the details of this structure, let us recall that in general, double real antenna subtraction terms, which reproduce the behaviour of the double real contributions in all their single and double unresolved limits, contain five different configurations corresponding to:

- (a) one unresolved parton
- (b) two colour-connected unresolved partons (colour-connected)
- (c) two unresolved partons that are not colour-connected but share a common radiator (almost colour-connected)
- (d) two unresolved partons that are well separated from each other in the colour chain (colour-unconnected)
- (e) compensation terms for the over subtraction of large angle soft emission.

The antenna content of the subtraction terms for each of these configurations is the same for the final-final, initial-final and initial-initial configurations and it is summarised in table 1, which is taken from [31].²

For the evaluation of the NNLO corrections to heavy quark pair production in the $q\bar{q}$ channel, the configurations (c) and (e), which always occur together, are not needed and will not be discussed here either. Only (S, a), (S, b) and (S, d) subtraction terms are needed to approximate the double real contributions of eq. (5.2), such that the total subtraction term is given by

$$d\hat{\sigma}_{q\bar{q},\text{NNLO},N_c^2}^S = d\hat{\sigma}_{q\bar{q},\text{NNLO},N_c^2}^{S,a} + d\hat{\sigma}_{q\bar{q},\text{NNLO},N_c^2}^{S,b} + d\hat{\sigma}_{q\bar{q},\text{NNLO},N_c^2}^{S,d}. \tag{5.4}$$

²As discussed in [4, 29] for example, this content is strictly valid only for leading-colour like double real contributions which involve colour-ordered matrix elements squared. For subleading colour contributions involving interferences of colour-ordered matrix elements, more antenna functions are needed.

The (S, a) type subtraction term, denoted by $d\hat{\sigma}_{q\bar{q},\text{NNLO},N_c^2}^{S,a}$, subtracts the single unresolved limits and it is built with products of a tree-level three-parton antennae and five-parton reduced matrix elements. It is given by,

$$\begin{aligned}
 d\hat{\sigma}_{q\bar{q},\text{NNLO},N_c^2}^{S,a} = & \frac{1}{2} \mathcal{N}_{\text{NNLO}}^{q\bar{q},\text{RR}} N_c^2 \sum_{(i,j) \in P(5,6)} d\Phi_4(p_3, p_4, p_5, p_6; p_1, p_2) \\
 & \times \left[A_3^0(3_Q, i_g, \hat{1}_q) |\mathcal{M}_5^0((\tilde{3}i)_Q, \hat{1}_q; \hat{2}_{\bar{q}}, j_g, 4_{\bar{Q}})|^2 J_2^{(3)}(\widetilde{p_{3i}}, p_4, p_j) \right. \\
 & + A_3^0(4_{\bar{Q}}, j_g, \hat{2}_{\bar{q}}) |\mathcal{M}_5^0(3_Q, i_g, \hat{1}_q; \hat{2}_{\bar{q}}, (\tilde{4}j)_{\bar{Q}})|^2 J_2^{(3)}(p_3, \widetilde{p_{4j}}, p_i) \\
 & + d_3^0(3_Q, i_g, j_g) |\mathcal{M}_5^0((\tilde{3}i)_Q, (\tilde{i}j)_g, \hat{1}_q; \hat{2}_{\bar{q}}, 4_{\bar{Q}})|^2 J_2^{(3)}(\widetilde{p_{3i}}, p_4, \widetilde{p_{ij}}) \\
 & + d_3^0(4_{\bar{Q}}, j_g, i_g) |\mathcal{M}_5^0(3_Q, \hat{1}_q; \hat{2}_{\bar{q}}, (\tilde{j}i)_g, (\tilde{4}j)_{\bar{Q}})|^2 J_2^{(3)}(p_3, \widetilde{p_{4j}}, \widetilde{p_{ji}}) \\
 & + d_3^0(\hat{1}_q, j_g, i_g) |\mathcal{M}_5^0(3_Q, (\tilde{j}i)_g, \hat{1}_q; \hat{2}_{\bar{q}}, 4_{\bar{Q}})|^2 J_2^{(3)}(p_3, p_4, \widetilde{p_{ij}}) \\
 & \left. + d_3^0(\hat{2}_{\bar{q}}, i_g, j_g) |\mathcal{M}_5^0(3_Q, \hat{1}_q; \hat{2}_{\bar{q}}, (\tilde{i}j)_g, 4_{\bar{Q}})|^2 J_2^{(3)}(p_3, p_4, \widetilde{p_{ij}}) \right]. \quad (5.5)
 \end{aligned}$$

All three-parton antennae present in this subtraction term have been derived in unintegrated and in integrated form in [27, 36, 40]. Furthermore, as can be seen from table 1, the integrated form of $d\hat{\sigma}_{q\bar{q},\text{NNLO},N_c^2}^{S,a}$ must be added back at the three-parton level, and it will therefore contribute to the real-virtual counter term $d\hat{\sigma}_{q\bar{q},\text{NNLO},N_c^2}^T$, which will be presented in section 8.

The (S, b) type subtraction term, denoted by $d\hat{\sigma}_{q\bar{q},\text{NNLO},N_c^2}^{S,b}$, takes care of the double unresolved limits of the double real contributions in those subamplitudes in which both final state gluons are colour-connected. It is given by,

$$\begin{aligned}
 d\hat{\sigma}_{q\bar{q},\text{NNLO},N_c^2}^{S,b} = & \frac{1}{2} \mathcal{N}_{\text{NNLO}}^{q\bar{q},\text{RR}} N_c^2 \sum_{(i,j) \in P(5,6)} d\Phi_4(p_3, p_4, p_5, p_6; p_1, p_2) \quad (5.6) \\
 & \times \left[\left(A_4^0(3_Q, i_g, j_g, \hat{1}_q) - d_3^0(3_Q, i_g, j_g) A_3^0((\tilde{3}i)_Q, (\tilde{i}j)_g, \hat{1}_q) \right. \right. \\
 & \left. \left. - d_3^0(\hat{1}_q, j_g, i_g) A_3^0(3_Q, (\tilde{j}i)_g, \hat{1}_q) \right) |\mathcal{M}_4^0((\tilde{3}i\tilde{j})_Q, 4_{\bar{Q}}, \hat{2}_{\bar{q}}, \hat{1}_q)|^2 J_2^{(2)}(\widetilde{p_{3ij}}, p_4) \right. \\
 & + \left(A_4^0(4_{\bar{Q}}, j_g, i_g, \hat{2}_{\bar{q}}) - d_3^0(4_{\bar{Q}}, j_g, i_g) A_3^0((\tilde{4}j)_{\bar{Q}}, (\tilde{j}i)_g, \hat{2}_{\bar{q}}) \right. \\
 & \left. \left. - d_3^0(\hat{2}_{\bar{q}}, i_g, j_g) A_3^0(4_{\bar{Q}}, (\tilde{i}j)_g, \hat{2}_{\bar{q}}) \right) |\mathcal{M}_4^0(3_Q, (\tilde{4}i\tilde{j})_{\bar{Q}}, \hat{2}_{\bar{q}}, \hat{1}_q)|^2 J_2^{(2)}(p_3, \widetilde{p_{4ij}}) \right].
 \end{aligned}$$

Two different kinds of structures are involved in this subtraction term: $X_4^0 \times |\mathcal{M}_4^0|^2$ and $X_3^0 \times X_3^0 \times |\mathcal{M}_4^0|^2$. The former subtracts the double unresolved limits while introducing spurious single unresolved singularities, whereas the latter removes these spurious limits ensuring that the four-parton antenna is only active in the double unresolved regions. The four-parton antenna $A_4^0(3_Q, i_g, j_g, \hat{1}_q)$ present in this equation appears in a subtraction term for the first time. It was discussed in section 3 together with its infrared limits and its explicit form can be found in appendix C.

	a	b_4	$b_{3 \times 3}, c$	d	e
$d\hat{\sigma}_{\text{NNLO}}^S$	$X_3^0 \mathcal{M}_{m+3}^0 ^2$	$X_4^0 \mathcal{M}_{m+2}^0 ^2$	$X_3^0 X_3^0 \mathcal{M}_{m+2}^0 ^2$	$X_3^0 X_3^0 \mathcal{M}_{m+2}^0 ^2$	$S X_3^0 \mathcal{M}_{m+2}^0 ^2$
$\int_1 d\hat{\sigma}_{\text{NNLO}}^{S,1}$	$\mathcal{X}_3^0 \mathcal{M}_{m+3}^0 ^2$	–	$\mathcal{X}_3^0 X_3^0 \mathcal{M}_{m+2}^0 ^2$	–	$S X_3^0 \mathcal{M}_{m+2}^0 ^2$
$\int_2 d\hat{\sigma}_{\text{NNLO}}^{S,2}$	–	$\mathcal{X}_4^0 \mathcal{M}_{m+2}^0 ^2$	–	$\mathcal{X}_3^0 \mathcal{X}_3^0 \mathcal{M}_{m+2}^0 ^2$	–

Table 1. Type of contribution to the double real subtraction term $d\hat{\sigma}_{\text{NNLO}}^S$, together with the integrated form of each term. The unintegrated antenna and soft functions are denoted as X_3^0 , X_4^0 and S while their integrated forms are \mathcal{X}_3^0 , \mathcal{X}_4^0 and \mathcal{S} respectively. \mathcal{M}_n^0 denotes an n -particle tree-level colour-ordered amplitude.

As shown in table 1, the brackets in $d\hat{\sigma}_{q\bar{q},\text{NNLO},N_c^2}^{S,b}$ should be expanded in order to combine its integrated form with the three and two-parton contributions. The pieces involving products of three-parton antennae, which we denote as $d\hat{\sigma}_{q\bar{q},\text{NNLO},N_c^2}^{S,b3 \times 3}$ should be included in the three-parton contributions $d\hat{\sigma}_{q\bar{q},\text{NNLO},N_c^2}^T$ with only the “outer” antenna integrated, while the terms involving a four-parton antenna, $d\hat{\sigma}_{q\bar{q},\text{NNLO},N_c^2}^{S,b4}$ are naturally added in integrated form to the two-parton counter term $d\hat{\sigma}_{q\bar{q},\text{NNLO},N_c^2}^U$. The integration of $d\hat{\sigma}_{q\bar{q},\text{NNLO},N_c^2}^{S,b4}$ will require analogous methods as developed in [44] and will be addressed elsewhere.

Finally, the subtraction term of type (S, d) , denoted by $d\hat{\sigma}_{q\bar{q},\text{NNLO},N_c^2}^{S,d}$, is built out of products of two three-parton antennae and four-parton reduced matrix elements squared. Its role in the partonic process that we are presently considering is to ensure the correct subtraction of the initial-final double collinear limits of the double real contributions given in eq. (5.2). It is given by

$$\begin{aligned}
 d\hat{\sigma}_{q\bar{q},\text{NNLO},N_c^2}^{S,d} &= -\frac{1}{2} \mathcal{N}_{\text{NNLO}}^{q\bar{q},\text{RR}} N_c^2 \sum_{(i,j) \in P(5,6)} d\Phi_4(p_3, p_4, p_5, p_6; p_1, p_2) \\
 &\times A_3^0(3_Q, i_q, \hat{1}_q) A_3^0(4_{\bar{Q}}, j_g, \hat{2}_{\bar{q}}) |\mathcal{M}_4^0((\tilde{3}i)_Q, (\tilde{4}j)_{\bar{Q}}, \hat{2}_{\bar{q}}, \hat{1}_q)|^2 J_2^{(2)}(\tilde{p}_{3i}, \tilde{p}_{4j}).
 \end{aligned}
 \tag{5.7}$$

This subtraction term will be added back to the two-parton counter term $d\hat{\sigma}_{q\bar{q},\text{NNLO},N_c^2}^U$ with both three-parton antennae integrated over their corresponding antenna phase space. We shall not discuss this integration in this paper.

In section 9 we will present a series of numerical tests that show that the subtraction term $d\hat{\sigma}_{q\bar{q},\text{NNLO},N_c^2}^S$ of eq. (5.4) correctly approximates the double real contributions $d\hat{\sigma}_{q\bar{q},\text{NNLO},N_c^2}^{\text{RR}}$ in all its single and double unresolved limits.

6 General structure of the real-virtual contributions to $q\bar{q} \rightarrow t\bar{t}$ at leading-colour

The real-virtual contributions to top-antitop production in the quark-antiquark channel are obtained using the interference of the one-loop and tree-level amplitudes for the partonic

process $q\bar{q} \rightarrow t\bar{t}g$. The colour decomposition of the matrix element reads,

$$\begin{aligned}
 M_5^1(q_1\bar{q}_2 \rightarrow Q_3\bar{Q}_4g_5) = & \quad (6.1) \\
 & \sqrt{2}g_s^6 C(\epsilon) \left\{ \left[(T^{a_5})_{i_3i_1} \delta_{i_2i_4} \mathcal{M}_5^1(3_Q, 5_g, \hat{1}_q; ; \hat{2}_{\bar{q}}, 4_{\bar{Q}}) + (T^{a_5})_{i_2i_4} \delta_{i_3i_1} \mathcal{M}_5^1(3_Q, \hat{1}_q; ; \hat{2}_{\bar{q}}, 5_g, 4_{\bar{Q}}) \right] \right. \\
 & \left. - \frac{1}{N_c} \left[(T^{a_5})_{i_3i_4} \delta_{i_2i_1} \mathcal{M}_5^1(3_Q, 5_g, 4_{\bar{Q}}; ; \hat{2}_{\bar{q}}, \hat{1}_q) + (T^{a_5})_{i_2i_1} \delta_{i_3i_4} \mathcal{M}_5^1(3_Q, 4_{\bar{Q}}; ; \hat{2}_{\bar{q}}, 5_g, \hat{1}_q) \right] \right\},
 \end{aligned}$$

where each of the sub-amplitudes has the following decomposition into primitives

$$\mathcal{M}_5^1(\dots) = N_c \mathcal{M}_5^{[lc]}(\dots) + N_l \mathcal{M}_5^{[l]}(\dots) + N_h \mathcal{M}_5^{[h]}(\dots) - \frac{1}{N_c} \mathcal{M}_5^{[slc]}(\dots). \quad (6.2)$$

Interfering the matrix element in eq. (6.1) with the tree-level amplitude in eq. (2.10), combining the result with the phase space and the jet function, and retaining only the terms proportional to N_c^2 , we obtain

$$\begin{aligned}
 d\hat{\sigma}_{q\bar{q},\text{NNLO},N_c^2}^{\text{RV}} = & \mathcal{N}_{\text{NNLO}}^{\text{RV},q\bar{q}} N_c^2 \int \frac{dx_1}{x_1} \frac{dx_2}{x_2} d\Phi_3(p_3, p_4, p_5; x_1 p_1, x_2 p_2) \delta(1-x_1) \delta(1-x_2) \quad (6.3) \\
 & \times \left(|\mathcal{M}_5^{[lc]}(3_Q, 5_g, \hat{1}_q; ; 4_{\bar{Q}}, \hat{2}_{\bar{q}})|_{\text{NLO}}^2 + |\mathcal{M}_5^{[lc]}(3_Q, \hat{1}_q; ; \hat{2}_{\bar{q}}, 5_g, 4_{\bar{Q}})|_{\text{NLO}}^2 \right) J_2^{(3)}(p_3, p_4, p_5),
 \end{aligned}$$

where the trivial dependence on x_1 and x_2 is introduced for later convenience. The overall factor $\mathcal{N}_{\text{NNLO}}^{\text{RV},q\bar{q}}$ is

$$\mathcal{N}_{\text{NNLO}}^{\text{RV},q\bar{q}} = \mathcal{N}_{\text{LO}}^{q\bar{q}} \frac{\bar{C}(\epsilon)^2}{C(\epsilon)} = \mathcal{N}_{\text{NNLO}}^{\text{RR},q\bar{q}} C(\epsilon). \quad (6.4)$$

The leading-colour primitive amplitudes in eq. (6.3) contain ultraviolet poles that must be removed by renormalisation. Following the scheme of [8, 9], which was described in section 2.3.2, we renormalise the primitive amplitudes as

$$\begin{aligned}
 \mathcal{M}_{5,\text{ren}}^{[lc]}(\dots) = & \mathcal{M}_{5,b}^{[lc]}(\dots) - \frac{3}{2} \bar{C}(\epsilon) \frac{b_0}{\epsilon} \mathcal{M}_5^0(\dots) \\
 & - \frac{1}{2} (4\pi)^\epsilon \Gamma(1+\epsilon) \left(\frac{m_Q}{\mu} \right)^{-2\epsilon} \left(\frac{3}{2\epsilon} + \frac{2}{1-2\epsilon} \right) \left(\mathcal{M}_5^0(\dots) - \mathcal{M}_{5,1M}^0(\dots) \right), \quad (6.5)
 \end{aligned}$$

where $b_0 = 11/6$ and $\mathcal{M}_{5,1M}^0(\dots)$ denotes the tree-level amplitude with a mass insertion in the heavy fermion propagators.

After UV renormalisation, the real-virtual contributions $d\hat{\sigma}_{q\bar{q},\text{NNLO},N_c^2}^{\text{RV}}$ still contain infrared divergences of implicit and explicit types. The explicit ones originate from the loop integration of the partial amplitudes $|\mathcal{M}_5^{[lc]}(\dots)|_{\text{NLO}}^2$ and can be written as the following combination of colour-ordered infrared singularity operators

$$\begin{aligned}
 \mathcal{Poles} \left(d\hat{\sigma}_{q\bar{q},\text{NNLO},N_c^2}^{\text{RV}} \right) = & \quad (6.6) \\
 & \mathcal{N}_{\text{NNLO}}^{\text{RV},q\bar{q}} N_c^2 \int \frac{dx_1}{x_1} \frac{dx_2}{x_2} d\Phi_3(p_3, p_4, p_5; x_1 p_1, x_2 p_2) \delta(1-x_1) \delta(1-x_2) \\
 & \times \left[\left(2\mathbf{I}_{Qg}^{(1)}(\epsilon, s_{35}) + 2\mathbf{I}_{qg}^{(1)}(\epsilon, s_{15}) + 2\mathbf{I}_{Q\bar{q}}^{(1)}(\epsilon, s_{24}) \right) |\mathcal{M}_5^0(3_Q, 5_g, \hat{1}_q; ; \hat{2}_{\bar{q}}, 4_{\bar{Q}})|^2 \right. \\
 & \left. + \left(2\mathbf{I}_{Qg}^{(1)}(\epsilon, s_{45}) + 2\mathbf{I}_{qg}^{(1)}(\epsilon, s_{25}) + 2\mathbf{I}_{Q\bar{q}}^{(1)}(\epsilon, s_{13}) \right) |\mathcal{M}_5^0(3_Q, \hat{1}_q; ; \hat{2}_{\bar{q}}, 5_g, 4_{\bar{Q}})|^2 \right] J_2^{(3)}(p_3, p_4, p_5).
 \end{aligned}$$

As we shall see in section 8, these poles will be canceled by the singly integrated double real subtraction terms and mass factorisation counter terms.

The implicit infrared poles, on the other hand, originate from the configurations where the final state gluon becomes soft or collinear to either of the incoming particles. Those will be dealt with the genuine real-virtual subtraction term $d\hat{\sigma}_{q\bar{q},\text{NNLO},N_c^2}^{VS}$ which will also be constructed in section 8.

7 Real-virtual contributions to top-antitop production in the quark-antiquark channel with OPENLOOPS

For the calculation of the matrix elements that enter the real-virtual contributions in eq. (6.3) we employ OPENLOOPS [45], a fully automated generator of one-loop corrections to Standard Model processes. As discussed in the following, OPENLOOPS builds Feynman diagrams with a recursive algorithm that allows for a fast and numerically stable evaluation of loop amplitudes. The reduction of amplitudes to scalar integrals can be achieved by interfacing OPENLOOPS to tensor-integral [67, 68] or OPP reduction libraries [46, 69, 70].

In the context of NNLO calculations, the integration of (subtracted) contributions over soft and collinear regions poses non trivial technical challenges as compared to conventional NLO applications. In particular, the loss of precision resulting from the cancellation between amplitudes and subtraction terms in the soft and collinear regions needs to be compensated by sufficiently high numerical accuracy. However, this is quite challenging since infrared singularities tend to amplify numerical instabilities that arise from spurious singularities (like inverse Gram determinants) in the reduction algorithms. It is thus quite interesting to investigate to which extend automated generators can guarantee an adequate level of numerical stability for NNLO calculations. In this respect OPENLOOPS has already been shown to be successfully applicable to the calculation of the NNLO corrections to $pp \rightarrow Z\gamma$ [71]. In this case, using the q_T -subtraction technique [21], it was found that the tensor-reduction library COLLIER [72], which implements the methods of [67, 68, 73], is sufficiently stable to perform the entire calculation in double precision. Very recently, OPENLOOPS was also applied to $t\bar{t}$ production in association with up to two jets at NLO [74], which is closely related to the present NNLO calculation.

In this work, OPENLOOPS is used to evaluate the amplitudes for $q\bar{q} \rightarrow t\bar{t}g$. The interference with the related Born amplitudes, the sums over external colours and helicity states, as well as the ultraviolet renormalisation (6.5) are performed in a fully automated way. The UV-finite but still IR-divergent result is returned in the form of a Laurent series,

$$|\mathcal{M}|_{\text{NLO}}^2 = \frac{(4\pi)^\epsilon}{\Gamma(1-\epsilon)} \sum_{k=-2}^0 \mathcal{A}_k \epsilon^k, \tag{7.1}$$

which must be combined with the corresponding subtraction terms. For consistency with the helicity amplitudes implemented in OPENLOOPS, the tree matrix elements in eq. (6.6) need to be evaluated in $D = 4$ dimensions.

Tree amplitudes (\mathcal{M}^0) and loop amplitudes (\mathcal{M}^1) are expressed as sums over corresponding Feynman diagrams,

$$\mathcal{M}^k = \sum_d \mathcal{C}^{(d)} \mathcal{A}_k^{(d)}, \tag{7.2}$$

where the colour factors $\mathcal{C}^{(d)}$ associated with individual diagrams are factorised, and the corresponding colour-stripped amplitudes are denoted as $\mathcal{A}_k^{(d)}$. All colour structures are reduced to a standard basis $\{\mathcal{C}_i\}$, and the colour information needed to build colour-summed squared matrix elements is encoded in the colour-interference matrix,

$$\mathcal{K}_{ij} = \sum_{\text{col}} \mathcal{C}_i^* \mathcal{C}_j. \tag{7.3}$$

These colour bookkeeping operations are done only once, using a generic and automated algebraic algorithm, during the generation of the numerical code for a particular process. This approach provides high flexibility in the colour treatment, and the leading-colour approximation used in this paper could be easily implemented via a $1/N_c$ expansion of the colour-interference matrix (7.3). Additionally, in order to obtain the leading colour contribution of the counter-term amplitude, the substitutions $C_F \rightarrow N_c$, $C_A \rightarrow 0$, $T_F \rightarrow 0$ are applied to colour factors which are attributed to renormalisation constants.

The calculation of colour-stripped loop amplitudes within OPENLOOPS is based on the representation

$$\mathcal{A}_1^{(d)} = \int \frac{d^D q \mathcal{N}^{(d)}(q)}{D_0 D_1 \dots D_{n-1}}, \tag{7.4}$$

where the denominators $D_i = (q + p_i)^2 - m_i^2 + i\epsilon$ depend on the loop momentum q , external momenta p_i , and internal masses m_i . The numerator $\mathcal{N}^{(d)}(q)$ corresponds to a particular diagram or to a set of diagrams with the same loop topology. It is expressed as a polynomial of degree $R \leq n$ in the loop momentum,

$$\mathcal{N}^{(d)}(q) = \sum_{r=0}^R \mathcal{N}_{\mu_1 \dots \mu_r}^{(d)} q^{\mu_1} \dots q^{\mu_r}. \tag{7.5}$$

In contrast to traditional approaches, where the above expressions are constructed via explicit insertion of the Feynman rules, the OPENLOOPS method consists of a numerical recursion that builds the polynomial coefficients $\mathcal{N}_{\mu_1 \dots \mu_r}^{(d)}$ in an iterative way starting from related coefficients for lower-point topologies, i.e. topologies with a lower number of loop propagators. The recursion is formulated in $D = 4$ dimensions, and rational terms resulting from $\mathcal{O}(D - 4)$ contributions to the numerator are easily obtained in a process-independent way via so-called R_2 counter terms [75].

For the reduction of amplitudes to scalar integrals, the OPENLOOPS representation (7.4)–(7.5) allows one to use the tensor-integral or OPP reduction techniques. In the former case, the reduction is performed at the level of process-independent tensor integrals,

$$T_{n,r}^{\mu_1 \dots \mu_r} = \int \frac{d^D q q^{\mu_1} \dots q^{\mu_r}}{D_0 D_1 \dots D_{n-1}}, \tag{7.6}$$

which are then combined with the corresponding coefficients. In this approach, the COLLIER library implements systematic expansions in Gram determinants and other kinematic quantities [68], which avoid numerical instabilities due to spurious singularities. In the OPP reduction framework, the reduction is performed at the level of the full integrand in eq. (7.4). This requires multiple evaluations of the numerator function, and using the representation (7.5) in combination with the OPENLOOPS coefficients, $\mathcal{N}_{\mu_1 \dots \mu_r}^{(d)}$, renders OPP reduction similarly fast as tensor reduction [45].

In section 9 we will investigate the numerical stability of the amplitudes in the soft and collinear regions using OPENLOOPS in combination with the OPP reduction library CUTTOOLS [46]. In this context we will exploit the quadruple precision mode of CUTTOOLS both as a rescue system for matrix elements that are not sufficiently stable in double precision, and for precision tests of the real-virtual cancellations in the deep infrared regime.

8 Real-virtual subtraction terms

The purpose of the real-virtual counter term $d\hat{\sigma}_{q\bar{q},\text{NNLO},N_c^2}^{\text{T}}$ is to cancel the explicit ϵ -poles of the real-virtual contributions $d\hat{\sigma}_{q\bar{q},\text{NNLO},N_c^2}^{\text{RV}}$ and to simultaneously subtract their infrared limits in such a way that the difference $d\hat{\sigma}_{q\bar{q},\text{NNLO},N_c^2}^{\text{RV}} - d\hat{\sigma}_{q\bar{q},\text{NNLO},N_c^2}^{\text{T}}$ can be safely integrated numerically in four dimensions. The generic antenna content of this counter term has been derived for the massless case in [31, 32], and it remains unchanged in the massive case. We will here follow the formalism developed in these references, to which the reader is referred for details.

In general, real-virtual antenna counter terms contain singly integrated double real subtraction terms, NNLO mass factorisation counter terms and genuine real-virtual subtraction terms. For the leading-colour contributions to top pair production in the $q\bar{q}$ channel the counter term has the following structure

$$d\hat{\sigma}_{q\bar{q},\text{NNLO},N_c^2}^{\text{T}} = - \left(\int_1 d\hat{\sigma}_{q\bar{q},\text{NNLO},N_c^2}^{\text{S},a} + d\hat{\sigma}_{q\bar{q},\text{NNLO},N_c^2}^{\text{MF},1a} \right) \tag{8.1}$$

$$+ \left[d\hat{\sigma}_{q\bar{q},\text{NNLO},N_c^2}^{\text{VS},a} + d\hat{\sigma}_{q\bar{q},\text{NNLO},N_c^2}^{\text{VS},b} + d\hat{\sigma}_{q\bar{q},\text{NNLO},N_c^2}^{\text{VS},d} - \int_1 d\hat{\sigma}_{q\bar{q},\text{NNLO},N_c^2}^{\text{S},b\ 3\times 3} - d\hat{\sigma}_{q\bar{q},\text{NNLO},N_c^2}^{\text{MF},1b} \right].$$

In the most general case, real-virtual subtraction terms contain yet another component, labelled (VS, c) [31, 32], whose absence in this particular case is related to the absence of the subtraction terms labelled (S, c) and (S, e) at the double real level. Furthermore, in eq. (8.1) we have splitted the mass factorisation counter term $d\hat{\sigma}_{q\bar{q},\text{NNLO},N_c^2}^{\text{MF},1}$ into two terms $d\hat{\sigma}_{q\bar{q},\text{NNLO},N_c^2}^{\text{MF},1a}$ and $d\hat{\sigma}_{q\bar{q},\text{NNLO},N_c^2}^{\text{MF},1b}$. In the following, we shall present all the pieces of $d\hat{\sigma}_{q\bar{q},\text{NNLO},N_c^2}^{\text{T}}$, starting with the explicit expressions of these two mass factorisation counter terms.

8.1 The mass factorisation counter term $d\hat{\sigma}_{\text{NNLO}}^{\text{MF},1}$

For a given partonic process initiated by partons labelled i and j the mass factorisation counter term $d\hat{\sigma}_{ij,\text{NNLO}}^{\text{MF},1}$ is related to the NLO real emission partonic cross sections $d\hat{\sigma}_{kl,\text{NLO}}^{\text{R}}$

and its corresponding antenna subtraction term $d\hat{\sigma}_{kl,\text{NLO}}^{\text{S}}$. It is given by

$$d\hat{\sigma}_{ij,\text{NNLO}}^{\text{MF},1}(p_1, p_2) = -\bar{C}(\epsilon) \sum_{k,l} \int \frac{dx_1}{x_1} \frac{dx_2}{x_2} \Gamma_{ij;kl}^{(1)}(x_1, x_2) \left[d\hat{\sigma}_{kl,\text{NLO}}^{\text{R}} - d\hat{\sigma}_{kl,\text{NLO}}^{\text{S}} \right](x_1 p_1, x_2 p_2), \quad (8.2)$$

with the kernel $\Gamma_{ij;kl}^{(1)}(x_1, x_2)$ defined in eq. (2.30). It is useful to further decompose this mass factorisation counter term as follows:

$$d\hat{\sigma}_{ij,\text{NNLO}}^{\text{MF},1} = d\hat{\sigma}_{ij,\text{NNLO}}^{\text{MF},1a} + d\hat{\sigma}_{ij,\text{NNLO}}^{\text{MF},1b} \quad (8.3)$$

with

$$d\hat{\sigma}_{ij,\text{NNLO}}^{\text{MF},1a}(p_1, p_2) = -\bar{C}(\epsilon) \sum_{k,l} \int \frac{dx_1}{x_1} \frac{dx_2}{x_2} \Gamma_{ij;kl}^{(1)}(x_1, x_2) d\hat{\sigma}_{kl,\text{NLO}}^{\text{R}}(x_1 p_1, x_2 p_2), \quad (8.4)$$

$$d\hat{\sigma}_{ij,\text{NNLO}}^{\text{MF},1b}(p_1, p_2) = +\bar{C}(\epsilon) \sum_{k,l} \int \frac{dx_1}{x_1} \frac{dx_2}{x_2} \Gamma_{ij;kl}^{(1)}(x_1, x_2) d\hat{\sigma}_{kl,\text{NLO}}^{\text{S}}(x_1 p_1, x_2 p_2). \quad (8.5)$$

In the context of this paper, the mass factorisation counter term denoted by $d\hat{\sigma}_{q\bar{q},\text{NNLO},N_c^2}^{\text{MF},1a}$ is constructed as in eq. (8.4) with $d\hat{\sigma}_{q\bar{q},\text{NLO}}^{\text{R}}$ given in eq. (2.11). Retaining only the terms with an overall N_c^2 we have

$$\begin{aligned} d\hat{\sigma}_{q\bar{q},\text{NNLO},N_c^2}^{\text{MF},1a} &= -\mathcal{N}_{\text{NNLO}}^{\text{RV},q\bar{q}} N_c^2 \int \frac{dx_1}{x_1} \frac{dx_2}{x_2} d\Phi_3(p_3, p_4, p_5; x_1 p_1, x_2 p_2) \\ &\times \left\{ \frac{1}{2} \left(\Gamma_{q\bar{q}}^{(1)}(x_1) \delta(1-x_2) + \Gamma_{q\bar{q}}^{(1)}(x_2) \delta(1-x_1) \right) |\mathcal{M}_5^0(3_Q, 5_g, \hat{1}_q; \hat{2}_{\bar{q}}, 4_{\bar{Q}})|^2 \right. \\ &\left. + \frac{1}{2} \left(\Gamma_{q\bar{q}}^{(1)}(x_1) \delta(1-x_2) + \Gamma_{q\bar{q}}^{(1)}(x_2) \delta(1-x_1) \right) |\mathcal{M}_5^0(3_Q, \hat{1}_q; \hat{2}_{\bar{q}}, 5_g, 4_{\bar{Q}})|^2 \right\} J_2^{(3)}(p_3, p_4, p_5). \end{aligned} \quad (8.6)$$

We note that this contribution contains five-parton matrix elements. It can therefore develop spurious single unresolved limits which have to be compensated for by other terms in $d\hat{\sigma}_{q\bar{q},\text{NNLO},N_c^2}^{\text{T}}$ as we shall see below.

Furthermore, the mass factorisation counter term $d\hat{\sigma}_{q\bar{q},\text{NNLO},N_c^2}^{\text{MF},1b}$ is constructed as in eq. (8.5) with the NLO subtraction term $d\hat{\sigma}_{q\bar{q},\text{NLO}}^{\text{S}}$ given in eq. (2.14). Retaining only the terms with an overall N_c^2 colour we have

$$\begin{aligned} d\hat{\sigma}_{q\bar{q},\text{NNLO},N_c^2}^{\text{MF},1b} &= \frac{1}{2} \mathcal{N}_{\text{NNLO}}^{q\bar{q},\text{RV}} N_c^2 \int \frac{dx_1}{x_1} \frac{dx_2}{x_2} d\Phi_3(p_3, p_4, p_5; x_1 p_1, x_2 p_2) \\ &\times \left(\Gamma_{q\bar{q}}^{(1)}(x_1) \delta(1-x_2) + \Gamma_{q\bar{q}}^{(1)}(x_2) \delta(1-x_1) \right) \\ &\times \left[A_3^0(3_Q, 5_g, \hat{1}_q) |\mathcal{M}_4^0((\widetilde{35})_Q, 4_{\bar{Q}}, \hat{2}_{\bar{q}}, \hat{1}_q)|^2 J_2^{(2)}(\widetilde{p}_{35}, p_4) \right. \\ &\left. + A_3^0(4_{\bar{Q}}, 5_g, \hat{2}_q) |\mathcal{M}_4^0(3_Q, (\widetilde{45})_{\bar{Q}}, \hat{2}_{\bar{q}}, \hat{1}_q)|^2 J_2^{(2)}(p_3, \widetilde{p}_{45}) \right]. \end{aligned} \quad (8.7)$$

8.2 Cancellation of explicit infrared poles in $d\hat{\sigma}_{\text{NNLO},q\bar{q},N_c^2}^{\text{RV}}$

We continue with the construction of $d\hat{\sigma}_{q\bar{q},\text{NNLO},N_c^2}^{\text{T}}$ by showing that the explicit infrared poles present in the real-virtual contributions and given in eq. (6.6) are cancelled as

$$\text{Poles} \left(d\hat{\sigma}_{\text{NNLO},q\bar{q},N_c^2}^{\text{RV}} + \int_1 d\hat{\sigma}_{q\bar{q},\text{NNLO},N_c^2}^{\text{S},a} + d\hat{\sigma}_{q\bar{q},\text{NNLO},N_c^2}^{\text{MF},1a} \right) = 0. \quad (8.8)$$

The integrated subtraction term $\int_1 d\hat{\sigma}_{q\bar{q},\text{NNLO},N_c^2}^{\text{S},a}$ can be obtained from eq. (5.5) by integrating each of the three-parton antenna functions over the appropriate antenna phase spaces. It reads

$$\begin{aligned} \int_1 d\hat{\sigma}_{q\bar{q},\text{NNLO},N_c^2}^{\text{S},a} &= \mathcal{N}_{\text{NNLO}}^{\text{RV},q\bar{q}} N_c^2 \int \frac{dx_1}{x_1} \frac{dx_2}{x_2} d\Phi_3(p_3, p_4, p_5; x_1 p_1, x_2 p_2) \\ &\times \left[\left(\frac{1}{2} \mathcal{D}_{Qgg}^0(\epsilon, s_{35}, x_1, x_2) + \frac{1}{2} \mathcal{D}_{q,gg}^0(\epsilon, s_{\bar{1}5}, x_1, x_2) \right. \right. \\ &+ \left. \mathcal{A}_{q,Qg}^0(\epsilon, s_{\bar{2}4}, x_2, x_1) \right) |\mathcal{M}_5^0(3_Q, 5_g, \hat{1}_q; \hat{2}_{\bar{q}}, 4_{\bar{Q}})|^2 \\ &+ \left(\frac{1}{2} \mathcal{D}_{Qgg}^0(\epsilon, s_{45}, x_1, x_2) + \frac{1}{2} \mathcal{D}_{q,gg}^0(\epsilon, s_{\bar{5}5}, x_2, x_1) \right. \\ &+ \left. \left. \mathcal{A}_{q,Qg}^0(\epsilon, s_{\bar{1}3}, x_1, x_2) \right) |\mathcal{M}_5^0(3_Q, \hat{1}_q; \hat{2}_{\bar{q}}, 5_g, 4_{\bar{Q}})|^2 \right] J_2^{(3)}(p_3, p_4, p_5). \end{aligned} \quad (8.9)$$

The integrated antennae in the equation above have been derived in [27]. Only their pole parts will be needed in the context of this paper. The poles of the flavour violating antenna $\mathcal{A}_{q,Qg}^0$ were given in eq. (2.15), and those of the D-type antennae are given by

$$\text{Poles}(\mathcal{D}_{Qgg}^0(\epsilon, s_{ij}, x_1, x_2)) = -4\mathbf{I}_{Qg}^{(1)}(\epsilon, s_{ij})\delta(1-x_1)\delta(1-x_2) \quad (8.10)$$

$$\text{Poles}(\mathcal{D}_{q,gg}^0(\epsilon, s_{ij}, x_1, x_2)) = -4\mathbf{I}_{qg}^{(1)}(\epsilon, s_{ij})\delta(1-x_1)\delta(1-x_2) + \Gamma_{qq}^{(1)}(x_1)\delta(1-x_2). \quad (8.11)$$

The pole part of the singly integrated real subtraction term denoted as (S, a) is therefore given by

$$\begin{aligned} \text{Poles} \left(\int_1 d\hat{\sigma}_{q\bar{q},\text{NNLO},N_c^2}^{\text{S},a} \right) &= \mathcal{N}_{\text{NNLO}}^{\text{RV},q\bar{q}} N_c^2 \int \frac{dx_1}{x_1} \frac{dx_2}{x_2} d\Phi_3(p_3, p_4, p_5; x_1 p_1, x_2 p_2) \\ &\times \left\{ \left[-\delta(1-x_1)\delta(1-x_2) \left(2\mathbf{I}_{Qg}^{(1)}(\epsilon, s_{35}) + 2\mathbf{I}_{qg}^{(1)}(\epsilon, s_{15}) + 2\mathbf{I}_{Q\bar{q}}^{(1)}(\epsilon, s_{24}) \right) \right. \right. \\ &+ \left. \frac{1}{2} \left(\Gamma_{qq}^{(1)}(x_1)\delta(1-x_2) + \Gamma_{qq}^{(1)}(x_2)\delta(1-x_1) \right) \right] |\mathcal{M}_5^0(3_Q, 5_g, \hat{1}_q; \hat{2}_{\bar{q}}, 4_{\bar{Q}})|^2 \\ &+ \left[-\delta(1-x_1)\delta(1-x_2) \left(2\mathbf{I}_{Qg}^{(1)}(\epsilon, s_{45}) + 2\mathbf{I}_{qg}^{(1)}(\epsilon, s_{25}) + 2\mathbf{I}_{Q\bar{q}}^{(1)}(\epsilon, s_{13}) \right) \right. \\ &+ \left. \left. \frac{1}{2} \left(\Gamma_{qq}^{(1)}(x_1)\delta(1-x_2) + \Gamma_{qq}^{(1)}(x_2)\delta(1-x_1) \right) \right] |\mathcal{M}_5^0(3_Q, \hat{1}_q; \hat{2}_{\bar{q}}, 5_g, 4_{\bar{Q}})|^2 \right\} J_2^{(3)}(p_3, p_4, p_5). \end{aligned} \quad (8.12)$$

The measurement function $J_2^{(3)}$ in eq. (8.12) allows the final state gluon in the reduced five-particle matrix elements squared to become unresolved. The corresponding singular limits of this subtraction term are spurious, since they do not correspond to any physical limits of the real-virtual contribution $d\hat{\sigma}_{q\bar{q},\text{NNLO},N_c^2}^{\text{RV}}$. Those must therefore be cancelled by other terms in $d\hat{\sigma}_{q\bar{q},\text{NNLO},N_c^2}^{\text{T}}$. We shall shortly see below that this is indeed the case.

Combining eqs. (6.6), (8.12) and (8.6) it can easily be seen that eq. (8.8) holds.

8.3 Construction of $d\hat{\sigma}_{q\bar{q},\text{NNLO},N_c^2}^{\text{VS}}$

The real-virtual subtraction term $d\hat{\sigma}_{q\bar{q},\text{NNLO},N_c^2}^{\text{VS}}$ has three components:

$$d\hat{\sigma}_{q\bar{q},\text{NNLO},N_c^2}^{\text{VS}} = d\hat{\sigma}_{q\bar{q},\text{NNLO},N_c^2}^{\text{VS},a} + d\hat{\sigma}_{q\bar{q},\text{NNLO},N_c^2}^{\text{VS},b} + d\hat{\sigma}_{q\bar{q},\text{NNLO},N_c^2}^{\text{VS},d}. \quad (8.13)$$

The (VS, a) piece subtracts the single unresolved limits of the real-virtual contributions, the (VS, d) subtraction term corrects for the different renormalisation scales in the matrix elements and in the antennae, while the (VS, b) part has the twofold purpose of removing the spurious unresolved limits of $\int_1 d\hat{\sigma}_{q\bar{q},\text{NNLO},N_c^2}^{\text{S},a}$ and achieving at the same time the following explicit pole cancellation:

$$\text{Poles} \left(d\hat{\sigma}_{q\bar{q},\text{NNLO},N_c^2}^{\text{VS},a} + d\hat{\sigma}_{q\bar{q},\text{NNLO},N_c^2}^{\text{VS},b} + \int_1 d\hat{\sigma}_{q\bar{q},\text{NNLO},N_c^2}^{\text{S},b \ 3 \times 3} - d\hat{\sigma}_{q\bar{q},\text{NNLO},N_c^2}^{\text{MF},1b} \right) = 0. \quad (8.14)$$

We shall present these three subtraction contributions separately below.

8.3.1 Construction of $d\hat{\sigma}_{q\bar{q},\text{NNLO},N_c^2}^{\text{VS},a}$

Following the general framework described in [31], in order to subtract the single unresolved limits of the real-virtual contributions given in eq. (6.3) we construct our subtraction terms of the type (VS, a) with one-loop antennae multiplied by reduced tree-level matrix-elements and one-loop matrix-elements multiplied by tree-level antennae. They read,

$$\begin{aligned} d\hat{\sigma}_{q\bar{q},\text{NNLO},N_c^2}^{\text{VS},a} = & \mathcal{N}_{\text{NNLO}}^{\text{RV},q\bar{q}} N_c^2 \int \frac{dx_1}{x_1} \frac{dx_2}{x_2} d\Phi_3(p_3, p_4, p_5; x_1 p_1, x_2 p_2) \delta(1-x_1) \delta(1-x_2) \\ & \times \left\{ A_3^0 \left(3_Q, 5_g, \hat{1}_q \right) | \mathcal{M}_{4,1}^{[lc]} \left((\tilde{35})_Q, 4_{\bar{Q}}, \hat{2}_{\bar{q}}, \hat{1}_q \right) |_{\text{NLO}}^2 J_2^{(2)}(p_{\tilde{35}}, p_4) \right. \\ & + A_3^{1,lc} \left(3_Q, 5_g, \hat{1}_q \right) | \mathcal{M}_4^0 \left((\tilde{35})_Q, 4_{\bar{Q}}, \hat{2}_{\bar{q}}, \hat{1}_q \right) |^2 J_2^{(2)}(p_{\tilde{35}}, p_4) \\ & + A_3^0 \left(4_{\bar{Q}}, 5_g, \hat{2}_{\bar{q}} \right) | \mathcal{M}_{4,1}^{[lc]} \left(3_Q, (\tilde{45})_{\bar{Q}}, \hat{2}_{\bar{q}}, \hat{1}_q \right) |_{\text{NLO}}^2 J_2^{(2)}(p_3, p_{\tilde{45}}) \\ & \left. + A_3^{1,lc} \left(4_{\bar{Q}}, 5_g, \hat{2}_{\bar{q}} \right) | \mathcal{M}_4^0 \left(3_Q, (\tilde{45})_{\bar{Q}}, \hat{2}_{\bar{q}}, \hat{1}_q \right) |^2 J_2^{(2)}(p_3, p_{\tilde{45}}) \right\}. \quad (8.15) \end{aligned}$$

The three-parton antenna $A_3^{1,lc}$ appears here in a subtraction term for the first time. This antenna has been presented together with its singular limits in section 4. Its integration over the antenna phase space will as for $d\hat{\sigma}^{\text{S},b,4}$ require application of the methods presented in [44].

8.3.2 Construction of $d\hat{\sigma}_{q\bar{q},\text{NNLO},N_c^2}^{\text{VS},b}$

In order to construct our (VS, b)-type subtraction terms in such a way that the pole cancellation of eq. (8.14) holds, we have to examine the pole parts of $d\hat{\sigma}_{q\bar{q},\text{NNLO},N_c^2}^{\text{VS},a}$, $\int_1 d\hat{\sigma}_{q\bar{q},\text{NNLO},N_c^2}^{\text{S},b \ 3 \times 3}$ and $d\hat{\sigma}_{q\bar{q},\text{NNLO},N_c^2}^{\text{MF},1b}$ with the latter expression given before in eq. (8.7). The poles of $d\hat{\sigma}_{q\bar{q},\text{NNLO},N_c^2}^{\text{VS},a}$ are simply obtained using the expressions of the pole part of the four-parton

matrix element and of the antenna in eq. (8.15). The explicit infrared poles of the one loop antenna have been given in eq. (4.22), and those of the matrix elements are given by:

$$\begin{aligned} \mathcal{Poles} \left(|\mathcal{M}_{4,1}^{[lc]}(3_Q, 4_{\bar{Q}}, \hat{2}_{\bar{q}}, \hat{1}_q)|_{\text{NLO}}^2 \right) = \\ 2 \left(\mathbf{I}_{Q\bar{q}}^{(1)}(\epsilon, s_{13}, m_Q^2) + \mathbf{I}_{Q\bar{q}}^{(1)}(\epsilon, s_{24}, m_Q^2) \right) |\mathcal{M}_4^0(3_Q, 4_{\bar{Q}}, \hat{2}_{\bar{q}}, \hat{1}_q)|^2. \end{aligned} \quad (8.16)$$

Relabelling the final state momenta, we find

$$\begin{aligned} \mathcal{Poles} \left(d\hat{\sigma}_{q\bar{q}, \text{NNLO}, N_c^2}^{\text{VS}, a} \right) = \mathcal{N}_{\text{NNLO}}^{q\bar{q}, \text{RV}} N_c^2 \int \frac{dx_1}{x_1} \frac{dx_2}{x_2} d\Phi_3(p_3, p_4, p_5; p_1, p_2) \\ \times \left\{ 2 \left[\mathbf{I}_{Q\bar{q}}^{(1)}(\epsilon, s_{24}) + \mathbf{I}_{Qg}^{(1)}(\epsilon, s_{35}) + \mathbf{I}_{qg}^{(1)}(\epsilon, s_{15}) \right] \right. \\ \times A_3^0(3_Q, 5_g, \hat{1}_q) |\mathcal{M}_4^0((\tilde{35})_Q, 4_{\bar{Q}}, \hat{2}_{\bar{q}}, \hat{1}_q)|^2 J_2^{(2)}(\tilde{p}_{35}, p_4) \\ \left. + 2 \left[\mathbf{I}_{Q\bar{q}}^{(1)}(\epsilon, s_{13}) + \mathbf{I}_{Qg}^{(1)}(\epsilon, s_{45}) + \mathbf{I}_{qg}^{(1)}(\epsilon, s_{25}) \right] \right. \\ \left. \times A_3^0(4_{\bar{Q}}, 5_g, \hat{2}_{\bar{q}}) |\mathcal{M}_4^0(3_Q, (\tilde{45})_{\bar{Q}}, \hat{2}_{\bar{q}}, \hat{1}_q)|^2 J_2^{(2)}(p_3, \tilde{p}_{45}) \right\}. \end{aligned} \quad (8.17)$$

The singly integrated subtraction term, $\int_1 d\hat{\sigma}_{q\bar{q}, \text{NNLO}, N_c^2}^{\text{S}, b \, 3 \times 3}$, on the other hand, is obtained by integrating the “outer” antennae in eq. (5.6) over the corresponding three-parton antenna phase space. We find

$$\begin{aligned} \int_1 d\hat{\sigma}_{q\bar{q}, \text{NNLO}, N_c^2}^{\text{S}, b \, 3 \times 3} = -\mathcal{N}_{\text{NNLO}}^{\text{RV}, q\bar{q}} N_c^2 \int \frac{dx_1}{x_1} \frac{dx_2}{x_2} d\Phi_3(p_3, p_4, p_5; x_1 p_1, x_2 p_2) \\ \times \left\{ \left(\frac{1}{2} \mathcal{D}_{Qgg}^0(\epsilon, s_{35}, x_1, x_2) + \frac{1}{2} \mathcal{D}_{q,gg}^0(\epsilon, s_{15}, x_1, x_2) \right) \right. \\ \times A_3^0(3_Q, 5_g, \hat{1}_q) |\mathcal{M}_4^0((\tilde{35})_Q, 4_{\bar{Q}}, \hat{2}_{\bar{q}}, \hat{1}_q)|^2 J_2^{(2)}(p_{\tilde{35}}, p_4) \\ \left. + \left(\frac{1}{2} \mathcal{D}_{Qgg}^0(\epsilon, s_{45}, x_1, x_2) + \frac{1}{2} \mathcal{D}_{q,gg}^0(\epsilon, s_{25}, x_2, x_2) \right) \right. \\ \left. \times A_3^0(4_{\bar{Q}}, 5_g, \hat{2}_{\bar{q}}) |\mathcal{M}_4^0(3_Q, (\tilde{45})_{\bar{Q}}, \hat{2}_{\bar{q}}, \hat{1}_q)|^2 J_2^{(2)}(p_3, p_{\tilde{45}}) \right\}, \end{aligned} \quad (8.18)$$

and using eqs. (2.15), (8.10) and (8.11) we get

$$\begin{aligned} \mathcal{Poles} \left(\int_1 d\hat{\sigma}_{q\bar{q}, \text{NNLO}, N_c^2}^{\text{S}, b \, 3 \times 3} \right) = \mathcal{N}_{\text{NNLO}}^{q\bar{q}, \text{RV}} N_c^2 \int \frac{dx_1}{x_1} \frac{dx_2}{x_2} d\Phi_3(p_3, p_4, p_5; x_1 p_1, x_2 p_2) \\ \times \left\{ \left[\delta(1-x_1)\delta(1-x_2) \left(2\mathbf{I}_{Qg}^{(1)}(\epsilon, s_{35}) + 2\mathbf{I}_{qg}^{(1)}(\epsilon, s_{15}) \right) - \frac{1}{2} \Gamma_{q\bar{q}}^{(1)}(x_1)\delta(1-x_2) \right] \right. \\ \times A_3^0(3_Q, 5_g, \hat{1}_q) |\mathcal{M}_4^0((\tilde{35})_Q, 4_{\bar{Q}}, \hat{2}_{\bar{q}}, \hat{1}_q)|^2 J_2^{(2)}(\tilde{p}_{35}, p_4) \\ \left. + \left[\delta(1-x_1)\delta(1-x_2) \left(2\mathbf{I}_{Qg}^{(1)}(\epsilon, s_{45}) + 2\mathbf{I}_{qg}^{(1)}(\epsilon, s_{25}) \right) - \frac{1}{2} \Gamma_{q\bar{q}}^{(1)}(x_2)\delta(1-x_1) \right] \right. \\ \left. \times A_3^0(4_{\bar{Q}}, 5_g, \hat{2}_{\bar{q}}) |\mathcal{M}_4^0(3_Q, (\tilde{45})_{\bar{Q}}, \hat{2}_{\bar{q}}, \hat{1}_q)|^2 J_2^{(2)}(p_3, \tilde{p}_{45}) \right\}. \end{aligned} \quad (8.19)$$

Combining equations (8.17), (8.19) and (8.7) we find that

$$\begin{aligned}
 \mathcal{Poles} \left(d\hat{\sigma}_{q\bar{q},\text{NNLO},N_c^2}^{\text{VS},a} - \int_1 d\hat{\sigma}_{q\bar{q},\text{NNLO},N_c^2}^{\text{S},b\,3\times 3} - d\hat{\sigma}_{q\bar{q},\text{NNLO},N_c^2}^{\text{MF},1b} \right) = \\
 \mathcal{N}_{\text{NNLO}}^{q\bar{q},\text{RV}} N_c^2 \int \frac{dx_1}{x_1} \frac{dx_2}{x_2} d\Phi_3(p_3, p_4, p_5; x_1 p_1, x_2 p_2) \\
 \times \left\{ 2\mathbf{I}_{Q\bar{q}}^{(1)}(\epsilon, s_{24}, m_Q^2) \delta(1-x_1) \delta(1-x_2) A_3^0(3_Q, 5_g, \hat{1}_q) |\mathcal{M}_4^0((\tilde{35})_Q, 4_{\bar{Q}}, \hat{2}_{\bar{q}}, \hat{1}_q)|^2 J_2^{(2)}(\widetilde{p_{35}}, p_4) \right. \\
 + 2\mathbf{I}_{Q\bar{q}}^{(1)}(\epsilon, s_{13}, m_Q^2) \delta(1-x_1) \delta(1-x_2) A_3^0(4_{\bar{Q}}, 5_g, \hat{2}_{\bar{q}}) |\mathcal{M}_4^0(3_Q, (\tilde{45})_{\bar{Q}}, \hat{2}_{\bar{q}}, \hat{1}_q)|^2 J_2^{(2)}(p_3, \widetilde{p_{45}}) \\
 - \frac{1}{2} \Gamma_{q\bar{q}}^{(1)}(x_1) \delta(1-x_2) A_3^0(4_{\bar{Q}}, 5_g, \hat{2}_q) |\mathcal{M}_4^0(3_Q, (\tilde{45})_{\bar{Q}}, \hat{2}_{\bar{q}}, \hat{1}_q)|^2 J_2^{(2)}(p_3, \widetilde{p_{45}}) \\
 \left. - \frac{1}{2} \Gamma_{q\bar{q}}^{(1)}(x_2) \delta(1-x_1) A_3^0(3_Q, 5_g, \hat{1}_q) |\mathcal{M}_4^0((\tilde{35})_Q, 4_{\bar{Q}}, \hat{2}_{\bar{q}}, \hat{1}_q)|^2 J_2^{(2)}(\widetilde{p_{35}}, p_4) \right\}. \quad (8.20)
 \end{aligned}$$

In order for eq. (8.14) to be satisfied, $d\hat{\sigma}_{q\bar{q},\text{NNLO},N_c^2}^{\text{VS},b}$ must be constructed in such a way that its pole part is opposite to the equation above. We must therefore identify the integrated antenna functions that yield the $\mathbf{I}_{ij}^{(1)}$ operators and splitting kernels in eq. (8.20). In this case, the integrated antennae that should be employed are initial-final flavour-violating A-type antennae, and it can be seen that eq. (8.14) is satisfied if we write

$$\begin{aligned}
 d\hat{\sigma}_{q\bar{q},\text{NNLO},N_c^2}^{\text{VS},b} = \mathcal{N}_{\text{NNLO}}^{q\bar{q},\text{RV}} N_c^2 \int \frac{dx_1}{x_1} \frac{dx_2}{x_2} d\Phi_3(p_3, p_4, p_5; x_1 p_1, x_2 p_2) \quad (8.21) \\
 \times \left\{ \mathcal{A}_{q,Qg}^0(\epsilon, s_{13}, x_1, x_2) A_3^0(4_{\bar{Q}}, 5_g, \hat{2}_{\bar{q}}) |\mathcal{M}_4^0(3_Q, (\tilde{45})_{\bar{Q}}, \hat{2}_{\bar{q}}, \hat{1}_q)|^2 J_2^{(2)}(p_3, \widetilde{p_{45}}) \right. \\
 \left. + \mathcal{A}_{q,Qg}^0(\epsilon, s_{24}, x_2, x_1) A_3^0(3_Q, 5_g, \hat{1}_q) |\mathcal{M}_4^0((\tilde{35})_Q, 4_{\bar{Q}}, \hat{2}_{\bar{q}}, \hat{1}_q)|^2 J_2^{(2)}(\widetilde{p_{35}}, p_4) \right\}.
 \end{aligned}$$

Furthermore the subtraction term $d\hat{\sigma}_{q\bar{q},\text{NNLO},N_c^2}^{\text{VS},b}$ together with $\int_1 d\hat{\sigma}_{q\bar{q},\text{NNLO},N_c^2}^{\text{S},b\,3\times 3}$ and $d\hat{\sigma}_{q\bar{q},\text{NNLO},N_c^2}^{\text{MF},1b}$ reproduces the spurious single unresolved behaviour of $\int_1 d\hat{\sigma}_{q\bar{q},\text{NNLO},N_c^2}^{\text{S},a}$ and $d\hat{\sigma}_{q\bar{q},\text{NNLO},N_c^2}^{\text{MF},1a}$ which is the second requirement the subtraction term (VS, b) has to fulfill.

8.3.3 Construction of $d\hat{\sigma}_{q\bar{q},\text{NNLO},N_c^2}^{\text{VS},d}$

Finally, the ultraviolet type subtraction term denoted by $d\hat{\sigma}_{q\bar{q},\text{NNLO},N_c^2}^{\text{VS},d}$ is proportional to the leading colour part of β_0 , $b_0 = 11/6$. It reads

$$\begin{aligned}
 d\hat{\sigma}_{q\bar{q},\text{NNLO},N_c^2}^{\text{VS},d} = \mathcal{N}_{\text{NNLO}}^{\text{RV},q\bar{q}} N_c^2 \int \frac{dx_1}{x_1} \frac{dx_2}{x_2} d\Phi_3(p_3, p_4, p_5; x_1 p_1, x_2 p_2) \delta(1-x_1) \delta(1-x_2) \quad (8.22) \\
 \times \left\{ b_0 \log\left(\frac{\mu^2}{|s_{135}|}\right) A_3^0(3_Q, 5_g, \hat{1}_q) |\mathcal{M}_4^0((\tilde{35})_Q, 4_{\bar{Q}}, \hat{2}_{\bar{q}}, \hat{1}_q)|^2 J_2^{(2)}(\widetilde{p_{35}}, p_4) \right. \\
 \left. + b_0 \log\left(\frac{\mu^2}{|s_{245}|}\right) A_3^0(4_{\bar{Q}}, 5_g, \hat{2}_{\bar{q}}) |\mathcal{M}_4^0(3_Q, (\tilde{45})_{\bar{Q}}, \hat{2}_{\bar{q}}, \hat{1}_q)|^2 J_2^{(2)}(p_3, \widetilde{p_{45}}) \right\}.
 \end{aligned}$$

8.3.4 The complete real-virtual subtraction term $d\hat{\sigma}_{q\bar{q},\text{NNLO},N_c^2}^{\text{T}}$

Putting everything together, the three-parton level contribution $d\hat{\sigma}_{q\bar{q},\text{NNLO},N_c^2}^{\text{T}}$ to be combined with the real-virtual contributions $d\hat{\sigma}_{q\bar{q},\text{NNLO},N_c^2}^{\text{RV}}$ can be conveniently written in the

following way

$$\begin{aligned}
 d\hat{\sigma}_{q\bar{q},\text{NNLO},N_c^2}^{\text{T}} &= \mathcal{N}_{\text{NNLO}}^{q\bar{q},\text{RV}} N_c^2 \int \frac{dx_1}{x_1} \frac{dx_2}{x_2} d\Phi_3(p_3, p_4, p_5; x_1 p_1, x_2 p_2) \quad (8.23) \\
 &\times \left\{ - \left(\frac{1}{2} \mathcal{D}_{Qgg}^0(\epsilon, s_{35}, x_1, x_2) + \frac{1}{2} \mathcal{D}_{q,gg}^0(\epsilon, s_{\bar{1}5}, x_1, x_2) + \mathcal{A}_{q,Qg}^0(\epsilon, s_{\bar{2}4}, x_2, x_1) \right. \right. \\
 &- \frac{1}{2} \Gamma_{q\bar{q}}^{(1)}(x_1) \delta(1-x_2) - \frac{1}{2} \Gamma_{q\bar{q}}^{(1)}(x_2) \delta(1-x_1) \left. \right) |\mathcal{M}_5^0(3_Q, 5_g, \hat{1}_q; \hat{2}_{\bar{q}}, 4_{\bar{Q}})|^2 J_2^{(3)}(p_3, p_4, p_5) \\
 &- \left(\frac{1}{2} \mathcal{D}_{Qgg}^0(\epsilon, s_{45}, x_1, x_2) + \frac{1}{2} \mathcal{D}_{q,gg}^0(\epsilon, s_{\bar{2}5}, x_2, x_1) + \mathcal{A}_{q,Qg}^0(\epsilon, s_{\bar{1}3}, x_1, x_2) \right. \\
 &- \frac{1}{2} \Gamma_{q\bar{q}}^{(1)}(x_1) \delta(1-x_2) - \frac{1}{2} \Gamma_{q\bar{q}}^{(1)}(x_2) \delta(1-x_1) \left. \right) |\mathcal{M}_5^0(3_Q, \hat{1}_q; \hat{2}_{\bar{q}}, 5_g, 4_{\bar{Q}})|^2 J_2^{(3)}(p_3, p_4, p_5) \\
 &+ \left[A_3^{1,lc}(3_Q, 5_g, \hat{1}_q) \delta(1-x_1) \delta(1-x_2) + \left(\frac{1}{2} \mathcal{D}_{Qgg}^0(\epsilon, s_{35}, x_1, x_2) + \frac{1}{2} \mathcal{D}_{q,gg}^0(\epsilon, s_{\bar{1}5}, x_1, x_2) \right. \right. \\
 &- \left. \left. \mathcal{A}_{q,Qg}^0(\epsilon, s_{\bar{1}35}, x_1, x_2) \right) A_3^0(3_Q, 5_g, \hat{1}_q) \right] |\mathcal{M}_4^0((\tilde{35})_Q, 4_{\bar{Q}}, \hat{2}_{\bar{q}}, \hat{1}_q)|^2 J_2^{(2)}(p_{\tilde{35}}, p_4) \\
 &+ \left[A_3^{1,lc}(4_{\bar{Q}}, 5_g, \hat{2}_{\bar{q}}) \delta(1-x_1) \delta(1-x_2) + \left(\frac{1}{2} \mathcal{D}_{Qgg}^0(\epsilon, s_{45}, x_1, x_2) + \frac{1}{2} \mathcal{D}_{q,gg}^0(\epsilon, s_{\bar{2}5}, x_2, x_1) \right. \right. \\
 &- \left. \left. \mathcal{A}_{q,Qg}^0(\epsilon, s_{\bar{2}45}, x_2, x_1) \right) A_3^0(4_{\bar{Q}}, 5_g, \hat{2}_{\bar{q}}) \right] |\mathcal{M}_4^0(3_Q, (\tilde{45})_{\bar{Q}}, \hat{2}_{\bar{q}}, \hat{1}_q)|^2 J_2^{(2)}(p_3, p_{\tilde{45}}) \\
 &+ A_3^0(3_Q, 5_g, \hat{1}_q) \left[|\mathcal{M}_{4,1}^{[lc]}((\tilde{35})_Q, 4_{\bar{Q}}, \hat{2}_{\bar{q}}, \hat{1}_q)|_{\text{NLO}}^2 \delta(1-x_1) \delta(1-x_2) \right. \\
 &+ \left(\mathcal{A}_{q,Qg}^0(\epsilon, s_{\bar{1}35}, x_1, x_2) + \mathcal{A}_{q,Qg}^0(\epsilon, s_{\bar{2}4}, x_2, x_1) \right. \\
 &- \left. \frac{1}{2} \Gamma_{q\bar{q}}^{(1)}(x_1) \delta(1-x_2) - \frac{1}{2} \Gamma_{q\bar{q}}^{(1)}(x_2) \delta(1-x_1) \left. \right) |\mathcal{M}_4^0((\tilde{35})_Q, 4_{\bar{Q}}, \hat{2}_{\bar{q}}, \hat{1}_q)|^2 \right] J_2^{(2)}(p_{\tilde{35}}, p_4) \\
 &+ A_3^0(4_{\bar{Q}}, 5_g, \hat{2}_{\bar{q}}) \left[|\mathcal{M}_{4,1}^{[lc]}(3_Q, (\tilde{45})_{\bar{Q}}, \hat{2}_{\bar{q}}, \hat{1}_q)|_{\text{NLO}}^2 \delta(1-x_1) \delta(1-x_2) \right. \\
 &+ \left(\mathcal{A}_{q,Qg}^0(\epsilon, s_{\bar{2}45}, x_2, x_1) + \mathcal{A}_{q,Qg}^0(\epsilon, s_{\bar{1}3}, x_1, x_2) \right. \\
 &- \left. \frac{1}{2} \Gamma_{q\bar{q}}^{(1)}(x_1) \delta(1-x_2) - \frac{1}{2} \Gamma_{q\bar{q}}^{(1)}(x_2) \delta(1-x_1) \left. \right) |\mathcal{M}_4^0(3_Q, (\tilde{45})_{\bar{Q}}, \hat{2}_{\bar{q}}, \hat{1}_q)|^2 \right] J_2^{(2)}(p_3, p_{\tilde{45}}) \\
 &+ b_0 \log \left(\frac{\mu^2}{|s_{\bar{1}35}|} \right) A_3^0(3_Q, 5_g, \hat{1}_q) \delta(1-x_1) \delta(1-x_2) |\mathcal{M}_4^0((\tilde{35})_Q, 4_{\bar{Q}}, \hat{2}_{\bar{q}}, \hat{1}_q)|^2 J_2^{(2)}(p_{\tilde{35}}, p_4) \\
 &+ b_0 \log \left(\frac{\mu^2}{|s_{\bar{2}45}|} \right) A_3^0(4_{\bar{Q}}, 5_g, \hat{2}_{\bar{q}}) \delta(1-x_1) \delta(1-x_2) |\mathcal{M}_4^0(3_Q, (\tilde{45})_{\bar{Q}}, \hat{2}_{\bar{q}}, \hat{1}_q)|^2 J_2^{(2)}(p_3, p_{\tilde{45}}) \left. \right\}.
 \end{aligned}$$

The pole part of the terms which contain tree-level five-parton matrix elements squared exactly cancel the explicit ϵ -poles of the real-virtual contributions $d\hat{\sigma}_{q\bar{q},\text{NNLO},N_c^2}^{\text{RV}}$. On the other hand, the content of the square brackets [...] is free of poles in ϵ .

From all terms in $d\hat{\sigma}_{q\bar{q},\text{NNLO},N_c^2}^{\text{T}}$, only those corresponding to real-virtual subtraction terms

$$d\hat{\sigma}_{q\bar{q},\text{NNLO},N_c^2}^{\text{VS}} = d\hat{\sigma}_{q\bar{q},\text{NNLO},N_c^2}^{\text{VS},a} + d\hat{\sigma}_{q\bar{q},\text{NNLO},N_c^2}^{\text{VS},b} + d\hat{\sigma}_{q\bar{q},\text{NNLO},N_c^2}^{\text{VS},d} \quad (8.24)$$

must be integrated and added back at the two-parton level with the double virtual contributions. The individual contributions in this sum were given in eqs. (8.15), (8.21) and (8.22).

We have shown in this section that, by construction, the counter term $d\hat{\sigma}_{q\bar{q},\text{NNLO},N_c^2}^{\text{T}}$ exactly cancels the explicit infrared poles of the real-virtual contributions. For the three-parton final state $d\hat{\sigma}_{q\bar{q},\text{NNLO},N_c^2}^{\text{RV}} - d\hat{\sigma}_{q\bar{q},\text{NNLO},N_c^2}^{\text{T}}$ to be numerically integrable in four dimensions, it remains to be shown that the real-virtual counter term $ds_{q\bar{q},\text{NNLO},N_c^2}^{\text{T}}$ constitutes a good approximation of the real-virtual contributions in the soft and collinear limits. We shall address this issue in the next section with a series of numerical tests employing the amplitudes obtained with OPENLOOPS as described in section 7.

9 Numerical tests of soft and collinear cancellations

The double real and real-virtual contributions to heavy quark pair production in the $q\bar{q}$ channel presented in sections 5 and 7 have been implemented in a `Fortran` code together with the corresponding subtraction terms $d\hat{\sigma}_{q\bar{q},\text{NNLO},N_c^2}^{\text{S}}$ and $d\hat{\sigma}_{q\bar{q},\text{NNLO},N_c^2}^{\text{T}}$. In this section we investigate how well these subtraction terms fulfil their purpose of approximating $d\hat{\sigma}_{q\bar{q},\text{NNLO},N_c^2}^{\text{RR}}$ and $d\hat{\sigma}_{q\bar{q},\text{NNLO},N_c^2}^{\text{RV}}$ in all unresolved limits. In the case of the real-virtual contributions, the quality of the cancellations in the infrared regions provides also important insights into the numerical stability of the amplitudes.

For each singular region we used a series of phase-space samples generated with `RAMBO` [76] by requiring an increasingly small distance, parametrised in terms of appropriate parameters x_k , from the relevant singularity. In the next two sections, we will quantify the level of the real-real and real-virtual cancellations as

$$\delta_{\text{RR}} = \left| \frac{d\hat{\sigma}_{q\bar{q},\text{NNLO},N_c^2}^{\text{RR}}}{d\hat{\sigma}_{q\bar{q},\text{NNLO},N_c^2}^{\text{S}}} - 1 \right|, \tag{9.1}$$

and

$$\delta_{\text{RV}} = \left| \frac{d\hat{\sigma}_{q\bar{q},\text{NNLO},N_c^2}^{\text{RV}}}{d\hat{\sigma}_{q\bar{q},\text{NNLO},N_c^2}^{\text{T}}} - 1 \right|, \tag{9.2}$$

respectively. To demonstrate the consistency and stability of the subtractions we will show that the δ_{RR} and δ_{RV} distributions converge to zero in all relevant $x_k \rightarrow 0$ limits. On the right-hand-side of (9.2) the consistent subtraction of explicit infrared singularities in the numerator and denominator is implicitly understood. Each of the employed samples consists of about 10^4 points with $\sqrt{\hat{s}} = 1 \text{ TeV}$,³ and $m_Q = 174.3 \text{ GeV}$.

9.1 Tests of the double real contributions

We start by discussing infrared cancellations for the double real contribution $q\bar{q} \rightarrow Q\bar{Q}gg$ in leading colour approximation. To this end we generated $2 \rightarrow 4$ phase space points near all possible single and double unresolved limits. The $2 \rightarrow 4$ tree-level matrix elements in (9.1) have been computed with an in-house `Mathematica` program based on `Qgraf` [77] and numerically checked against `MadGraph` [78] for a few phase space points.

³For simplicity, \hat{s} will be denoted by s in this section.

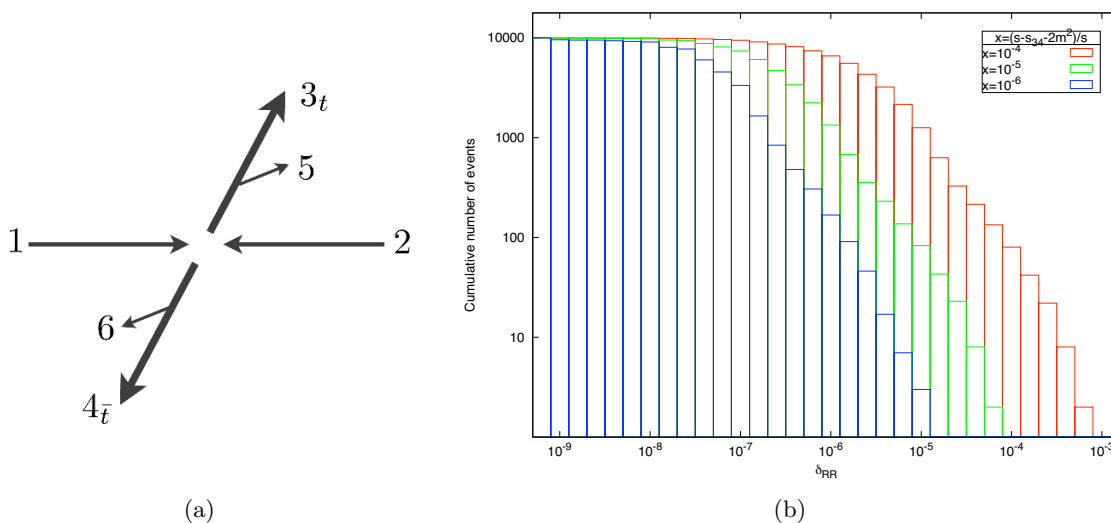


Figure 1. (a) Sketch of a double soft event. (b) Cumulative distributions of δ_{RR} for 10^4 double soft phase space points with three different values of x .

9.1.1 Double soft limits

As shown in figure 1(a), a double soft phase space point is characterised by the heavy quark pair taking nearly the full energy of the event, and therefore a suitable variable to control the proximity of the events to the singular limit is $x = (s - s_{34} - 2m_Q^2)/s$. In figure 1(b) we show cumulative distributions of δ_{RR} for three different values of x . Each bin contains the total number of points for which the relative difference between matrix element and subtraction term is larger than δ_{RR} . The good convergence of the subtraction terms to the double real contributions as the singularity is approached can be seen in the fact that the events accumulate more rapidly near $\delta_{RR} = 0$ as the control variable x is taken to be smaller.

9.1.2 Triple collinear limits

Since we do not subtract collinear limits involving the massive fermions because they are regulated by the large value of m_Q , the only types of triple collinear limits that we must consider are of initial-final nature as depicted in figure 2(a). The control variable in this case is defined as $x = s_{i56}/s$, where $i = 1, 2$. In figure 2(b) we show how, as we take smaller values of x , i.e. as we get closer in phase space to the singularity of the real radiation matrix element, there is a more rapid accumulation of events around $\delta_{RR} = 0$, signalling again that the approximation is correct. These results correspond to the triple collinear limit $p_1 || p_5 || p_6$. Similar results are obtained for $p_2 || p_5 || p_6$.

9.1.3 Soft-collinear limits

As shown in figure 3(a), soft-collinear limits occur when one of the final state gluons becomes soft and the remaining one becomes collinear to an initial state leg. To probe the soft-collinear regions of phase space we generate events with a soft gluon and rotate the

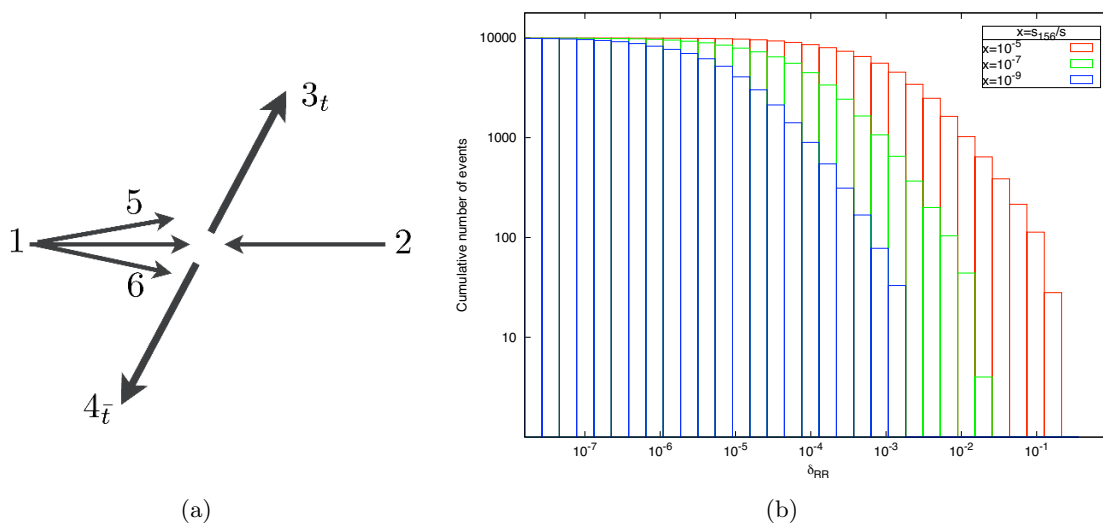


Figure 2. (a) Sketch of a triple collinear event. (b) Cumulative distributions of δ_{RR} for 10^4 triple collinear phase space points with three different values of x .

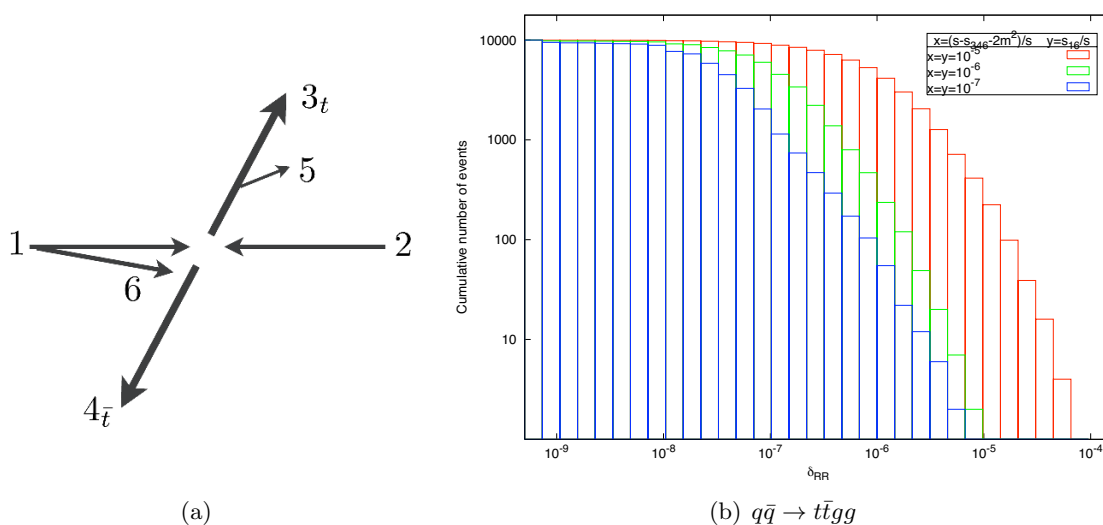


Figure 3. (a) Sketch of a soft-collinear event. (b) Cumulative distributions of δ_{RR} for 10^4 soft-collinear phase space points with three different values of x and y .

final state to make the hard gluon collinear to one of the initial state legs. We employ two control variables x and y . If we consider the limit where gluon (5) is soft and (6) becomes collinear to the incoming leg (1), x is defined as $x = (s - s_{346} - 2m_Q^2)/s$ and y is given by $y = s_{16}/s$. As can be seen if figure 3(b) the convergence of the subtraction term to the partonic double real contribution is once more achieved.

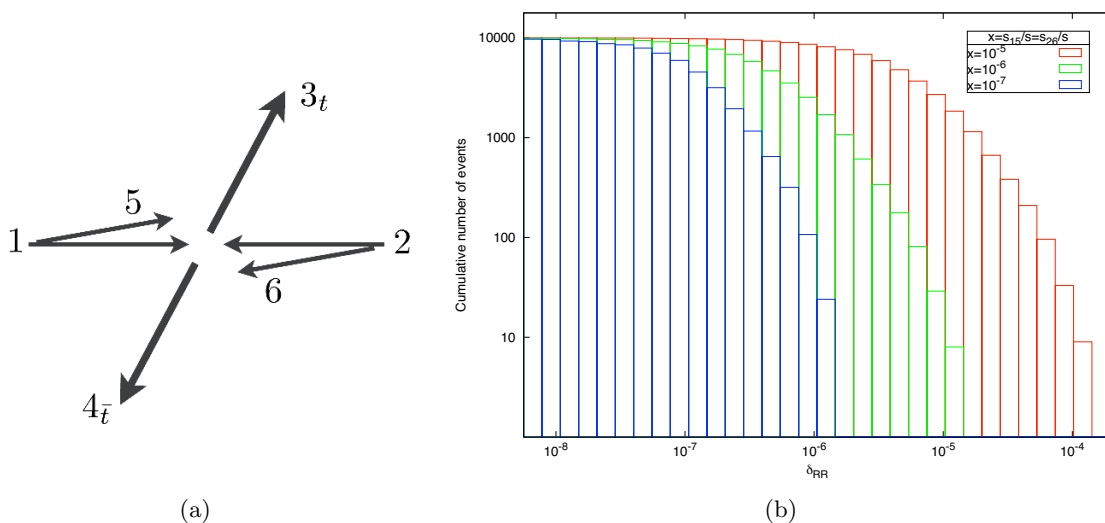


Figure 4. (a) Sketch of a double collinear event. (b) Cumulative distributions of δ_{RR} for 10^4 double collinear phase space points with three different values of x .

9.1.4 Double collinear limits

Due to the fact that the quasi-collinear limits involving the heavy (anti) quark do not require subtraction, the only double collinear limits in which the double real contributions can diverge are the two simultaneous single collinear limits depicted in figure 4(a). To control the proximity of the phase space points to the double collinear singularity $p_1||p_5$, $p_2||p_6$ we employ the variable $x = s_{15}/s = s_{26}/s$. As can be seen from figure 4(b), our numerical results show that behaviour of the double real corrections in their double collinear limits, is correctly described by our subtraction terms. Similar results are obtained for the double collinear limit $p_1||p_6$, $p_2||p_5$.

9.1.5 Single soft limits

Single soft limits are characterised by having the three hard final state particles taking nearly the full center-of-mass energy of the event leaving one of the final state gluons with an almost vanishing energy. Consequently, if the soft-gluon momentum is p_5 , we define the control variable as $x = (s_{346} - s - 2m_Q^2)/s$. In figure 5(b) we show how as the singularity is approached by making x closer to zero, events accumulate more rapidly near $\delta_{RR} = 0$. Analogous results are obtained when the soft-gluon momentum is p_6 .

9.1.6 Final-final single collinear limit

As depicted in figure 6(a), final-final collinear limits occur when the final state gluons with momentum p_5 and p_6 become collinear. This divergence is approached as the ratio $x = s_{56}/s$ gets closer to zero.

As discussed previously in [4, 26, 39, 42], because of the presence of angular correlations between the splitting functions and the reduced matrix elements, in single collinear limits corresponding to the gluon splittings $g \rightarrow gg$ and $g \rightarrow q\bar{q}$, antenna subtraction terms do

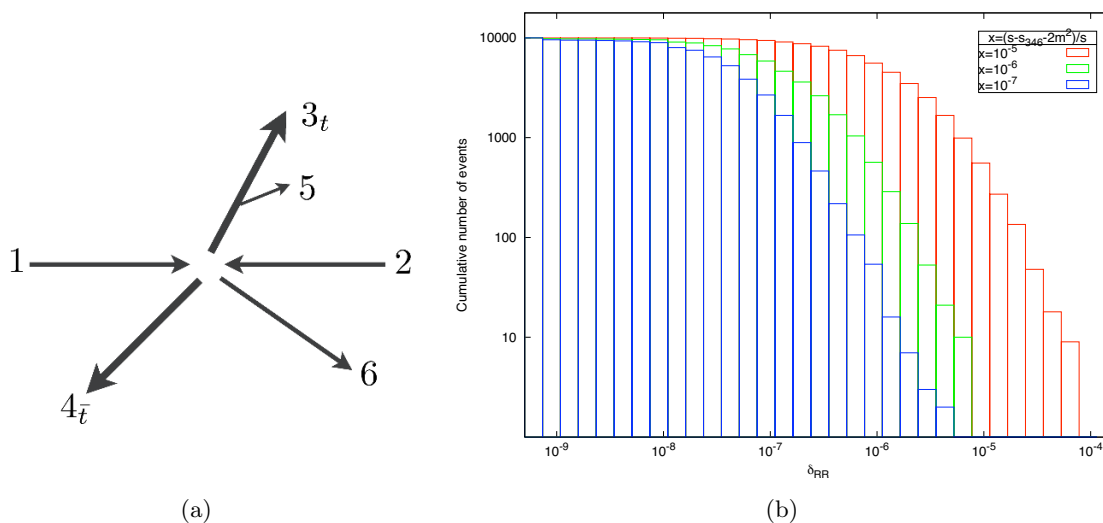


Figure 5. (a) Sketch of a single soft event. (b) Cumulative distributions of δ_{RR} for 10^4 single soft phase space points with three different values of x .

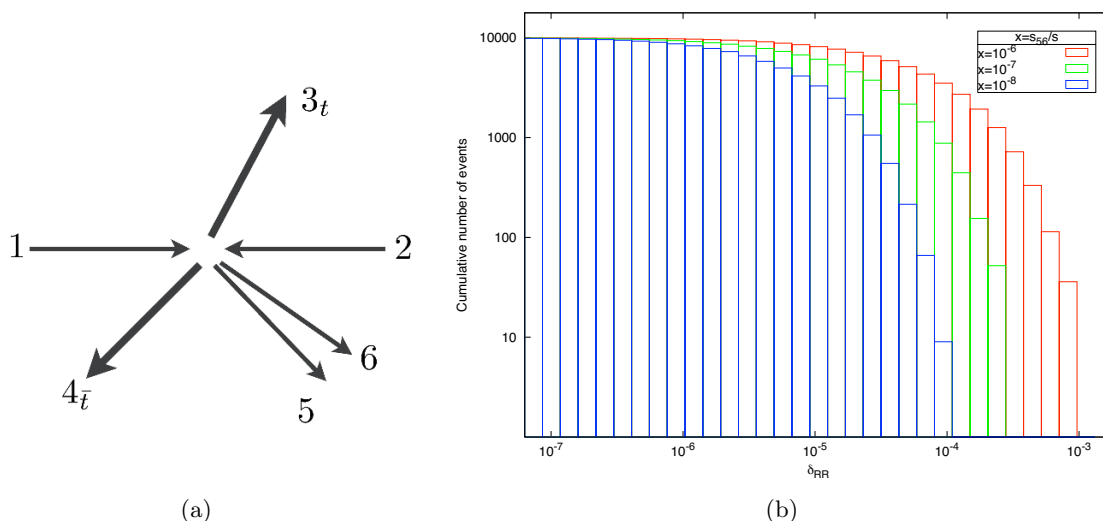


Figure 6. (a) Sketch of a final-final single collinear limit. (b) Cumulative distributions of δ_{RR} for 10^4 final-final single collinear phase space points with three different values of x .

not reproduce the behaviour of the real radiation matrix elements in an exact point-by-point manner but in a two-to-two point manner. This is due to the fact that the angular correlations which spoil the convergence are averaged out when a single collinear phase space point is combined with another single collinear point which differs from the original by a $\pi/2$ rotation of the collinear pair around the collinear axis. A thorough discussion of this issue can be found in [42]. In the histogram of figure 6(b) the aforementioned angular averaging has been performed.

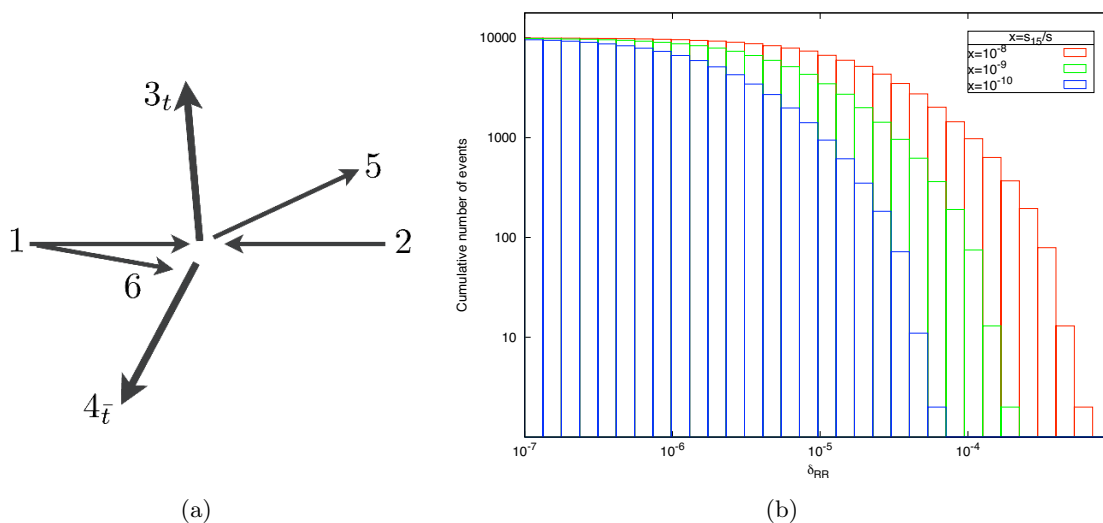


Figure 7. (a) Sketch of an initial-final single collinear limit. (b) Cumulative distributions of δ_{RR} for 10^4 initial-final single collinear phase space points with three different values of x .

9.1.7 Initial-final single collinear limits

The topology of the single initial-final collinear events is illustrated in figure 7(a), and the corresponding control variable is defined analogously to the final-final case. There are four different collinear limits in the partonic process $q\bar{q} \rightarrow Q\bar{Q}gg$, namely $p_i||p_j$ with $i = 1, 2$ and $j = 5, 6$. Figure 7(b) contains our results for the limit $p_1||p_6$, which clearly show that the subtraction terms correctly approximate the double real radiation contributions in this limit. The singularity in figure 7(b) is parametrised in terms of $x = s_{16}/s$, and similar histograms are obtained for the other three limits of this kind.

9.2 Tests of the real-virtual contributions

In this section we study the cancellation between the real-virtual matrix elements and the corresponding subtraction terms. Due to the lower multiplicity of the $2 \rightarrow 3$ final state and the fact that the heavy quark mass regulates all final-final single collinear limits, the singular structure of the real-virtual contributions is simpler than that of the double real pieces. Indeed, only the soft limit $p_5 \rightarrow 0$ and the initial-final collinear limits $p_i||p_5$ ($i = 1, 2$) must be considered.

The real-virtual cancellations provide a strong check both of the correctness of the subtraction terms presented in section 8 and of the numerical stability of the OPENLOOPS amplitudes discussed in section 7. In the vicinity of the soft and collinear singularities matrix elements and subtraction terms are strongly enhanced, and the cancellation can amount to several digits. While this requires augmented numerical accuracy in the unsubtracted amplitudes, numerical instabilities related to Gram determinants can be strongly amplified in the vicinity of the singularities. It is thus crucial to prevent that the infrared cancellations are spoiled by numerical instabilities of the amplitudes. To this end, OPENLOOPS implements an instability trigger, which monitors the numerical accuracy of the

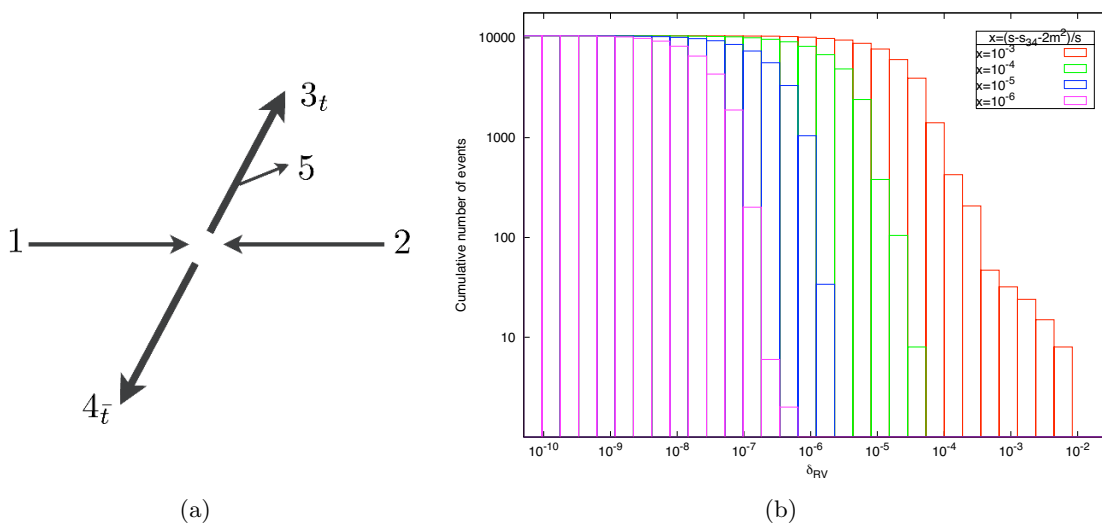


Figure 8. (a) Sketch of soft event limit. (b) Distribution of R for 10^4 soft phase space points with three different values of x .

results by means of a scaling test. The amplitudes are evaluated a second time by rescaling all dimensionful input parameters by a constant factor ξ , and the output is rescaled back by a factor ξ^{-d} depending on its mass dimension d . The agreement with the original matrix element serves as an accuracy estimate, and phase-space points that are not sufficiently stable are automatically reevaluated with a rescue system. Results presented in the following have been obtained with CUTTOOLS as a reduction back end of OPENLOOPS, using the quadruple-precision mode of CUTTOOLS as a rescue system for unstable points. Matrix elements are first evaluated in double precision and are reevaluated in quadruple precision if their estimated double-precision accuracy is less than 3 correct digits or smaller than the observed cancellation δ_{RV} with the subtraction term. The stability of the quadruple-precision output is assessed with an additional scaling test. Due to the fact that the scaling test tends to overestimate the accuracy, following a universal distribution, one must demand for an accuracy which is higher than the cancellation by about the width of this distribution. For calibration we determine the width from double precision scalings, using a quadruple precision result as reference point, finding a width of around one decimal digit. If needed, the accuracy estimate can be improved using multiple scalings.

Figure 8(b) shows the degree of cancellation δ_{RV} in the soft region for samples of 10^4 phase space points for several values of the control variable $x = (s - s_{34} - 2m_Q^2)/s$, which describes the softness of the phase space points. As the singularity is approached with smaller values of x , the subtraction term $d\hat{\sigma}_{q\bar{q},NNLO,N_c^2}^T$ converges to the real-virtual corrections $d\hat{\sigma}_{q\bar{q},NNLO,N_c^2}^{RV}$ as expected. Similarly, figure 9(b) demonstrates the consistency of the cancellation in the collinear region, parametrised by the control variable $x = s_{15}/s$.

For what concerns the numerical stability of the matrix elements, in the collinear region it turns out that for the depicted values of the control variable, double precision provides sufficient stability (in the sense of the criterion described above) for the vast majority of

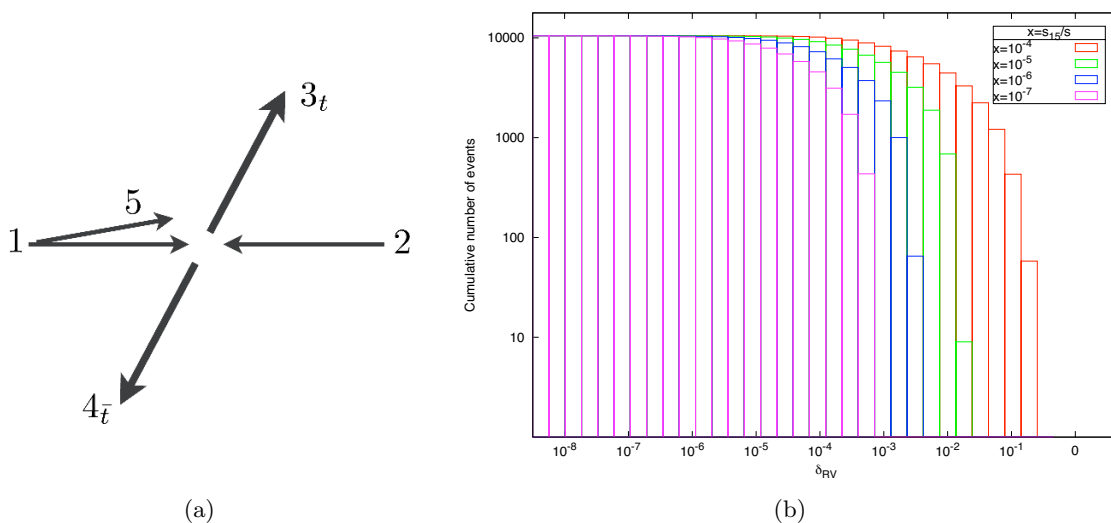


Figure 9. (a) Sketch of collinear event limit. (b) Distribution of R for 10^4 collinear phase space points with three different values of x .

the phase space points. This also holds in the soft regions with $x = 10^{-3}$ and $x = 10^{-4}$. Starting at the soft sample with $x = 10^{-5}$, a sizable fraction of the matrix elements must be evaluated in quadruple precision. However, it should be pointed out that this deep infrared region ($x = 10^{-5}$ corresponds to a gluon energy around 5 MeV) is not relevant for physical applications based on antenna subtraction. In fact, as will be shown in section 10, double precision results are sufficiently stable to obtain integrated cross sections with permil level accuracy.

Detailed findings on the numerical stability and the reliability of the trigger system are summarised in table 2. The trigger system to detect unstable points from scalings can lead to false positive results, meaning that points will be evaluated in quadruple precision although they were actually stable enough. This is a side effect of avoiding false negative results, meaning points which are regarded as stable although they are not. Note that in the $x = 10^{-6}$ soft sample even quadruple precision is no more enough to observe full cancellation for all points, and $\mathcal{O}(5\%)$ of the points are tagged as unstable. This shows in the tail of the corresponding distribution in figure 8(b), where the two bins around $x = 10^{-6.5}$ are populated only by unstable points.

10 Stability of the integration over the three-particle phase space

As a further and more realistic test of the stability of the real-virtual matrix elements and of the related subtraction terms we have integrated the difference $d\sigma_{q\bar{q},\text{NNLO},N_c^2}^{\text{RV}} - d\sigma_{q\bar{q},\text{NNLO},N_c^2}^{\text{T}}$ inclusively over the three-particle phase space employing a parton level event generator. In this integration, we impose a technical cut on the gluon p_T using the control variable $y_{\text{cut}} = p_T^g/\sqrt{\hat{s}}$, in such a way that no events are generated too close to the soft and collinear singularities. Naturally, since the entire phase space ought to be covered in the

sample	unstable	triggered	false negative
soft $x = 10^{-3}$	0.0004	0.0009	0
soft $x = 10^{-4}$	0.008	0.06	0.0001
soft $x = 10^{-5}$	0.31	0.70	0.002
soft $x = 10^{-6}$	0.96	1	0.001
collinear $x = 10^{-4}$	0	0	0
collinear $x = 10^{-5}$	0	0	0
collinear $x = 10^{-6}$	0.0001	0.0008	0
collinear $x = 10^{-7}$	0.009	0.12	0.0002

Table 2. For the samples of phase space points of figures 8(b) and 9(b) the fraction of points is shown which are unstable in double precision (“unstable”), meaning that the accuracy is not high enough to observe full cancellation between matrix element and subtraction term. “triggered” is the fraction of points which is detected as unstable by the trigger system described in the text, and subsequently evaluated in quadruple precision, and “false negative” is the fraction of points which are unstable, but not triggered.

integration, y_{cut} must be taken small. While the unsubtracted $d\sigma^{\text{RV}}$ contribution would lead to a logarithmic divergence in the limit $y_{\text{cut}} \rightarrow 0$, the subtraction term guarantees a smooth convergence at small y_{cut} . In practice the integral should reach a plateau for a sufficiently small value of the cut, $y_{\text{cut}}^{\text{max}}$, i.e. for any $y_{\text{cut}} < y_{\text{cut}}^{\text{max}}$ the integral of $d\sigma^{\text{RV}} - d\sigma^{\text{T}}$ should remain stable within Monte Carlo integration errors. This is clearly confirmed in figure 10, where we plot the ratio

$$\frac{\sigma_{q\bar{q},\text{NNLO},N_c^2}^{\text{RV}} - \sigma_{q\bar{q},\text{NNLO},N_c^2}^{\text{T}}}{\sigma_{q\bar{q},\text{LO}} \tag{10.1}$$

for $pp \rightarrow t\bar{t}$ as a function of y_{cut} . For both the NNLO real-virtual subtracted contributions and the LO normalisation we used $\sqrt{s} = 7 \text{ TeV}$, $m_t = 174.3 \text{ GeV}$ and set the renormalisation and factorisation scales to $\mu_R = \mu_F = m_t$. We employed the MSTW2008nnlo90cl and MSTW2008lo90cl PDF sets for the NNLO and the LO contributions respectively. The high stability of the integration results for values of y_{cut} below $y_{\text{cut}}^{\text{max}} \sim 10^{-3}$ provides solid evidence of the correctness of the real-virtual subtraction terms of eq. (8.23). Moreover, using OPENLOOPS in combination with CUTTOOLS, it turns out that the stability plateau is reached before encountering significant instabilities in double precision. For $y_{\text{cut}} = 10^{-3}(10^{-4})$ we find that only 1 out of $10^5(10^4)$ events requires a quadruple precision reevaluation. This allows for a highly efficient evaluation of the real-virtual contributions based on double precision for the vast majority of the phase space points.

11 Summary and outlook

In this paper, we presented the double real and real-virtual NNLO contributions to hadronic $t\bar{t}$ production in the quark-antiquark annihilation channel. The computation is performed in leading colour approximation using the antenna subtraction method, which was extended to deal with the presence of a massive fermion pair in the final state. The real-real

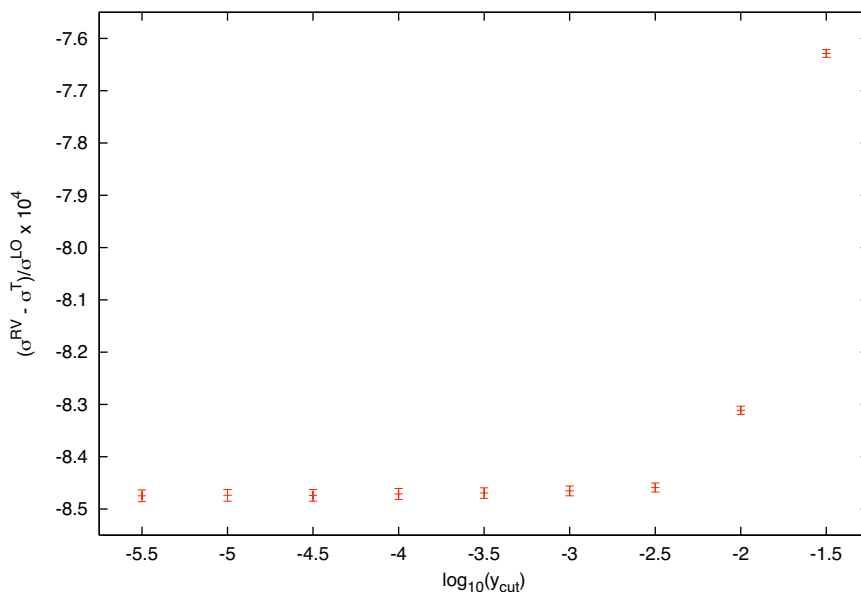


Figure 10. Inclusive phase space integral of $d\sigma_{q\bar{q},\text{NNLO},N_c^2}^{\text{RV}} - d\sigma_{q\bar{q},\text{NNLO},N_c^2}^{\text{T}}$ normalised to $\sigma_{q\bar{q},\text{LO}}$ for different values of y_{cut} . The error bars correspond to the Monte Carlo uncertainty.

subtraction terms, presented in section 5, approximate the corresponding $2 \rightarrow 4$ tree matrix elements in all single and double unresolved limits, while the real-virtual subtraction terms, presented in section 8, remove the explicit infrared poles present in the $2 \rightarrow 3$ one-loop matrix elements, as well as the implicit singularities that occur in the soft and collinear limits. The relevant new tree-level four-parton and three-parton massive initial-final antennae functions, together with their unresolved counterparts, have been derived in sections 3 and 4.

The correctness of the subtraction and its numerical stability have been demonstrated with detailed cancellation checks in section 9. To this end, the convergence of the subtracted real-real and real-virtual contributions was studied by means of event samples generated in several phase space slices with increasingly small distance from all relevant single and double-unresolved limits.

To compute the one-loop $q\bar{q} \rightarrow t\bar{t}g$ real-virtual contributions we used OPENLOOPS in combination with the CUTTOOLS implementation of OPP reduction. This provides interesting insights into the potential benefits of new automated one-loop generators in the framework of NNLO calculations. While the high CPU speed of OPENLOOPS represents an obvious attractive feature, numerical instabilities could represent a very serious issue for NNLO applications. In fact, while the strong cancellations between one-loop amplitudes and related subtraction terms call for augmented numerical accuracy in the soft and collinear regions, the typical Gram-determinant instabilities of one-loop amplitudes tend to be strongly enhanced in the infrared regions. It is thus important to make sure that the infrared subtractions are not spoiled by numerical instabilities of the one-loop matrix elements. To this end, using scaling tests as well as the quadruple precision mode of the CUTTOOLS library, we performed detailed studies of the interplay between one-loop insta-

bilities and infrared cancellations. On the one hand, it turns out that quadruple precision is essential (and at some point even insufficient) to avoid excessive numerical instabilities in the deep infrared regime. On the other hand, we found that such instabilities arise only at very small gluon energies and are essentially irrelevant for an NNLO calculation based on antenna subtraction. In particular, using a realistic infrared cut-off, one-loop amplitudes in double precision turn out to be sufficiently stable for the vast majority (more than 99.99%) of the phase space points. The fact that quadruple precision can be avoided almost completely implies a drastic efficiency improvement for the integration of the real-virtual NNLO contributions.

In order to complete the NNLO corrections to top-antitop production in the quark-antiquark channel at leading colour, the 2-parton contributions $d\hat{\sigma}_{\text{NNLO}}^{\text{VV}}$ and its corresponding counterterm $d\hat{\sigma}_{\text{NNLO}}^{\text{U}}$ need to be added to the 3 and 4-parton contributions ($d\hat{\sigma}_{\text{NNLO}}^{\text{RV}}$ and $d\hat{\sigma}_{\text{NNLO}}^{\text{RR}}$) and their corresponding subtraction term $d\hat{\sigma}_{\text{NNLO}}^{\text{T}}$ and $d\hat{\sigma}_{\text{NNLO}}^{\text{S}}$ derived in this paper. The 2-loop contributions participating in $d\hat{\sigma}_{\text{NNLO}}^{\text{VV}}$ are known. However $d\hat{\sigma}_{\text{NNLO}}^{\text{U}}$ is presently unknown. In it, essential unknown ingredients are the integrated 4-parton tree level antenna $A_4^0(1_Q, 3_g, 4_g, \hat{2}_q)$ and the integrated one-loop antenna $A_3^{1,lc}(1_Q, 3_g, \hat{2}_q)$ which have been presented in unintegrated form together with their infrared limits for the first time in this paper.

The results presented in this paper constitute a major step towards a complete NNLO calculation, based on antenna subtraction, of top-pair production in the quark-antiquark channel. Our final goal is then the construction of an NNLO parton-level event generator for the two, three and four partonic contributions, which will be applicable to any fully differential observable at hadron colliders.

Acknowledgments

We are grateful to S. Dittmaier and J. Pires for many useful discussions. This research was supported by the Swiss National Science Foundation (SNF) under contracts PP00P2-139192, PP00P2-128552, and PBEZP2-145917 and in part by the European Commission through the ‘LHCPhenoNet’ (PITN-GA-2010-264564), ‘HiggsTools’ (PITN-GA-2012-316704) Initial Training Networks and the ERC Advanced Grant ‘MC@NNLO’ (340983), which are hereby acknowledged.

A Single unresolved tree-level universal factors

In single unresolved limits, tree-level colour-ordered matrix elements squared and antenna functions yield universal single unresolved factors. These well-known universal factors associated to collinear limits are Altarelli-Parisi splitting functions [51], and those occurring in soft limits are soft eikonal factors. Those needed in the context of this paper are given below.

A.1 The collinear splitting functions

In this paper we have considered the collinear radiation emitted from a massive fermion to be regulated by the mass of this fermion. Consequently, we shall here restrict our-

selves to present the usual massless Altarelli-Parisi splitting functions arising in collinear configurations involving only massless partons.

When a pair of massless final state particles i and j with momentum p_i and p_j become collinear and cluster into a parent parton of momentum $p_k = p_i + p_j$ the kinematics of the collinear configuration can be described as

$$p_i \rightarrow z p_k \quad p_j \rightarrow (1 - z)p_k, \tag{A.1}$$

where z is the momentum fraction of one of the partons in the collinear pair. The specific form of the splitting function depends on the species of partons i and j . There are three different splitting functions, corresponding to the three possible final-final parton-parton splittings. In conventional dimensional regularisation, they are given by

$$P_{qg \rightarrow q}(z) = \frac{1 + (1 - z)^2 - \epsilon z^2}{z} \tag{A.2}$$

$$P_{q\bar{q} \rightarrow g}(z) = \frac{z^2 + (1 - z)^2 - \epsilon}{1 - \epsilon} \tag{A.3}$$

$$P_{gg \rightarrow g}(z) = 2 \left[\frac{z}{1 - z} + \frac{1 - z}{z} + z(1 - z) \right]. \tag{A.4}$$

When one of the collinear particles is in the initial state, the kinematics of the collinear limit can be described as

$$p_j \rightarrow z p_i \quad p_k \rightarrow (1 - z)p_i, \tag{A.5}$$

and the four splitting functions corresponding to the four different parton-parton splittings read

$$P_{q\hat{q} \rightarrow g}(z) = \frac{1 + z^2 - \epsilon(1 - z)^2}{(1 - \epsilon)(1 - z)^2} = \frac{1}{1 - z} \frac{1}{1 - \epsilon} P_{qg \rightarrow q}(1 - z) \tag{A.6}$$

$$P_{\hat{q}g \rightarrow \hat{q}}(z) = \frac{1 + (1 - z)^2 - \epsilon z^2}{z(1 - z)} = \frac{1}{1 - z} P_{qg \rightarrow q}(z) \tag{A.7}$$

$$P_{q\hat{g} \rightarrow \hat{q}}(z) = \frac{z^2 + (1 - z)^2 - \epsilon}{1 - z} = \frac{1 - \epsilon}{1 - z} P_{q\bar{q} \rightarrow g}(z) \tag{A.8}$$

$$P_{g\hat{g} \rightarrow \hat{g}}(z) = \frac{2(1 - z + z^2)^2}{z(1 - z)^2} = \frac{1}{1 - z} P_{gg \rightarrow g}(z). \tag{A.9}$$

The additional factors $(1 - \epsilon)$ and $1/(1 - \epsilon)$ account for the different number of polarizations of quark and gluons in the cases in which the particle entering the hard processes changes its type. The antiquark-gluon splitting functions are identical to the quark-gluon ones due to the invariance of the splitting under charge conjugation. In this paper, only the latter splitting functions arising in initial-final collinear configurations are employed.

A.2 The massive soft eikonal factor

When a gluon with momentum p_j becomes soft in a colour-ordered tree-level amplitude where it is colour connected to partons i and k with masses m_i and m_k respectively, the associated soft factor is given by [27, 40]

$$S_{ijk}(m_i, m_k) = \frac{2s_{ik}}{s_{ij}s_{jk}} - \frac{2m_i^2}{s_{ij}^2} - \frac{2m_k^2}{s_{jk}^2}. \tag{A.10}$$

When $m_i = m_k = 0$ this factor reduces to the usual massless soft eikonal factor.

B Colour-ordered infrared singularity operators

The explicit pole structure of colour-ordered matrix elements can be written in terms of colour-ordered infrared singularity operators $\mathbf{I}_{ij}^{(1)}$. Within the antenna subtraction method, the pole part of antennae as well as that of integrated tree-level three-parton antennae can be also captured by these operators.

If only massless particles are involved, the following set of operators is sufficient (in addition to the splitting kernels $\Gamma_{ij}^{(1)}(x)$) to express the pole structure of a QCD amplitude as well as that of a one-particle inclusive integral of a tree-level amplitude [22, 36]:

$$\mathbf{I}_{q\bar{q}}^{(1)}(\epsilon, s_{q\bar{q}}) = -\frac{e^{\epsilon\gamma_E}}{2\Gamma(1-\epsilon)} \left(\frac{|s_{q\bar{q}}|}{\mu^2}\right)^{-\epsilon} \left[\frac{1}{\epsilon^2} + \frac{3}{2\epsilon}\right] \quad (\text{B.1})$$

$$\mathbf{I}_{qg}^{(1)}(\epsilon, s_{qg}) = -\frac{e^{\epsilon\gamma_E}}{2\Gamma(1-\epsilon)} \left(\frac{|s_{qg}|}{\mu^2}\right)^{-\epsilon} \left[\frac{1}{\epsilon^2} + \frac{5}{3\epsilon}\right] \quad (\text{B.2})$$

$$\mathbf{I}_{gg}^{(1)}(\epsilon, s_{gg}) = -\frac{e^{\epsilon\gamma_E}}{2\Gamma(1-\epsilon)} \left(\frac{|s_{gg}|}{\mu^2}\right)^{-\epsilon} \left[\frac{1}{\epsilon^2} + \frac{11}{6\epsilon}\right] \quad (\text{B.3})$$

$$\mathbf{I}_{qg,F}^{(1)}(\epsilon, s_{qg}) = \frac{e^{\epsilon\gamma_E}}{2\Gamma(1-\epsilon)} \left(\frac{|s_{qg}|}{\mu^2}\right)^{-\epsilon} \frac{1}{6\epsilon} \quad (\text{B.4})$$

$$\mathbf{I}_{gg,F}^{(1)}(\epsilon, s_{gg}) = \frac{e^{\epsilon\gamma_E}}{2\Gamma(1-\epsilon)} \left(\frac{|s_{gg}|}{\mu^2}\right)^{-\epsilon} \frac{1}{3\epsilon}. \quad (\text{B.5})$$

When massive fermions denoted by Q of mass m_Q are involved, the following operators must also be considered [27]

$$\mathbf{I}_{Q\bar{Q}}^{(1)}(\epsilon, s_{Q\bar{Q}}) = -\frac{e^{\epsilon\gamma_E}}{2\Gamma(1-\epsilon)} \left(\frac{|s_{Q\bar{Q}}|}{\mu^2}\right)^{-\epsilon} \left[\frac{1}{\epsilon} \left(1 - \frac{1+r_0}{2\sqrt{r_0}} \ln\left(\frac{1+\sqrt{r_0}}{1-\sqrt{r_0}}\right)\right)\right] \quad (\text{B.6})$$

$$\mathbf{I}_{Q\bar{q}}^{(1)}(\epsilon, s_{Q\bar{q}}) = -\frac{e^{\epsilon\gamma_E}}{2\Gamma(1-\epsilon)} \left(\frac{|s_{Q\bar{q}}|}{\mu^2}\right)^{-\epsilon} \left[\frac{1}{2\epsilon^2} + \frac{5}{4\epsilon} + \frac{1}{2\epsilon} \ln\left(\frac{m_Q^2}{|s_{Q\bar{q}}|}\right)\right] \quad (\text{B.7})$$

$$\mathbf{I}_{Qg}^{(1)}(\epsilon, s_{Qg}) = -\frac{e^{\epsilon\gamma_E}}{2\Gamma(1-\epsilon)} \left(\frac{|s_{Qg}|}{\mu^2}\right)^{-\epsilon} \left[\frac{1}{2\epsilon^2} + \frac{17}{12\epsilon} + \frac{1}{2\epsilon} \ln\left(\frac{m_Q^2}{|s_{Qg}|}\right)\right] \quad (\text{B.8})$$

$$\mathbf{I}_{Qg,F}^{(1)}(\epsilon, s_{Qg}) = \frac{e^{\epsilon\gamma_E}}{2\Gamma(1-\epsilon)} \left(\frac{|s_{Qg}|}{\mu^2}\right)^{-\epsilon} \frac{1}{6\epsilon}, \quad (\text{B.9})$$

with

$$r_0 = 1 - \frac{4m_Q^2}{s_{Q\bar{Q}} + 2m_Q^2}. \quad (\text{B.10})$$

C The complete expression of $A_4^0(1_Q, 3_g, 4_g, \hat{2}_q)$

The full expression of the initial-final flavour-violating antenna $A_4^0(1_Q, 3_g, 4_g, \hat{2}_q)$ discussed in section 3 is given by

$$\begin{aligned}
 A_4^0(1_Q, 3_g, 4_g, \hat{2}_q) = & \frac{1}{(Q^2 + m_Q^2)} \left[-\frac{2}{s_{24}s_{34}} (2s_{12} + s_{13} - s_{134} - s_{234}) \right. \\
 & + \frac{1}{s_{13}s_{134}} (-9s_{12} + 5s_{234} + 3s_{24} - 8s_{34}) + \frac{1}{s_{134}^2} (3s_{12} + 4s_{13} - 3s_{234} + 3s_{34}) \\
 & + \frac{1}{s_{13}s_{234}} (-8s_{12} + 5s_{134} + 5s_{24} - 7s_{34}) + \frac{1}{s_{234}^2} (3s_{12} - 3s_{134} - 4s_{24} + 3s_{34}) \\
 & + \frac{1}{s_{13}s_{24}} (-2s_{12} + s_{134} + s_{234} - 4s_{34}) + \frac{1}{s_{24}s_{234}^2} (-s_{34}^2 - s_{12}s_{34} + s_{134}s_{34}) \\
 & + \frac{1}{s_{24}s_{134}} (8s_{12} + 5s_{13} - 5s_{234} + 7s_{34}) + \frac{1}{s_{13}s_{134}^2} (s_{34}^2 + s_{12}s_{34} - s_{234}s_{34}) \\
 & + \frac{1}{s_{24}s_{234}} (9s_{12} + 3s_{13} - 5s_{134} + 8s_{34}) + \frac{2}{s_{34}s_{134}^2} (s_{13}^2 + 2s_{12}s_{13} - 2s_{234}s_{13}) \\
 & + \frac{1}{s_{134}s_{234}} (10s_{12} + 7s_{13} - 7s_{24} + 8s_{34}) + \frac{9}{s_{13}} - \frac{17}{s_{134}} - \frac{17}{s_{234}} - \frac{9}{s_{24}} \\
 & + \frac{1}{s_{134}s_{234}s_{24}} (-4s_{12}^2 - 3s_{13}s_{12} - 6s_{34}s_{12} - s_{13}^2 - 3s_{34}^2 - 3s_{13}s_{34}) \\
 & + \frac{1}{s_{13}s_{24}s_{234}} (4s_{12}^2 - 3s_{134}s_{12} + 6s_{34}s_{12} + s_{134}^2 + 3s_{34}^2 - 3s_{134}s_{34}) \\
 & + \frac{1}{s_{13}s_{24}s_{134}} (4s_{12}^2 - 3s_{234}s_{12} + 6s_{34}s_{12} + s_{234}^2 + 3s_{34}^2 - 3s_{234}s_{34}) \\
 & + \frac{1}{s_{13}s_{134}s_{234}} (4s_{12}^2 - 3s_{24}s_{12} + 6s_{34}s_{12} + s_{24}^2 + 3s_{34}^2 - 3s_{24}s_{34}) \\
 & + \frac{1}{s_{13}s_{24}s_{134}s_{234}} (-2s_{12}^3 - 4s_{34}s_{12}^2 - 3s_{34}^2s_{12} - s_{34}^3) \\
 & + \frac{2}{s_{13}s_{34}} (2s_{12} - s_{134} - s_{234} - s_{24}) - \frac{1}{s_{34}s_{134}} (14s_{12} + 12s_{13} - 9s_{234} - 7s_{24}) \\
 & - \frac{1}{s_{34}s_{234}} (14s_{12} + 7s_{13} - 9s_{134} - 12s_{24}) + \frac{2}{s_{34}^2s_{134}^2} (s_{12}s_{13}^2 - s_{13}^2s_{234}) \\
 & + \frac{2}{s_{34}s_{234}^2} (s_{24}^2 - 2s_{12}s_{24} + 2s_{134}s_{24}) + \frac{2}{s_{34}^2s_{234}^2} (s_{12}s_{24}^2 - s_{134}s_{24}^2) \\
 & + \frac{1}{s_{13}s_{34}s_{234}} (-2s_{12}^2 + 2s_{134}s_{12} + 2s_{24}s_{12} - s_{134}^2 - s_{24}^2 - 2s_{134}s_{24}) \\
 & + \frac{2}{s_{134}s_{234}s_{34}} (4s_{12}^2 + 2s_{13}s_{12} - 2s_{24}s_{12} + s_{13}^2 + s_{24}^2 - 2s_{13}s_{24}) \\
 & + \frac{1}{s_{13}s_{24}s_{34}} (2s_{12}^2 - 2s_{134}s_{12} - 2s_{234}s_{12} + s_{134}^2 + s_{234}^2) \\
 & + \frac{1}{s_{134}s_{24}s_{34}} (2s_{12}^2 + 2s_{13}s_{12} - 2s_{234}s_{12} + s_{13}^2 + s_{234}^2 - 2s_{13}s_{234}) \\
 & + \frac{14}{s_{34}} + \frac{2}{s_{34}^2} (s_{12} + 2s_{13} - s_{134} - s_{234} - 2s_{24})
 \end{aligned}$$

$$\begin{aligned}
& - \frac{4s_{12}s_{13}s_{24}}{s_{134}s_{234}s_{34}^2} - \frac{2}{s_{134}s_{34}^2} (s_{13}^2 + 2s_{12}s_{13} - 2s_{234}s_{13} - 2s_{24}s_{13}) \\
& + \frac{2}{s_{234}s_{34}^2} (-s_{24}^2 + 2s_{12}s_{24} + 2s_{13}s_{24} - 2s_{134}s_{24}) \\
& + m_Q^2 \left(\frac{1}{s_{13}s_{134}s_{24}} (-4s_{12} + 8s_{234} - 3s_{34}) - \frac{1}{s_{13}s_{24}s_{134}s_{234}} (s_{12}s_{34} + s_{34}^2) \right. \\
& + \frac{2}{s_{13}^2s_{24}} (2s_{12} - s_{134} - 2s_{234} + 2s_{34}) + \frac{4}{s_{13}s_{34}s_{134}} (s_{12} - s_{234} - s_{24}) \\
& + \frac{2}{s_{13}^2s_{134}} (2s_{12} - 2s_{234} - s_{24} + 2s_{34}) + \frac{4}{s_{13}s_{24}s_{34}s_{134}} (s_{12}s_{234} - s_{234}^2) \\
& - \frac{4}{s_{13}^2s_{134}s_{24}} (-2s_{12}s_{234} + 2s_{12}s_{34} + s_{12}^2 - 2s_{234}s_{34} + s_{234}^2 + s_{34}^2) + \frac{4}{s_{134}^2} \\
& + \frac{4s_{12}s_{24}}{s_{13}s_{134}s_{234}s_{34}} + \frac{s_{34} - 4s_{12}}{s_{13}s_{134}s_{234}} + \frac{4}{s_{13}s_{134}^2} (s_{12} - s_{234} + s_{34}) \\
& + \frac{4}{s_{134}^2s_{34}} (s_{12} - s_{234}) - \frac{s_{34}}{s_{13}s_{234}s_{24}} - \frac{4s_{24}}{s_{13}s_{234}s_{34}} - \frac{4s_{234}}{s_{13}s_{24}s_{34}} + \frac{1}{s_{134}s_{24}} \\
& + \frac{5}{s_{13}s_{234}} + \frac{5}{s_{13}s_{24}} - \frac{4}{s_{13}s_{34}} - \frac{4}{s_{13}^2} - \frac{s_{34}}{s_{134}s_{234}s_{24}} + \frac{2}{s_{134}s_{234}} - \frac{4}{s_{134}s_{34}} \Big) \\
& \left. + m_Q^4 \left(\frac{4}{s_{13}^2s_{134}^2} (s_{12} - s_{234} + s_{34}) - \frac{4}{s_{13}^2s_{134}} \right) \right] + \mathcal{O}(\epsilon), \tag{C.1}
\end{aligned}$$

with $Q^2 = -(p_1 - p_2 + p_3 + p_4)^2$, $s_{134} = s_{13} + s_{14} + s_{34}$, and $s_{234} = -s_{23} - s_{24} + s_{34}$, using our convention $s_{ij} = 2p_i p_j$

Open Access. This article is distributed under the terms of the Creative Commons Attribution License ([CC-BY 4.0](https://creativecommons.org/licenses/by/4.0/)), which permits any use, distribution and reproduction in any medium, provided the original author(s) and source are credited.

References

- [1] ATLAS collaboration, *Measurements of top quark pair relative differential cross-sections with ATLAS in pp collisions at $\sqrt{s} = 7$ TeV*, *Eur. Phys. J. C* **73** (2013) 2261 [[arXiv:1207.5644](https://arxiv.org/abs/1207.5644)] [[INSPIRE](#)].
- [2] CMS collaboration, *Measurement of differential top-quark pair production cross sections in the lepton+jets channel in pp collisions at 8 TeV*, [CMS-PAS-TOP-12-027](#).
- [3] CMS collaboration, *Measurement of the differential ttbar cross section in the dilepton channel at 8 TeV*, [CMS-PAS-TOP-12-028](#).
- [4] G. Abelof and A. Gehrmann-De Ridder, *Double real radiation corrections to $t\bar{t}$ production at the LHC: the all-fermion processes*, *JHEP* **04** (2012) 076 [[arXiv:1112.4736](https://arxiv.org/abs/1112.4736)] [[INSPIRE](#)].
- [5] C. Anastasiou and S.M. Aybat, *The one-loop gluon amplitude for heavy-quark production at NNLO*, *Phys. Rev. D* **78** (2008) 114006 [[arXiv:0809.1355](https://arxiv.org/abs/0809.1355)] [[INSPIRE](#)].
- [6] P. Bärnreuther, M. Czakon and A. Mitov, *Percent Level Precision Physics at the Tevatron: First Genuine NNLO QCD Corrections to $q\bar{q} \rightarrow t\bar{t} + X$* , *Phys. Rev. Lett.* **109** (2012) 132001 [[arXiv:1204.5201](https://arxiv.org/abs/1204.5201)] [[INSPIRE](#)].

- [7] I. Bierenbaum, M. Czakon and A. Mitov, *The singular behavior of one-loop massive QCD amplitudes with one external soft gluon*, *Nucl. Phys. B* **856** (2012) 228 [[arXiv:1107.4384](#)] [[INSPIRE](#)].
- [8] R. Bonciani, A. Ferroglia, T. Gehrmann, D. Maître and C. Studerus, *Two-Loop Fermionic Corrections to Heavy-Quark Pair Production: The Quark-Antiquark Channel*, *JHEP* **07** (2008) 129 [[arXiv:0806.2301](#)] [[INSPIRE](#)].
- [9] R. Bonciani, A. Ferroglia, T. Gehrmann and C. Studerus, *Two-Loop Planar Corrections to Heavy-Quark Pair Production in the Quark-Antiquark Channel*, *JHEP* **08** (2009) 067 [[arXiv:0906.3671](#)] [[INSPIRE](#)].
- [10] R. Bonciani, A. Ferroglia, T. Gehrmann, A. von Manteuffel and C. Studerus, *Two-Loop Leading Color Corrections to Heavy-Quark Pair Production in the Gluon Fusion Channel*, *JHEP* **01** (2011) 102 [[arXiv:1011.6661](#)] [[INSPIRE](#)].
- [11] M. Czakon, *Tops from Light Quarks: Full Mass Dependence at Two-Loops in QCD*, *Phys. Lett. B* **664** (2008) 307 [[arXiv:0803.1400](#)] [[INSPIRE](#)].
- [12] M. Czakon, *Double-real radiation in hadronic top quark pair production as a proof of a certain concept*, *Nucl. Phys. B* **849** (2011) 250 [[arXiv:1101.0642](#)] [[INSPIRE](#)].
- [13] M. Czakon and A. Mitov, *NNLO corrections to top-pair production at hadron colliders: the all-fermionic scattering channels*, *JHEP* **12** (2012) 054 [[arXiv:1207.0236](#)] [[INSPIRE](#)].
- [14] B. Kniehl, Z. Merebashvili, J.G. Korner and M. Rogal, *Heavy quark pair production in gluon fusion at next-to-next-to-leading $O(\alpha_s^4)$ order: One-loop squared contributions*, *Phys. Rev. D* **78** (2008) 094013 [[arXiv:0809.3980](#)] [[INSPIRE](#)].
- [15] J.G. Korner, Z. Merebashvili and M. Rogal, *NNLO $O(\alpha_s^4)$ results for heavy quark pair production in quark-antiquark collisions: The one-loop squared contributions*, *Phys. Rev. D* **77** (2008) 094011 [*Erratum ibid.* **D 85** (2012) 119904] [[arXiv:0802.0106](#)] [[INSPIRE](#)].
- [16] M. Czakon, P. Fiedler and A. Mitov, *Total Top-Quark Pair-Production Cross section at Hadron Colliders Through $O(\alpha_s^4)$* , *Phys. Rev. Lett.* **110** (2013) 252004 [[arXiv:1303.6254](#)] [[INSPIRE](#)].
- [17] T. Binoth and G. Heinrich, *An automatized algorithm to compute infrared divergent multiloop integrals*, *Nucl. Phys. B* **585** (2000) 741 [[hep-ph/0004013](#)] [[INSPIRE](#)].
- [18] C. Anastasiou, K. Melnikov and F. Petriello, *A new method for real radiation at NNLO*, *Phys. Rev. D* **69** (2004) 076010 [[hep-ph/0311311](#)] [[INSPIRE](#)].
- [19] T. Binoth and G. Heinrich, *Numerical evaluation of phase space integrals by sector decomposition*, *Nucl. Phys. B* **693** (2004) 134 [[hep-ph/0402265](#)] [[INSPIRE](#)].
- [20] C. Anastasiou, F. Herzog and A. Lazopoulos, *On the factorization of overlapping singularities at NNLO*, *JHEP* **03** (2011) 038 [[arXiv:1011.4867](#)] [[INSPIRE](#)].
- [21] S. Catani and M. Grazzini, *An NNLO subtraction formalism in hadron collisions and its application to Higgs boson production at the LHC*, *Phys. Rev. Lett.* **98** (2007) 222002 [[hep-ph/0703012](#)] [[INSPIRE](#)].
- [22] A. Gehrmann-De Ridder, T. Gehrmann and E.W.N. Glover, *Antenna subtraction at NNLO*, *JHEP* **09** (2005) 056 [[hep-ph/0505111](#)] [[INSPIRE](#)].
- [23] M. Czakon, *A novel subtraction scheme for double-real radiation at NNLO*, *Phys. Lett. B* **693** (2010) 259 [[arXiv:1005.0274](#)] [[INSPIRE](#)].
- [24] R. Boughezal, K. Melnikov and F. Petriello, *A subtraction scheme for NNLO computations*, *Phys. Rev. D* **85** (2012) 034025 [[arXiv:1111.7041](#)] [[INSPIRE](#)].

- [25] S. Frixione, *A general approach to jet cross-sections in QCD*, *Nucl. Phys. B* **507** (1997) 295 [[hep-ph/9706545](#)] [[INSPIRE](#)].
- [26] G. Abeloﬀ and A. Gehrmann-De Ridder, *Double real radiation corrections to $t\bar{t}$ production at the LHC: the $gg \rightarrow t\bar{t}q\bar{q}$ channel*, *JHEP* **11** (2012) 074 [[arXiv:1207.6546](#)] [[INSPIRE](#)].
- [27] G. Abeloﬀ and A. Gehrmann-De Ridder, *Antenna subtraction for the production of heavy particles at hadron colliders*, *JHEP* **04** (2011) 063 [[arXiv:1102.2443](#)] [[INSPIRE](#)].
- [28] S. Catani, S. Dittmaier, M.H. Seymour and Z. Trócsányi, *The dipole formalism for next-to-leading order QCD calculations with massive partons*, *Nucl. Phys. B* **627** (2002) 189 [[hep-ph/0201036](#)] [[INSPIRE](#)].
- [29] J. Currie, A. Gehrmann-De Ridder, E.W.N. Glover and J. Pires, *NNLO QCD corrections to jet production at hadron colliders from gluon scattering*, *JHEP* **01** (2014) 110 [[arXiv:1310.3993](#)] [[INSPIRE](#)].
- [30] J. Currie, E.W.N. Glover and S. Wells, *Infrared Structure at NNLO Using Antenna Subtraction*, *JHEP* **04** (2013) 066 [[arXiv:1301.4693](#)] [[INSPIRE](#)].
- [31] A. Gehrmann-De Ridder, E.W.N. Glover and J. Pires, *Real-Virtual corrections for gluon scattering at NNLO*, *JHEP* **02** (2012) 141 [[arXiv:1112.3613](#)] [[INSPIRE](#)].
- [32] A. Gehrmann-De Ridder, T. Gehrmann, E.W.N. Glover and J. Pires, *Double Virtual corrections for gluon scattering at NNLO*, *JHEP* **02** (2013) 026 [[arXiv:1211.2710](#)] [[INSPIRE](#)].
- [33] W. Bernreuther, C. Bogner and O. Dekkers, *The real radiation antenna function for $S \rightarrow Q\bar{Q}q\bar{q}$ at NNLO QCD*, *JHEP* **06** (2011) 032 [[arXiv:1105.0530](#)] [[INSPIRE](#)].
- [34] W. Bernreuther, C. Bogner and O. Dekkers, *The real radiation antenna functions for $S \rightarrow Q\bar{Q}gg$ at NNLO QCD*, *JHEP* **10** (2013) 161 [[arXiv:1309.6887](#)] [[INSPIRE](#)].
- [35] R. Boughezal, A. Gehrmann-De Ridder and M. Ritzmann, *Antenna subtraction at NNLO with hadronic initial states: double real radiation for initial-initial configurations with two quark flavours*, *JHEP* **02** (2011) 098 [[arXiv:1011.6631](#)] [[INSPIRE](#)].
- [36] A. Daleo, T. Gehrmann and D. Maître, *Antenna subtraction with hadronic initial states*, *JHEP* **04** (2007) 016 [[hep-ph/0612257](#)] [[INSPIRE](#)].
- [37] A. Daleo, A. Gehrmann-De Ridder, T. Gehrmann and G. Luisoni, *Antenna subtraction at NNLO with hadronic initial states: initial-final configurations*, *JHEP* **01** (2010) 118 [[arXiv:0912.0374](#)] [[INSPIRE](#)].
- [38] T. Gehrmann and P.F. Monni, *Antenna subtraction at NNLO with hadronic initial states: real-virtual initial-initial configurations*, *JHEP* **12** (2011) 049 [[arXiv:1107.4037](#)] [[INSPIRE](#)].
- [39] A. Gehrmann-De Ridder, T. Gehrmann, E.W.N. Glover and G. Heinrich, *Infrared structure of $e^+e^- \rightarrow 3$ jets at NNLO*, *JHEP* **11** (2007) 058 [[arXiv:0710.0346](#)] [[INSPIRE](#)].
- [40] A. Gehrmann-De Ridder and M. Ritzmann, *NLO Antenna Subtraction with Massive Fermions*, *JHEP* **07** (2009) 041 [[arXiv:0904.3297](#)] [[INSPIRE](#)].
- [41] A. Gehrmann-De Ridder, T. Gehrmann and M. Ritzmann, *Antenna subtraction at NNLO with hadronic initial states: double real initial-initial configurations*, *JHEP* **10** (2012) 047 [[arXiv:1207.5779](#)] [[INSPIRE](#)].
- [42] E.W. Nigel Glover and J. Pires, *Antenna subtraction for gluon scattering at NNLO*, *JHEP* **06** (2010) 096 [[arXiv:1003.2824](#)] [[INSPIRE](#)].

- [43] A. Gehrmann-De Ridder, T. Gehrmann, E.W.N. Glover and J. Pires, *Second order QCD corrections to jet production at hadron colliders: the all-gluon contribution*, *Phys. Rev. Lett.* **110** (2013) 162003 [[arXiv:1301.7310](#)] [[INSPIRE](#)].
- [44] G. Abelo, O. Dekkers and A. Gehrmann-De Ridder, *Antenna subtraction with massive fermions at NNLO: Double real initial-final configurations*, *JHEP* **12** (2012) 107 [[arXiv:1210.5059](#)] [[INSPIRE](#)].
- [45] F. Cascioli, P. Maierhofer and S. Pozzorini, *Scattering Amplitudes with Open Loops*, *Phys. Rev. Lett.* **108** (2012) 111601 [[arXiv:1111.5206](#)] [[INSPIRE](#)].
- [46] G. Ossola, C.G. Papadopoulos and R. Pittau, *CutTools: A program implementing the OPP reduction method to compute one-loop amplitudes*, *JHEP* **03** (2008) 042 [[arXiv:0711.3596](#)] [[INSPIRE](#)].
- [47] S. Badger, R. Sattler and V. Yundin, *One-Loop Helicity Amplitudes for $t\bar{t}$ Production at Hadron Colliders*, *Phys. Rev. D* **83** (2011) 074020 [[arXiv:1101.5947](#)] [[INSPIRE](#)].
- [48] W. Beenakker, H. Kuijf, W.L. van Neerven and J. Smith, *QCD Corrections to Heavy Quark Production in $p\bar{p}$ Collisions*, *Phys. Rev. D* **40** (1989) 54 [[INSPIRE](#)].
- [49] P. Nason, S. Dawson and R.K. Ellis, *The One Particle Inclusive Differential Cross-Section for Heavy Quark Production in Hadronic Collisions*, *Nucl. Phys. B* **327** (1989) 49 [Erratum *ibid.* **B 335** (1990) 260] [[INSPIRE](#)].
- [50] S. Catani, S. Dittmaier and Z. Trócsányi, *One loop singular behavior of QCD and SUSY QCD amplitudes with massive partons*, *Phys. Lett. B* **500** (2001) 149 [[hep-ph/0011222](#)] [[INSPIRE](#)].
- [51] G. Altarelli and G. Parisi, *Asymptotic Freedom in Parton Language*, *Nucl. Phys. B* **126** (1977) 298 [[INSPIRE](#)].
- [52] F.A. Berends and W.T. Giele, *Multiple Soft Gluon Radiation in Parton Processes*, *Nucl. Phys. B* **313** (1989) 595 [[INSPIRE](#)].
- [53] J.M. Campbell and E.W.N. Glover, *Double unresolved approximations to multiparton scattering amplitudes*, *Nucl. Phys. B* **527** (1998) 264 [[hep-ph/9710255](#)] [[INSPIRE](#)].
- [54] D. de Florian and M. Grazzini, *The structure of large logarithmic corrections at small transverse momentum in hadronic collisions*, *Nucl. Phys. B* **616** (2001) 247 [[hep-ph/0108273](#)] [[INSPIRE](#)].
- [55] S. Weinzierl, *Subtraction terms for one loop amplitudes with one unresolved parton*, *JHEP* **07** (2003) 052 [[hep-ph/0306248](#)] [[INSPIRE](#)].
- [56] Z. Bern, L.J. Dixon, D.C. Dunbar and D.A. Kosower, *One loop n point gauge theory amplitudes, unitarity and collinear limits*, *Nucl. Phys. B* **425** (1994) 217 [[hep-ph/9403226](#)] [[INSPIRE](#)].
- [57] Z. Bern, V. Del Duca and C.R. Schmidt, *The infrared behavior of one loop gluon amplitudes at next-to-next-to-leading order*, *Phys. Lett. B* **445** (1998) 168 [[hep-ph/9810409](#)] [[INSPIRE](#)].
- [58] D.A. Kosower, *All order collinear behavior in gauge theories*, *Nucl. Phys. B* **552** (1999) 319 [[hep-ph/9901201](#)] [[INSPIRE](#)].
- [59] D.A. Kosower and P. Uwer, *One loop splitting amplitudes in gauge theory*, *Nucl. Phys. B* **563** (1999) 477 [[hep-ph/9903515](#)] [[INSPIRE](#)].

- [60] Z. Bern, V. Del Duca, W.B. Kilgore and C.R. Schmidt, *The infrared behavior of one loop QCD amplitudes at next-to-next-to leading order*, *Phys. Rev. D* **60** (1999) 116001 [[hep-ph/9903516](#)] [[INSPIRE](#)].
- [61] S. Catani and M. Grazzini, *The soft gluon current at one loop order*, *Nucl. Phys. B* **591** (2000) 435 [[hep-ph/0007142](#)] [[INSPIRE](#)].
- [62] D.A. Kosower, *Multiple singular emission in gauge theories*, *Phys. Rev. D* **67** (2003) 116003 [[hep-ph/0212097](#)] [[INSPIRE](#)].
- [63] D.A. Kosower, *All orders singular emission in gauge theories*, *Phys. Rev. Lett.* **91** (2003) 061602 [[hep-ph/0301069](#)] [[INSPIRE](#)].
- [64] S. Catani, D. de Florian and G. Rodrigo, *The triple collinear limit of one loop QCD amplitudes*, *Phys. Lett. B* **586** (2004) 323 [[hep-ph/0312067](#)] [[INSPIRE](#)].
- [65] Z. Bern, L.J. Dixon and D.A. Kosower, *Two-loop $g \rightarrow gg$ splitting amplitudes in QCD*, *JHEP* **08** (2004) 012 [[hep-ph/0404293](#)] [[INSPIRE](#)].
- [66] S.D. Badger and E.W.N. Glover, *Two loop splitting functions in QCD*, *JHEP* **07** (2004) 040 [[hep-ph/0405236](#)] [[INSPIRE](#)].
- [67] A. Denner and S. Dittmaier, *Reduction of one loop tensor five point integrals*, *Nucl. Phys. B* **658** (2003) 175 [[hep-ph/0212259](#)] [[INSPIRE](#)].
- [68] A. Denner and S. Dittmaier, *Reduction schemes for one-loop tensor integrals*, *Nucl. Phys. B* **734** (2006) 62 [[hep-ph/0509141](#)] [[INSPIRE](#)].
- [69] G. Ossola, C.G. Papadopoulos and R. Pittau, *Reducing full one-loop amplitudes to scalar integrals at the integrand level*, *Nucl. Phys. B* **763** (2007) 147 [[hep-ph/0609007](#)] [[INSPIRE](#)].
- [70] P. Mastrolia, G. Ossola, T. Reiter and F. Tramontano, *Scattering AMplitudes from Unitarity-based Reduction Algorithm at the Integrand-level*, *JHEP* **08** (2010) 080 [[arXiv:1006.0710](#)] [[INSPIRE](#)].
- [71] M. Grazzini, S. Kallweit, D. Rathlev and A. Torre, *$Z\gamma$ production at hadron colliders in NNLO QCD*, *Phys. Lett. B* **731** (2014) 204 [[arXiv:1309.7000](#)] [[INSPIRE](#)].
- [72] A. Denner, S. Dittmaier and L. Hofer, *COLLIER: a fortran-based complex one-loop library in extended regularizations*, in preparation.
- [73] A. Denner and S. Dittmaier, *Scalar one-loop 4-point integrals*, *Nucl. Phys. B* **844** (2011) 199 [[arXiv:1005.2076](#)] [[INSPIRE](#)].
- [74] S. Hoeche et al., *Next-to-leading order QCD predictions for top-quark pair production with up to two jets merged with a parton shower*, [arXiv:1402.6293](#) [[INSPIRE](#)].
- [75] P. Draggiotis, M.V. Garzelli, C.G. Papadopoulos and R. Pittau, *Feynman Rules for the Rational Part of the QCD 1-loop amplitudes*, *JHEP* **04** (2009) 072 [[arXiv:0903.0356](#)] [[INSPIRE](#)].
- [76] R. Kleiss, W.J. Stirling and S.D. Ellis, *A New Monte Carlo Treatment of Multiparticle Phase Space at High-energies*, *Comput. Phys. Commun.* **40** (1986) 359 [[INSPIRE](#)].
- [77] P. Nogueira, *Automatic Feynman graph generation*, *J. Comput. Phys.* **105** (1993) 279 [[INSPIRE](#)].
- [78] J. Alwall, M. Herquet, F. Maltoni, O. Mattelaer and T. Stelzer, *MadGraph 5: Going Beyond*, *JHEP* **06** (2011) 128 [[arXiv:1106.0522](#)] [[INSPIRE](#)].